UNIVERSITÀ DEGLI STUDI DI TRIESTE E UNIVERSITÀ CA' FOSCARI VENEZIA

XXXVI CICLO DEL DOTTORATO DI RICERCA IN CHIMICA

MULTI–ANALYTICAL APPROACHES APPLIED TO THE STUDY OF ANCIENT COINS

Settore scientifico-disciplinare: CHIM/01 CHIMICA ANALITICA

DOTTORANDA
GIOVANNA MARUSSI

COORDINATORE
PROF. ENZO ALESSIO

SUPERVISORE DI TESI
PROF. GIANPIERO ADAMI

ANNO ACCADEMICO 2022/2023

UNIVERSITÀ DEGLI STUDI DI TRIESTE E UNIVERSITÀ CA' FOSCARI VENEZIA

XXXVI CICLO DEL DOTTORATO DI RICERCA IN CHIMICA

MULTI–ANALYTICAL APPROACHES APPLIED TO THE STUDY OF ANCIENT COINS

Settore scientifico-disciplinare: CHIM/01 CHIMICA ANALITICA

DOTTORANDA
GIOVANNA MARUSSI

COORDINATORE
PROF. ENZO ALESSIO

SUPERVISORE DI TESI
PROF. GIANPIERO ADAMI

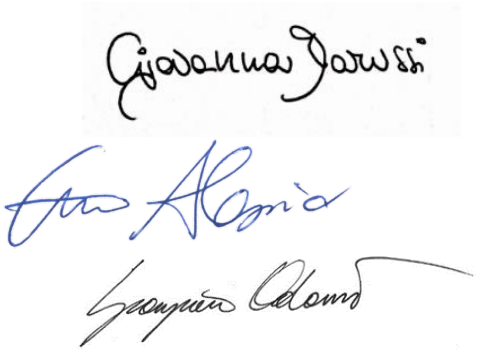

ANNO ACCADEMICO 2022/2023

Table of Contents

SECTION 2

Non−destructive and micro−destructive chemical analysis of Late Antique gold solidi (4^{th}–6^{th} century) from Balkan hoards

SECTION 3

A Multi−Analytical Approach on Silver−Copper Coins of the Roman Empire to Elucidate the Economy of the 3rd Century A.D.

SECTION 4

Enhancing Understanding of the Sasanian Dynasty: Archaeometric Investigations of Silver Drachmas (6th–7th Century AD) Using X−Ray Fluorescence Analysis

List of figures

1. Introduction

3. Sampling and characterization techniques

SECTION 1 – From Collection or Archaeological Finds? A Non-Destructive Analytical Approach to Distinguish between Two Sets of Bronze Coins of the Roman Empire

SECTION 2 - Non−destructive and micro−destructive chemical analysis of Late Antique gold solidi (4th–6th century) from Balkan hoards

1. A multi−technique preliminary study of 49 gold solidi from the Late Antique period (4th–6th century AD)

2. Combining synchrotron radiation techniques for the analysis of gold coins from the Roman Empire

SECTION 3 - A Multi−Analytical Approach on Silver−Copper Coins of the Roman Empire to Elucidate the Economy of the 3rd Century A.D.

SECTION 4 - Enhancing Understanding of the Sasanian Dynasty: Archaeometric Investigations of Silver Drachmas (6th–7th Century AD) Using X−Ray Fluorescence Analysis

List of tables

SECTION 1 – From Collection or Archaeological Finds? A Non-Destructive Analytical Approach to Distinguish between Two Sets of Bronze Coins of the Roman Empire

SECTION 2 - Non−destructive and micro−destructive chemical analysis of Late Antique gold solidi (4th–6th century) from Balkan hoards

1. A multi−technique preliminary study of 49 gold solidi from the Late Antique period (4th–6th century AD)

2. Combining synchrotron radiation techniques for the analysis of gold coins from the Roman Empire

SECTION 3 - A Multi−Analytical Approach on Silver−Copper Coins of the Roman Empire to Elucidate the Economy of the 3rd Century A.D.

SECTION 4 - Enhancing Understanding of the Sasanian Dynasty: Archaeometric Investigations of Silver Drachmas (6th–7th Century AD) Using X−Ray Fluorescence Analysis

Abstract

Chemistry was first applied to the field of conservation in the 18th century. Today, analytical chemistry plays a crucial role in characterising artistic and cultural heritage, as well as supporting archaeometric studies related to origin, dating, and attribution. This discipline is employed to identify the causes and mechanisms of degradation, and to develop and evaluate the performance of materials and restoration methods. In particular, ancient coins are significant cultural heritage artefacts with high historical and artistic value. Indeed, the inscriptions and figures on their surfaces can assist historians and numismatists in identifying the period, mint of issue, country, and ruler associated with the coin's age.

Archaeological systems are highly complex, composed of several chemical species within inhomogeneous matrices. To obtain maximum information about the composition of the specimens under examination, it is essential to combine different analytical techniques, both non–destructive and micro–destructive, with varying sensitivities. Besides alloying elements, attention should also be given to the presence of minor elements (<0.1%). These elements are fundamental for obtaining insights into the origin of the primary metal, alloy alteration processes affecting coin value, changes in coin manufacturing, degradation and corrosion processes, as well as the place of burial.

The aim of this thesis is to explore the potential of analytical chemistry applied to the study of ancient coins. This research presents various studies carried out on coin specimens from different time periods, illustrating how the choice of a correct multi−analytical approach can provide answers to questions raised by historians, numismatists, and collectors.

Firstly, the results of non–destructive analyses (μ–EDXRF and ATR–FTIR) conducted on the surface patina of six bronze coins from the Roman−Imperial era are presented. The combination of these two techniques allowed for the classification of these coins into two distinct groups: those recovered from archaeological excavations on Monte Cesén (Treviso, Italy) and a group preserved at the Museum of Natural History and Archaeology of Montebelluna (Treviso, Italy).

The second part of this study involved the examination of 49 Late Antique gold solidi using both conventional laboratory techniques, such as μ−EDXRF, ICP−AES and ICP−MS, as well as techniques employing synchrotron radiation. Thanks to the

availability of a gold standard, it became possible to determine the fineness of all 49 coins. In addition, trace elements were quantified, enabling the formulation of hypotheses about the origin of the gold used to mint the coins and the location of their burial. Through the application of SR−XRF and SR−XANES, it was possible to distinguish between the elements constituting the surface concretions and those composing the original alloy. Furthermore, analyses at the Fe K−edge led to the conclusion that the likely burial place of the gold solidi was in the Mediterranean area.

Significant analysis and cataloguing work were carried out on 160 silver−copper alloy coins minted during the Roman Empire. This study harnessed the combined capabilities of μ–EDXRF, SEM–EDX, ICP–AES, and ICP–MS to accurately identify and quantify the alloy percentages as well as the main trace elements. The distinction between the two currency types – denarius and antoninianus – became evident from the different silver and copper percentages in these specimens. Specifically, there was a noticeable decline in silver content as the year of minting increased. This phenomenon highlights the progression of the economic crisis during the 3rd century, culminating in 215 AD with the introduction of the new coin, the antoninianus. Among the trace elements, high concentrations of lead and tin were consistent with the use of argentiferous galena for silver extraction and older brass or bronze objects for the production of silver–copper coins, respectively.

Finally, a study was conducted on 29 drachmas dating back to the Sasanian dynasty (224–651 AD). An exclusively non–destructive analysis was performed using μ–EDXRF. Leveraging the availability of a sterling silver standard, it was possible to conduct a semi–quantitative analysis, offering insights into the fineness of the coins under examination. In addition, ratios between the elements detected in the XRF spectra were calculated in order to obtain additional information on the raw materials employed in coin minting. In the end, chemical analyses revealed a group of coins of exceptional quality, corroborating historical assumptions.

Riassunto

La chimica è stata applicata per la prima volta nel campo della conservazione nel XVIII secolo. Attualmente, la chimica analitica svolge un ruolo cruciale nella caratterizzazione del patrimonio artistico e culturale, oltre a supportare gli studi archeometrici relativi all'origine, alla datazione e all'attribuzione. Questa disciplina viene utilizzata per identificare le cause e i meccanismi di degrado e per sviluppare e valutare le prestazioni dei materiali e dei metodi di restauro. In particolare, le monete antiche sono importanti manufatti del patrimonio culturale con un elevato valore storico e artistico. Infatti, le iscrizioni e le figure presenti sulle loro superfici possono aiutare gli storici e i numismatici ad identificare il periodo, la zecca di emissione, il paese e il sovrano associato all'epoca della moneta.

I sistemi archeologici sono estremamente complessi, poiché sono costituiti da molte specie chimiche in matrici disomogenee. Ai fini di ottenere il massimo delle informazioni sulla composizione degli esemplari esaminati, è essenziale combinare diverse tecniche analitiche, sia non−distruttive che micro−distruttive, con diverse sensibilità. Oltre agli elementi di lega, bisogna porre attenzione anche sulla presenza degli elementi minori (<0.1%). Questi elementi sono fondamentali per ottenere informazioni sull'origine del metallo primario, sui processi di alterazione delle leghe che influenzano il valore delle monete, sui cambiamenti nella produzione delle monete, sui processi di degradazione e corrosione, nonché sul luogo di sepoltura.

Lo scopo di questa tesi è quello di esplorare le potenzialità della chimica analitica applicata allo studio delle monete antiche. Questa ricerca presenta vari studi condotti su esemplari di monete di diversi periodi storici, illustrando come la scelta di un corretto approccio multi−analitico aiuti a rispondere alle domande poste da storici, numismatici e collezionisti.

In primo luogo, vengono presentati i risultati ottenuti da un'analisi non distruttiva (μ–EDXRF e ATR–FTIR) della patina superficiale di sei monete di bronzo di epoca romano−imperiale. La combinazione di queste due tecniche ha permesso la classificazione di queste monete in due gruppi distinti: quelli rinvenuti negli scavi archeologici del Monte Cesén (Treviso) e un gruppo conservato presso il Museo di Storia Naturale e Archeologia di Montebelluna (Treviso).

La seconda parte dello studio ha riguardato l'esame di 49 solidi d'oro tardo−antichi utilizzando sia tecniche di laboratorio convenzionali, come μ−EDXRF, ICP−AES e ICP−MS, che tecniche che impiegano la radiazione di sincrotrone. Grazie alla disponibilità di uno standard d'oro, è stato possibile determinare la finezza di tutte le 49 monete. Inoltre, sono stati quantificati gli elementi in traccia, consentendo di formulare ipotesi sull'origine dell'oro utilizzato per coniare le monete e sul luogo in cui sono state sepolte. Attraverso l'applicazione di SR−XRF e SR−XANES, è stato possibile distinguere gli elementi che costituivano le concrezioni superficiali da quelli che costituivano la lega originale. Inoltre, lo spettro di assorbimento XANES della soglia K del ferro ha portato alla conclusione che il luogo di sepoltura dei solidi d'oro si trovava probabilmente nell'area mediterranea.

Un importante lavoro di analisi e catalogazione è stato condotto su 160 monete in lega argento−rame coniate durante l'Impero Romano. Questo studio ha sfruttato le capacità combinate di μ–EDXRF, SEM–EDX, ICP–AES e ICP–MS per identificare e quantificare con precisione le percentuali di lega e i principali elementi in traccia. La differenza fra le due valute – denario e antoniniano – è risultata evidente dalle diverse percentuali di argento e rame presenti in questi esemplari. In particolare, si è notata una notevole diminuzione del contenuto di argento all'aumentare dell'anno di coniazione. Questo fenomeno evidenzia la progressione della crisi economica del III secolo, culminata nel 215 d.C. con l'introduzione della nuova moneta, l'antoniniano. Tra gli elementi in traccia, le alte concentrazioni di piombo e stagno sono coerenti, rispettivamente, con l'uso della galena argentifera per l'estrazione dell'argento e con l'utilizzo di vecchi oggetti in bronzo o ottone per la produzione di monete in argento−rame.

Infine, è stato condotto uno studio su 29 dracme risalenti alla dinastia Sasanide (224–651 d.C.). È stata eseguita un'analisi esclusivamente non distruttiva utilizzando la μ–EDXRF. Sfruttando la disponibilità di uno standard di argento sterling, è stato possibile condurre un'analisi semi−quantitativa che ha fornito informazioni sulla finezza delle monete in esame. Inoltre, sono stati calcolati i rapporti tra gli elementi rilevati dagli spettri XRF al fine di ottenere maggiori informazioni sulle materie prime utilizzate nella coniazione delle monete. In conclusione, le analisi chimiche hanno rivelato un gruppo di monete di qualità eccezionale, confermando le ipotesi storiche.

1. Introduction

The knowledge of a cultural heritage entails not only the recognition of its historical and artistic value, but also the determination of its composition and the technique of its execution through scientific investigations. These investigations are primarily based on the principles of chemistry and physics (Campanella et al., 2011).

Analytical chemistry – a field of chemistry focused on the development and applications of chemical analysis – plays a crucial role in characterising works of art and cultural heritage and in supporting archaeometric studies.

Archaeological systems are highly complex, consisting of numerous chemical species in inhomogeneous matrices. Therefore, in order to obtain more information about the samples under study, it is important to combine non−destructive techniques with micro–destructive ones. The latter are more informative as they provide data on the composition of the "bulk" – the innermost part – of the objects, not just the surfaces (Adriaens, 2004; Mazzeo et al., 2011).

The results obtained are then analysed by different experts, who are key figures in the study of cultural heritage, including art and archaeological conservators and restorers, analytical chemists and physicists, biologists, engineers, materials science experts, etc. (Madariaga, 2015). Therefore, cultural heritage science can be defined as a multidisciplinary field.

1.1 Archaeometry: definition and relevance in the scientific community

In etymology, the term archaeometry (from the Greek *archaeos*– meaning "ancient", and *–metron* meaning "measure" or "measurement") denotes a set of measurements carried out with various instruments on ancient materials. This concept dates back to the early 1950s, when C. Hawkes, a professor of European Archaeology at Oxford University, coined the word to characterise the increasing importance of dating, physico–chemical analysis, and quantification in archaeology. In 1958, the international journal *Archaeometry* was founded, followed in 1961 by the first annual scientific meetings of the *International Symposium on Archaeometry* (Wells, 2014). From then on, archaeometric research accelerated worldwide with the publication of several textbooks and international journals on the subject.

Today, archaeometry, or archaeological science, is a field of study that includes all the scientific technologies and methods to assist archaeologists in studying and interpreting archaeological materials and answering historical questions and problems (Colombini, 2011; Liritzis et al., 2020).

Archaeometric investigations employ both instrumental and non–instrumental approaches and focus on the study of materials, substances, chemical and biological residues.

Initially, the applications of archaeometry were limited to dating, provenance, production methods, and artefacts usage. Today, thanks to advances and developments in several sciences, in particular computer modelling and statistics, along with access to modern technologies, archaeometry has gained a more significant position among other sciences (Razani et al., 2021).

1.2 Chemical analysis of ancient coins: an overview

Ancient coins are important cultural heritage artefacts with high historical, artistic, and cultural value. The inscriptions and figures on their surface can help historians and numismatists to identify the period, mint of issue, country, and ruler of the coin's era. For this reason, coins are considered a valuable source of useful information about the minting period and have been widely studied in cultural heritage science (Salem and Mohamed, 2019). In fact, through their examination and analysis, it is possible to ascertain the provenance of the raw materials, the minting technique, the government policy, and the economic conditions of the time when the coins were minted (Mabuchi et al., 1979).

The chemical analysis of ancient coins is far from recent. As early as the 16th century, scholars mentioned the examination of ancient coins in their essays, such as Agricola in 1550 (Metcalf, 2011). The first documented chemical analyses date back to the late 18th and early 19th centuries. In 1798, M. H. Klaproth published the first quantitative analysis of six orichalcum coins from the 1st century (Klaproth, 1798). Thereafter, interest in this topic grew, but it mainly focused on quantifying major metals. Until 1908, there were few attempts to determine trace elements, or even microstructures. After this time, there were studies that focused on the presence of minor elements, but they were limited by the low–sensitivity analytical techniques available at the time. An illustrative example is Brambach's study in which 216 copper alloy coins dating from 320–330 AD were melted,

resulting in a sample of about 675 g. The obtained sample was analysed and found to contain 1.98% silver (Metcalf, 2011).

In the 1960s and 1970s, new analytical techniques that did not require coin sampling were developed. Two such techniques are distinguished: X–Ray Fluorescence (XRF) and Neutron Activation Analysis (NAA) (Ponting, 2012). These techniques contributed to the growth of research in the chemical analysis of ancient coins because of their non–destructive nature, which fascinated archaeologists and museum curators. However, these techniques have a significant limitation: they are unsuitable for determining the fineness of coins with an enriched surface layer.

In the 1990s, researchers in the field realised that the use of non–destructive analytical techniques alone was not sufficient to fully understand the composition of ancient coins. In 1994, Ponting proposed a micro–destructive approach based on the use of Atomic Absorption Spectrometry (AAS). It required the use of a drill to remove a specific amount of material from the edge of the coin. By discarding the first 2 mm of depth, it was possible to avoid evaluation errors due to corrosion or deliberate silvering techniques (Ponting, 1994a). Indeed, by comparing the results of his micro–destructive analyses on 274 coins with those obtained on similar coins by Ziegler (George, 2019), Ponting clearly demonstrated that non–destructive techniques alone are not accurate enough to obtain the overall composition of coins made of complex alloys (Ponting, 1994b).

In recent years, new analytical techniques have been developed using only a few micrograms of material, such as Laser Ablation–Inductively Coupled Plasma–Mass Spectrometry (LA–ICP–MS). In this technique, a laser is focused on the solid sample, ablating a tiny hole on its surface. Depending on the chosen LA protocol and the material to be analysed, a heterogeneous mixture of clusters, particles, and aggregates is released, which can be introduced directly into the plasma (Pitts and May, 2023). The detection limits for optimised LA–ICP–MS are higher than for liquid–mode ICP–MS but are still in the low ppb range for most elements. This technique offers several advantages: no sample preparation is required, complications associated with highly dissolved solid solutions are eliminated, and there is no interference with solvents (Trejos et al., 2003). However, concerning ancient coins, there is some disagreement about the depth achieved by this technique. Proponents argue that an adequate laser can reach a depth of 300 µm, while other experts have pointed out that to maintain the accuracy of analysis for a 100 µm diameter hole, the depth should not exceed 100 µm (Butcher and Ponting, 2015).

Today, there are several non–invasive analytical techniques used in the field of cultural heritage, based on different beams that allow direct measurements on the sample or area of interest (Madariaga, 2015). Unfortunately, in the case of silver–copper alloy coins, the variable depth of surface enrichment cannot be quantified without examining them in section. Additionally, the depth reached by the beam depends on different factors, such as the energy of the incident primary radiation, the absorption coefficient, the energy of the secondary X–rays, the atmosphere, and the composition of the matrix; thus, it depends on the Lambert–Beer law (Haschke, 2014).

As a result, after a few hundred microns, the analyst can assume that the metal core has been reached, but there is no assurance. As stated by Butcher and Ponting (2015), the only reliable method to determine the extent of surface enrichment is the study of cross–sections, although this approach is highly destructive and is often not recommended in the field of cultural heritage. In this regard, Hrnjić et al. (2020) examined the cross−sections of 12 historical silver–copper alloy coins with various chronologies, origins, and compositions to investigate the different surface enrichment in silver. In their study, they analysed the section perpendicular to the flat coin without damaging the relief using micro–X–Ray Fluorescence (μ–XRF) for alloying elements and LA–ICP–MS to study trace elements. As a result of this work, Hrnjić et al. confirmed that surface enrichment in the case of ancient Ag–Cu alloy coins can also be identified non–destructively with XRF by calculating the intensity ratio Ag Kα/Ag Lα, as already suggested by Linke et al. (2004). Indeed, depending on the composition of the matrix, the Ag Kα radiation (energy: 22.16 keV) comes from a depth of about 100 μm, while the Ag Lα line appearing at 2.98 keV comes from a maximum depth of 2 μm. Coins with a lower ratio suggest a relative enrichment of silver on the surface, while higher ratios indicate the presence of corrosion products with an elemental composition different from the bulk. In any case, if surface screening of many Ag–Cu coins is desired, the researcher must consider the compositional inhomogeneity of the coins and use multiple standards to evaluate surface enrichment.

Besides the main elements, trace elements are also important in the study of ancient coins. They can provide information about the locations of the mines from which the metals were extracted and the manufacturing procedures (Hrnjić et al., 2021; Zaykov et al., 2018), as well as reveal possible forgeries (Charalambous, 2015).

In the case of silver coins, an important trace element is gold. The Au/Ag ratio of a coin normally reflects those of the ore and thus gold is usually taken as an indicator of the origin of the silver used. Indeed, this metal does not oxidize when ore is melted down to obtain silver (Flament and Marchetti, 2004). However, modern forging techniques separate gold from silver, making the presence of Au strong evidence of authenticity. Similarly, another element that can help scholars to distinguish a counterfeit silver coin from an authentic one is lead. In antiquity, the noble metal was extracted from argentiferous lead ores, such as cerussite or argentiferous galena (Salem and Mohamed, 2019). Furthermore, Pb is known to be an indicator of the quality of the technological process used to purify Ag. Generally, a low Pb concentration is associated with a high level of Ag refining (Nriagu, 1985). Lastly, another minority element that may often be present in silver coins is bismuth, which is strongly associated with gold, so this element may also indicate the origin of silver (Šmit and Šemrov, 2006).

On the contrary, in the case of gold coins, elements such as Sn, Sb, Pt, Pd, Ir, Rh, As, Zn, Ru, and Te can be used to trace the origin of the noble metal (Guerra, 2004; Guerra and Calligaro, 2004). In particular, Sn, Sb, Pt, and Pd have demonstrated to be the most important for provenance (Guerra, 2005), in particular Pt and Sn are essential to distinguish secondary from primary gold deposits (Dube, 2006): tin is common in alluvial gold, as cassiterite. Platinum and palladium are important gold tracers because ancient processes, such as melting, cupellation, or cementation, did not separate these two elements from gold due to their low reactivity and high melting points (Blet-Lemarquand et al., 2015). However, it is important to remember that Platinum Group Elements (PGE) tend to form inclusions of different densities that could be removed during cupellation, thus decreasing the amount of the two tracer elements in the gold artefacts (Guerra and Calligaro, 2004).

Trace element concentrations are usually range from 1000 and 0.1 µg g^{-1}. Non–invasive analytical techniques are often not sensitive enough to determine and quantify trace element concentrations below 1 µg g^{-1}. This is the case of XRF and NAA (Burger et al., 2017; Liritzis et al., 2020). For this reason, destructive sampling followed by sample digestion and analysis in liquid mode with Inductively Coupled Plasma–Atomic Emission Spectroscopy (ICP–AES) or Inductively Coupled Plasma–Mass Spectrometry (ICP–MS) are often required (Giumlia-Mair, 2005).

As sampling can be difficult in the case of very thin or small objects, or is not permitted by the Superintendence, museum curators, or private owners, other techniques based on nuclear physics can be used as an alternative, such as Ion Beam Analysis (IBA), of which PIXE (Particle Induced X–ray Emission) and PIXE–XRF (Particle Induced X–ray Emission combined with X–Ray Fluorescence) are examples (Guerra et al., 2008a). PIXE is a non–destructive technique that can simultaneously detect several elements (from sodium to uranium) at different concentrations. However, when analysing corroded coins or coins with silver surface enrichment without sample preparation, the accuracy of PIXE decreases (Ben Abdelouahed et al., 2010). Therefore, in the case of cultural heritage, especially in the case of ancient coins in different preservation states, there is a trend towards multi–analytical approach, combining different analytical techniques in order to better understand the sample as a whole.

1.3 Changes over time: corrosion and influence of the burial environment

Ancient coins are metallic specimens; thus, their state of preservation largely depends on the burial environment and the chemical and physical changes they have undergone. Moreover, as Ullén et al. (2004) state, due to technological progress and resulting pollution, the deterioration of metal objects has accelerated over the last 50−100 years, as can be seen in Figure 1. In northern Europe, soil acidification is a serious problem because typically only a thin layer of soil covers non–calcareous bedrock, making the soil very sensitive to acid deposition (Nord et al., 2005). Since the pollution problem is relatively recent, it is irrelevant for assessing the corrosion status of an artefact whether it has been buried in the soil for 300 or 3000 years (Nord, 2002).

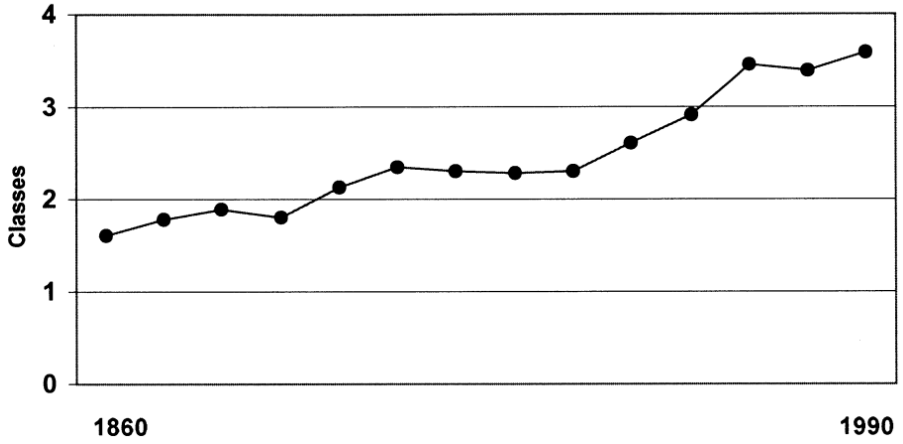

Figure 1. Average degree of deterioration of 2800 prehistoric bronze artefacts found in Sweden, both in graves and in individual finds. Class 1 represents well–preserved objects, while class 4 poorly preserved objects (Ullén et al., 2004).

The features of the burial site of archaeological artefacts are crucial for their preservation: geological and chemical composition, soil grain size, resistivity, humidity, and pH are some of the aspects that must be considered when studying the alteration of ancient objects (Robbiola et al., 1998). Furthermore, another important factor in the deterioration of ancient metal artefacts is the archaeological context, such as graves, settlements, or deposits. In fact, the type of tomb controls the degree of exposure to air and water of the buried objects. As Ullén et al. (2004) attest in their work, specimens from deposits (votive or storage) generally survive in better conditions than those excavated in burials, and this also includes scattered finds.

Climatic factors have the greatest influence on the preservation conditions of ancient coins: direct precipitation (e.g., acid rain or soot), rapid changes in temperature and humidity, as well as gaseous pollutants (e.g., SO_2, NOx, etc.), attack by microorganisms, and exposure to UV radiation endanger these precious objects through physical and chemical attacks (Mottner, 2007).

Therefore, a moderately aerated and moist or acidic and salt–rich soil favour corrosion of metals and alloys (Gerwin and Baumhauer, 2000; Nord et al., 2005). In contrast, a clay–rich sediment that does not allow oxygen and moisture to penetrate is less damaging to the preservation of ancient artefacts. The corrosion layer that forms on the surface of coins is usually inhomogeneous, both in composition and thickness, which can be as thin as 1–2 mm (Volpi et al., 2023).

The composition of the patina depends on the substrate. In the case of copper coins, copper (I) and copper (II) compounds are usually formed depending on the burial site.

Copper tends to oxidise in the presence of oxygen, forming cuprite (1) and tenorite (2), which are red–brown compounds (Pagano et al., 2023):

$$4\ Cu + O_2 \rightleftarrows 2\ Cu_2O\ (cuprite) \quad (1)$$

$$2\ Cu + O_2 \rightleftarrows 2\ CuO\ (tenorite) \quad (2)$$

Once formed, the oxides can react with carbon dioxide, carried by moisture and soil aeration, giving rise to compounds such as malachite (3) and azurite (4) (He et al., 2011):

$$2\ Cu_2O + 2\ H_2O + 2\ CO_2 + O_2 \rightleftarrows 2\ Cu_2(OH)_2CO_3\ (malachite) \quad (3)$$

$$6\ Cu_2O + 4\ H_2O + 8\ CO_2 + 3\ O_2 \rightleftarrows 4\ Cu_3(CO_3)_2(OH)_2\ (azurite) \quad (4)$$

However, what most scares restorers and art scholars is the so–called “bronze disease”. Cuprite, in fact, can react with chlorine in the soil in a humid environment, producing copper chloride (5). Copper chloride exposed to atmospheric humidity cyclically reacts with oxygen and water from atmospheric moisture to form the green coloured atacamite $CuCl_2 \cdot 3Cu(OH)_2$ and hydrochloric acid (6). The latter reacts, in turn, with copper to form new copper chloride (5). In this way, the cycle continues until Cu, O_2 and H_2O are exhausted, defacing the archaeological object (Bozzini et al., 2017; Ingo et al., 2006).

$$Cu_2O + 2\ Cl^- + 2H^+ \rightleftarrows 2CuCl\ (nantokite) + H_2O \quad (5)$$

$$4\ CuCl + 4\ H_2O + O_2 \rightleftarrows CuCl_2 \cdot 3Cu(OH)_2\ (atacamite) + 2\ H^+ + 2\ Cl^- \quad (6)$$

This cycle can be summarised in reaction (7):

$$2\ Cu_2O + 2\ H_2O + 2\ HCl + O_2 \rightleftarrows CuCl_2 \cdot 3Cu(OH)_2\ (bronze\ disease) \quad (7)$$

Atacamite possesses four isomers, which are formed depending on the chemical and physical parameters of the burial site and the structure of the alloy (Bozzini et al., 2017). As bronze corrosion is a cyclic and autocatalytic process, when removing the surface patina from ancient artefacts, care must be taken to avoid exposure to the atmosphere of

active copper chloride compounds that could react with oxygen and water, initiating the bronze cancer cycle (Giannossa et al., 2013).

In the case of silver–copper alloy coins, corrosion is more complicated and depends on both the composition of the alloy and the environmental conditions. Indeed, the phenomenon of Silver Surface Enrichment (SSE) is often observed, due to the electrode potential difference between Ag and Cu. In this process, the copper–rich phase oxidises and tends to form cuprite and tenorite, which are then leached, resulting in preferential Cu depletion and apparent Ag enrichment at the surface (Ager et al., 2016; Hrnjić et al., 2020). The thickness of the silver–enriched phase can reach several hundred microns, well beyond the penetration depth of normal non–destructive analytical techniques. This makes it more difficult to determine the fineness of ancient silver and copper coins (Ager et al., 2013).

In addition to copper and silver oxides, chlorargyrite is often found as a corrosion product of Ag–Cu alloys according to the reaction (8). This product, also known as "horn silver", is a typically porous and brittle black, grey, purple, or brown deposit (Ingo et al., 2018):

$$4\,Ag + O_2 + 4\,HCl \rightleftarrows 4\,AgCl\ (chlorargyrite) + 2\,H_2O \qquad (8)$$

On the other hand, if the artefact is in the presence of sulphur, an element closely linked to air pollution, acanthite can be formed (Fabrizi et al., 2019), as shown in reaction (9):

$$4\,Ag + O_2 + 2\,H_2S \rightleftarrows 2\,Ag_2S\ (acanthite) + 2\,H_2O \qquad (9)$$

Chlorargyrite can also be formed by reaction with copper (II) ions in the presence of oxygen and water (Martins and Martins, 2011). However, chlorine also partially reacts with copper, producing CuCl and $CuCl_2 \cdot 3Cu(OH)_2$ and its polymorphs, which are linked to "bronze disease" (Ingo et al., 2018) (10).

$$Cu^{2+} + 2\,Cl^- + Ag \rightleftarrows AgCl + CuCl \qquad (10)$$

To summarise the various processes that can occur on silver–copper alloy artefacts, consider the diagram presented in the work of Doménech et al. (2012) as an example

(Figure 2). They studied the corrosion products of copper and silver in coins from medieval Spain using the Voltammetry of IMmobilized Particles technique (VIMP).

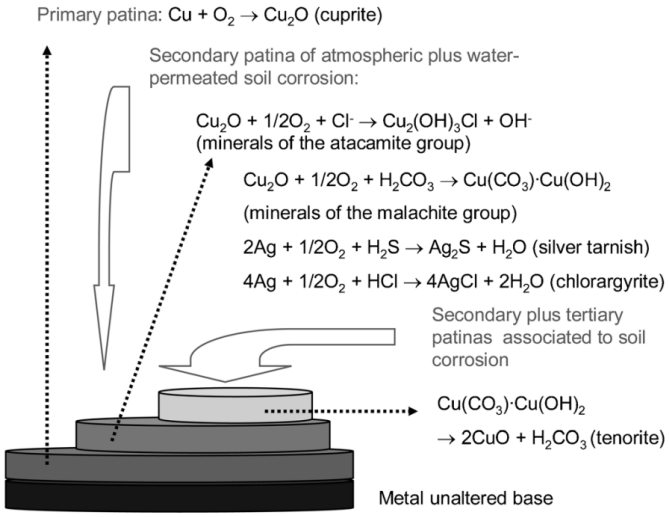

Figure 2: The main corrosion processes and corrosion products occurring on antique copper–silver alloy artefacts (Doménech et al., 2012).

Although complicated, the study of the corrosion layer in ancient coins provides important data on the burial site and the deterioration mechanisms that occurred or are still occurring. Furthermore, this information can help identify counterfeit coins with artificially grown patina (Salem and Mohamed, 2019). For this reason, in order to obtain this information, it would be better not to clean the coins, a procedure that is unfortunately often performed in numismatics.

2. Aim of the thesis

Chemistry was first applied in the field of cultural heritage in the 18th century and has since become an integral part to diagnostic studies and conservation treatments of archaeological materials. It is an interdisciplinary study, involving the collaboration among various specialists, including archaeologists, restorers, conservation scientists, and chemists (Mazzeo, 2017).

The analytical chemists working with cultural heritage choose the analytical instrumentation and approach based on the nature of the object to be analysed. While museum curators and collection owners usually prefer non–destructive techniques for the analysis of ancient artefacts, a combination of non–destructive and micro–destructive techniques used in an integrated manner is necessary for their complete characterization (De Castro and Jurado-López, 2019). This context sets the stage for the present thesis work, where several coin specimens from different historical periods are analysed using various analytical techniques to address questions posed by numismatic historians and the commissioners of the work.

Collectors often treat the surfaces of antique coins to enhance their appearance and lustre. However, this practice typically removes the patina, i.e., the surface layer of the coin altered by the interaction between the metal alloy it is composed and the surrounding environment where it is stored. Therefore, for identifying the burial place of coins, the patina is usually very important. This forms the basis for the work described in Section 1, in which copper folles and a soil sample from the presumed excavation area will be analysed using exclusively non–destructive techniques. A multi–analytical approach will be employed to answer the questions posed by numismatists.

A crucial aspect of archaeometry is the multi–analytical approach, capable of fully characterising an archaeological sample, both in terms of composition and alteration over the centuries. In Section 2, precisely a multi–analytical approach will be used to analyse Late Antique gold solidi. Surface analytical technique (μ–EDXRF) will be combined with micro–destructive techniques investigating the bulk of the coins (ICP–AES and ICP–MS) in order to obtain their overall composition. More sensitive analyses using synchrotron light (SR–XRF and SR–XANES) will be employed to validate the results obtained with the conventional laboratory techniques.

Archaeometric analyses can answer various questions, including the study of devaluation in antiquity, which directly affected the weight of the coin and/or the precious metal content. A notable example is the crisis of the 3rd century, a period in Roman history roughly between 235 and 284 AD, marked by barbarian invasions, secessions, internal unrest, political instability, and the crisis of the traditional economic system. In Section 3, we will use several analytical techniques to assess how the economic crisis manifested in the silver content of the traditional Roman currency, the denarius, and the new currency, the antoninianus, introduced to address the declining value of the denarius.

Finally, the potential of X–Ray Fluorescence in the study of silver Sasanian drachmas will be assessed (Section 4). XRF is undoubtedly the most widely used technique in the field of cultural heritage. In the case of well–preserved coins, although it is a superficial technique, XRF can be employed for semi–quantitative analyses. By means of non–invasive analysis, the fineness of the coins will be determined semi–quantitatively, and any forgeries will be identified. This section will also focus on a group of drachmas issued during the reign of Khosrow II with a particular inscription: chemical analysis will be used to prove historical hypotheses.

3. Sampling and characterization techniques

In the field of cultural heritage, advanced analytical methods and techniques are essential for a better understanding of the objects under examination. Advanced analytical methods enable authenticity studies and contribute to the development of diagnostic techniques for conservation and restoration (Adriaens, 2004). The limitation is that no single analytical technique can fully characterise the sample under investigation. Each case is different, and the choice of technique depends on the question being answered. Obviously, this decision depends on many factors, such as the availability of the instrument, its accessibility, and the cost/benefit analysis. For this reason, before analysing an archaeological find, it is a good idea to optimise the approach by assessing whether it is possible to transport the sample to the laboratory, if sampling is allowed, and what the aim of the analysis is. Depending on these aspects, one can choose a non−destructive rather than a micro−destructive analysis or a qualitative, semi−quantitative, or quantitative approach (Pollard and Bray, 2014).

3.1 Development of the sampling system for micro−destructive analysis

The surface of antique metal artefacts can be modified by several factors, such as oxidation reactions, corrosion processes, intentional alteration of the surface, and cleaning treatments. In addition, the alloy elements of the artefact may spread differently within the artefact over time. This means that the surface composition is no longer representative of the entire sample (Ager et al., 2016). In the case of gold coins, it has been shown that they are stable when well preserved and thus the surface reflects the composition of the original alloy (Cataldo et al., 2022; Green et al., 2021). However, if coins are made of other metals, surface enrichment and/or migration of alloying elements can be observed, resulting in a surface composition significantly different from that of the inner part of the coin.

The most reliable method to ensure that the result obtained from analysis fully represents the alloy prepared in antiquity is for the analyst to remove both surfaces of the coin, leaving a central piece of alloy. However, this approach is too destructive, so a compromise must be found that preserves the integrity of the coin as much as possible while still allowing for a representative and reliable analysis. In 1960, Hall proposed

drilling a small hole (1 mm in diameter) in the coin and analysing the resulting sample using an optical emission spectrometer (Hall, 1960). In 2012, Ponting improved the procedure by removing the sample with a perforation (0.6 mm diameter) in the edge of the coin and penetrating up to 10−15 mm into the bulk. By discarding the material obtained from the first millimetres of perforation, any corrosion or surface enrichment can be excluded from the subsequent examination. Thus, the hole generated does not affect the coin faces, which are often useful for historians and numismatists to date the period and mint of casting. Furthermore, if desired, the hole can be filled and hidden, so that the micro−sampling process is not visible to the naked eye (Butcher and Ponting, 2015; Ponting, 2012).

The material obtained from the micro−sampling can be analysed by Inductively Coupled Plasma−Atomic Emission Spectroscopy or Mass Spectrometry. In this way, it is possible to determine the true fineness of the alloy, the relative proportion of major elements, which provides valuable information on changes in monetary policies, economic trends, and material technology, as well as the presence of trace elements useful for coin authentication (Ager et al., 2016; Salem and Mohamed, 2019).

To date, this micro−sampling system continues to be the gold standard for measuring the original composition of ancient coins, as non−destructive techniques can provide erroneous results, especially in the case of plated coins, as pointed out by Gitler et al. (2008). Recently, Milot et al. (2021) proposed an alternative to drilling, especially for lead: the preliminary removal of the surface patina, followed by etching with abrasive SiC suspended in a solution of H_2O_2 + NH_4OH.

The work carried out during the PhD project involved coins of different alloys, so the method proposed by Ponting was chosen for alloy determination.

3.2 Multi−analytical approach and analytical techniques used

Cultural heritage, including archaeological samples, is heterogeneous and very complex. For this reason, a multi−analytical approach is usually preferred for its analysis, with the combination of different analytical techniques, both non−destructive and micro−invasive. This approach has become essential for understanding completely the material under analysis and the alteration and degradation processes it undergoes. Once this information

is obtained, it becomes easier to choose the most suitable restoration or conservation intervention.

Each case study is unique, so the analytical chemist must choose the most appropriate techniques based on the nature of the investigation and the aims of the work. In the case of ancient metal artefacts, several non−destructive methodologies can be used to preserve the sample's integrity. These include X−Ray Fluorescence (XRF), Scanning Electron Microscopy (SEM−EDS), X−Ray Diffraction (XRD), μ−Raman spectroscopy, and Fourier Transform Infrared Spectroscopy (FTIR).

In the specific case of ancient coins, the multi−analytical approach is useful to better understand the corrosion patterns and chemical composition of the non−corroded metal core (Di Fazio, 2022). In the latter case, it is important to combine non−destructive techniques, often superficial, with micro−invasive techniques necessary to study the bulk. However, since these are samples of high historical and artistic value, if part of the sample is removed, it is crucial to maximise the information while minimising the volume used to obtain it (Adriaens, 2004). Therefore, to optimise the analysis, it is advisable to design multi−analytical paths, starting with the sample preparation step.

In cultural heritage analysis, the complementarity of analytical instrumentation is a key point. Analytical chemists often apply their knowledge to serve historians, archaeologists and art scholars, creating a multidisciplinary community, which is the true strength of Archaeometry (De Castro and Jurado-López, 2019).

3.2.1 Non−destructive techniques

Ancient coins have significant historical value and unique rarity. For this reason, and due to the Italian legislation regarding the preservation of cultural heritage, scholars prefer non−destructive analysis, which maintains the integrity of the sample (Volpi et al., 2023). Therefore, no original material of the sample must be removed, and the object itself must not be modified during the examination (Linke et al., 2003). Moreover, in recent years, thanks to modern technology, portable instruments have become more widespread as they allow analyses on artefacts directly at the preservation site (Adriaens, 2004).

The non−destructive analytical techniques used during the PhD project are outlined below. The theory and applications of μ−EDXRF, SEM−EDX, FTIR−ATR, SR−XRF,

and SR−XANES in cultural heritage will be briefly explained, with particular focus on the study of ancient coins.

3.2.1.1 X−Ray Fluorescence spectroscopy

X−rays were discovered in 1895 by the German physicist W. C. Röntgen (Mould, 1995), but it was only in 1913 that H. G. J. Moseley established the relationship between atomic number and frequency, laying the foundation for identifying elements through the emission of characteristic lines (Min et al., 2014).

It was not until the 1950s that X−Ray Fluorescence began to be systematically used. It took many years to develop an instrument capable of exploiting the phenomenon discovered by Moseley. Moseley himself built the first spectrometer, which used electrons as its X−ray source, but almost 99% of the energy was dissipated as heat. In 1925, Coster and Nishina proposed to replace the incident electron beam with X−photons to induce the emission of the characteristic X−rays (Kim, 2007). Three years later, Glocker and Schreiber (1928) used the XRF spectrometer for quantitative analysis. However, it was only in the 1950s that the first mainly Wavelength−Dispersive XRF spectrometers (WD−XRF), based on Bragg diffraction, were introduced to the market (Guthrie, 2012; Jenkins, 1995).

In the 1970s, the lithium drift detector was developed, leading to Energy−Dispersive XRF spectrometers (ED−XRF), which allow X−photons of different energy to be transformed into electrical pulses of different intensity.

To date, XRF is one of the most widely used techniques in archaeometry, as it usually requires minimal sample preparation, is fast and can detect elements in the ppm range (Jenkins, 1995). In addition, it can be used for solid, liquid, and thin−film samples.

When an atom is irradiated with radiation of appropriate energy and intensity, it creates an electron vacancy − or electron hole − in the innermost orbitals through the photoelectric effect. Starting with the inner most, the orbitals are designated with the letters K, L, M, N, etc., corresponding to the quantum numbers n=1, n=2, n=3, n=4, etc. The atom then enters an unstable excited state, and an electron from an outermost orbital quickly fills this vacancy (10^{-16}–10^{-9} seconds) to return to the initial stable configuration. This electron's de−excitation produces an X−photon with energy equal to the energy difference between the two involved orbitals, resulting in an emission line in the

spectrum. In the literature, emission lines are usually indicated with Siegbahn notation, which includes the shell symbol followed by an alphanumeric index (α1, α2, β, etc.) indicating the exact origin of the transition electron.

Figure 1 illustrates the process of X−Ray Fluorescence. In this process, an incident photon strikes an atom, resulting in the ejection of one of the two electrons present in the K−shell. The vacancy created in the K−shell is then filled by an electron from one of the 3 sub−shells of the L−shell. This transition of electrons releases energy, leading to the emission of a so−called "characteristic photon". When using Siegbahn notation, this particular transition is referred to as Kα1.

Generally, K−lines are more intense than L−lines, which in turn are more intense than M−lines, and this pattern continues for higher electron shells. This hierarchy in intensity is due to the fact that transitions involving inner electron shells (e.g., K−shell) typically release higher−energy X−rays and are, therefore, more intense in XRF spectra compared to transitions involving outer electron shells (e.g., L−shell and M−shell).

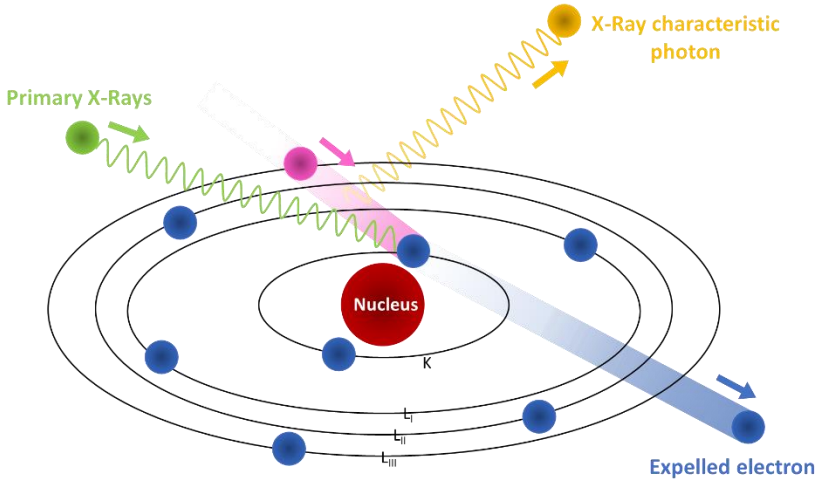

Figure 1: Schematic of characteristic X−ray radiation production at the atomic level.

Not all created holes produce fluorescence photons; there are competitive processes, such as Auger emission, i.e., the release of energy to a third electron − Auger electron − belonging to the outermost shell, which thus successfully leaves the atom. The probability of this phenomenon occurring increases as atomic number (Z) decreases and is exploited in Auger Electron Spectroscopy (AES). Auger emission reduces the number of fluorescence photons compared to the theoretical expected value.

The fluorescence yield *w* is defined as the ratio of fluorescence photons to the initial number of vacancies and is a function of the emitting atom. Experiments have shown that this ratio is always less than one and increases with increasing atomic number. This technique is thus insensitive to light elements (Z<11) due to their very low yield (Fig. 2).

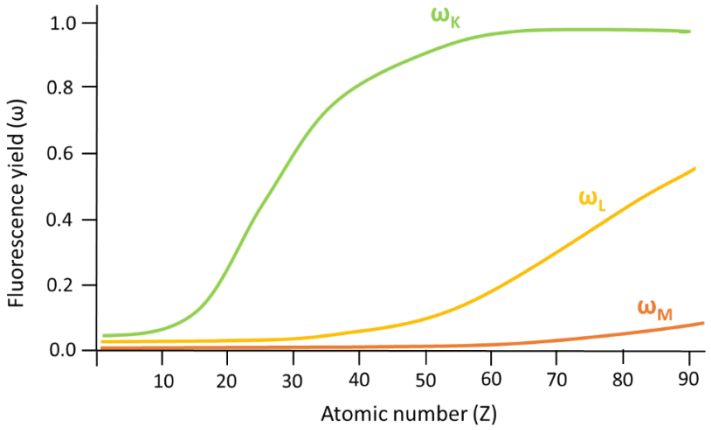

Figure 2: Fluorescence yield for K, L and M electrons.

The basic scheme of all XRF spectrometers includes:

- Primary X−Ray source
- Sample
- Detection system
- Signal amplifier
- Multi−Channel Analyser MCA (analogue/digital converter)
- Data acquisition and processing system

X−rays emitted by the source interact with the sample, placed at a certain distance, resulting in fluorescence emissions, which are collected by the detector. The X−photon energies are then converted into a voltage signal, which is subsequently amplified and converted from analogue to digital. The resulting spectrum represents the intensity of the X−rays (counts or counts per second) as a function of energy (eV) (Figure 3).

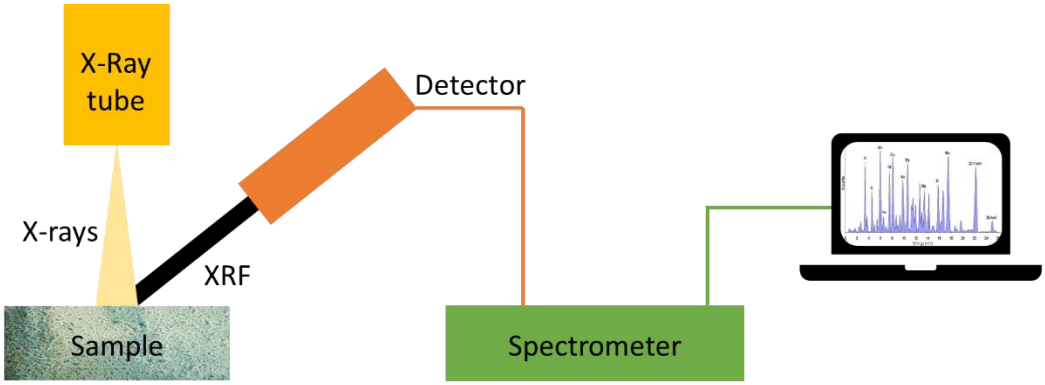

Figure 3: Schematic diagram of an XRF spectrometer.

Two types of XRF spectrometers are usually distinguished based on the detection system:

- ED−XRF, in which the detector − typically a semiconductor crystal, such as Si(Li) − can transform X−photons into electrical pulses proportional to the photon energy. This detector scatters the radiation emitted by the sample into its constituent elements, detecting them simultaneously.
- WD−XRF, in which the detector is a crystal − typically quartz, LiF, PbST or phthalic acid salts − which geometrically scatters the fluorescence radiation, selecting only those X−rays whose wavelength satisfies Bragg's law. Only one wavelength can be detected at a time (Goldstein et al., 2017).

Of the two types of spectrometers, ED−XRFs are more popular because they allow fast analysis, and in recent years, portable instruments with this geometry (p−XRF) have been developed, which are valuable in archaeometry and, in particular, in numismatics (Corsi et al., 2018).

The main limitation of XRF in the study of ancient coins is that it is a superficial technique. As explained in Section 1.3, metal artefacts can undergo corrosion or alteration processes, changing the composition of the surface. Therefore, the surface is no longer representative of the original composition and the XRF analysis does not allow for a quantitative calculation of the main elements of the alloy. Furthermore, if a metal artefact is well preserved and a quantitative analysis of its composition is to be carried out, calibration of the instrument with a Standard or Certified Reference Material (SRM or CRM) is required. For plausible results, the composition of the CRM should closely match the sample's composition, which is challenging due to the variable composition of ancient coins.

3.2.1.2 Secondary Emission Microscopy – Energy Dispersive Spectroscopy

The theory of Scanning Electron Microscopy was developed by M. Knoll (1935). Several groups improved and optimised instruments using secondary electrons during and after the Second World War. The first SEM image was obtained in 1951 by Oatley's group. Since then, commercial production of electron microscopes by the Cambridge Instrument Company began and today there are about a dozen SEM manufacturers worldwide (Egerton, 2016). The SEM technique exploits the emission of secondary and backscattering electrons, and characteristic X−rays of the elements that constitute the sample.

In electron microscopy, a beam of primary electrons is focused on the sample. This interaction produces various signals, i.e., backscattered electrons (BSE), secondary electrons (SE), Auger electrons, Bremsstrahlung X−rays, characteristic X−rays, and visible or UV light emission (cathodoluminescence, CL). Certain electron−matter interactions can also internally alter the sample, such as the generation of phonons (heat) and plasmons (collective electron oscillations) (Inkson, 2016).

SEM uses secondary electrons (SE), which are emitted due to an inelastic interaction, with only those produced near the surface (within a few tens of nm) managing to emerge from the sample and reach the detector. From these electrons, compositional and topographical information is obtained.

Backscattered electrons (BSE) result from the elastic interaction between the electrons in the beam and the nuclei of the atoms in the sample, providing information on atomic number and phase differences of the sample.

Characteristic X−rays allow the identification of the elements in the sample in terms of quantity and distribution.

A Scanning Electron Microscope typically consists of:

- Electron source, which can be a heated tungsten filament or a Field Emission Gun (FEG)
- Column consisting of several lenses, electrostatic or electromagnetic, to focus the beam on the sample
- Sample stage

- Series of detectors that collect signals generated by the interaction between the beam and the sample, which are used to reconstruct images (backscatter detector, secondary electron detector) or to obtain composition information (Energy Dispersive X−ray Analysis or EDX).

The entire system (Figure 4) is in vacuum, so the beam or signals generated do not encounter gas molecules that would interact with, resulting in a noisier image and less accurate analysis.

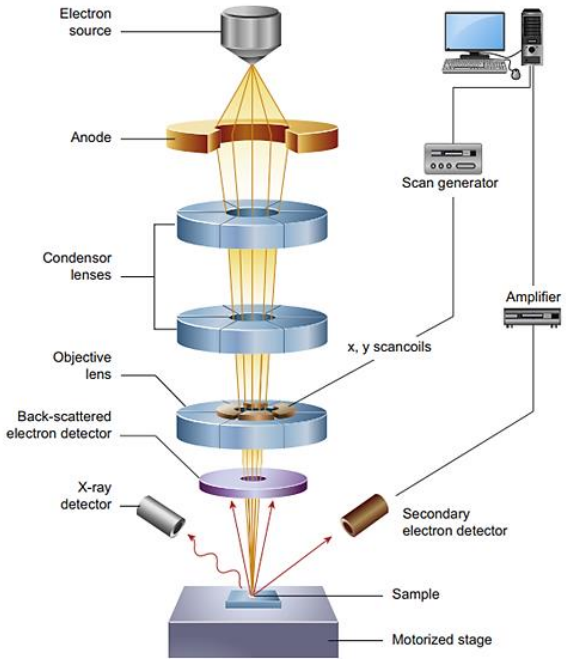

Figure 4: Schematic diagram of the components of an SEM microscope (Inkson, 2016).

Magnification is given by the ratio of the scanning distance in the image to the scanning distance on the sample. The SEM offers a wide range of magnification control, from 10 to 500,000 times, allowing for high spatial resolution and analysis of small sample areas without the need for thinning the sample. This feature has made SEM a valuable tool in archaeometry for analysing various objects such as ceramics, glass, metals, pigments, and polychrome sculptures (Schreiner et al., 2007).

However, SEM−EDX has some disadvantages, such as the detection limit of about 0.1 wt%, depending on atomic number and matrix composition (Linke et al., 2004). An important characteristic of samples subjected to SEM analysis is that they must be

conductive. If they are not, surface metallisation or ultra−high vacuum bombardment with Argon radicals can be used. In addition, they must be free of surface contamination (grease, moisture, dust). Thus, the surface of the samples must be cleaned before analysis, with solvent immersion and ultrasonic agitation (Inkson, 2016).

3.2.1.3 Fourier Transform Infrared Spectroscopy – Attenuated Total Reflection

Infrared (IR) spectroscopy relies on the interaction between radiation and matter. Molecules can absorb radiation at specific frequencies determined by the functional groups involved, i.e., the structure of the molecule. The energy is converted into rotational and vibrational motions, the absorption is quantized and results in a spectrum characterised by vibro−rotational bands with specific wave numbers. The most important types of vibration are stretching and bending, the latter including twisting, rocking, scissoring, and shaking (El-Azazy, 2018).

The advent of IR spectroscopy dates back to the early 1900s, with the recognition of specific and characteristic IR absorptions by chemical functional groups (Coblentz, 1911). The technique gained prominence during Second World War, when it was necessary to characterise synthetic rubber formulations for the war effort. In the early and mid−1940s, the first commercial instruments were introduced to the market by both Beckman and Perkin Elmer. The IR technique was widely used but underwent a significant scientific renaissance with the advent of Fourier Transform IR (FTIR) instruments in the late 1960s and early 1970s (Sommer, 2020).

In the late 1980s, the attenuated total reflection (ATR) sampling system was developed, removing the need for samples to be in the form of thin film less than 10 µm thick. ATR involves bringing the sample into close contact with an Internal Reflection Element (IRE) using a pressure applicator (Sommer, 2020). ATR crystals are typically made of materials like diamond, zinc selenide (ZnSe), germanium (Ge), or silicon (Si), which are transparent to IR and resistant to pressure.

The ATR−FTIR technique is based on the principle of internal reflection: when IR radiation from the spectrometer penetrates the crystal at a critical angle, a total internal reflection occurs, in which a standing wave of radiation, called “evanescent wave”, is generated by the IR light that is totally reflected inside the IRE. Part of the evanescent wave penetrates inside the sample for a few fractions of a micron and is absorbed (or

attenuated) to a small extent. After a few reflections, the attenuation of the IR beam intensity is sufficient to be detected by the spectrophotometer, resulting in an ATR−FTIR spectrum (Fig. 5).

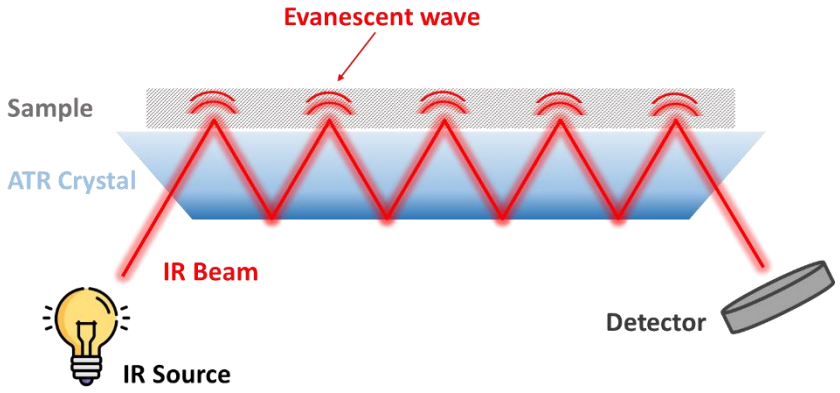

Figure 5: Evanescent wave formation process in an ATR crystal.

An ATR−FTIR spectrophotometer usually comprises:

- IR source
- Michaelson interferometer
- Sample on ATR crystal
- Detector
- Computer

The polychromatic IR radiation emitted by the source reaches a semi−reflecting mirror (beam splitter) which divides it into two beams: one travelling at a fixed distance (fixed mirror) and the other travelling at a variable distance (moving mirror). The beams reflected by these mirrors are then sent one more time to the semi−reflecting mirror, which brings the two beams together and sends them to the sample. Depending on the movement of the moving mirror, all the monochromatic radiation contained in the light emitted by the lamp produces an overall interference signal (interferogram), which contains information about the frequency and intensity of the emitted radiation. Once the signal reaches the detector, thanks to the Fourier transform, the light intensity signal as a function of time is converted into an intensity signal as a function of wave number, resulting in the IR spectrum (Figure 6).

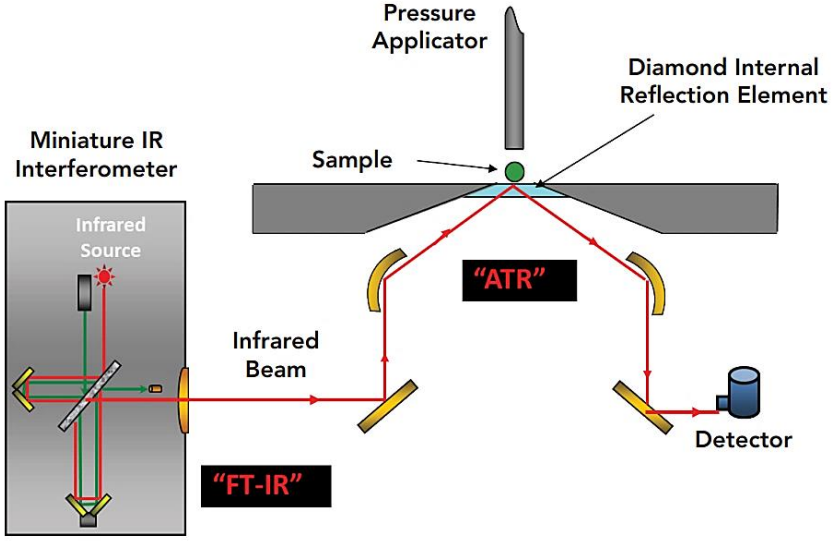

Figure 6: Schematic diagram of an ATR−FTIR spectrometer (Sommer, 2020).

FTIR spectroscopy is widely used in the field of cultural heritage due to its sensitivity and specificity. Moreover, thanks to new imaging devices, it can provide spatial and spectral information simultaneously, allowing for the chemical distribution of the sample in the investigated area. In particular, ATR−FTIR is used to analyse various objects in cultural heritage, including oil paintings, historical paper and polychrome, as well as the patina and corrosion pattern of the surface of ancient coins (Di Fazio et al., 2019). Thus, ATR−FTIR mapping and spectroscopic imaging contribute to solving specific analytical questions and conservation problems (Liu and Kazarian, 2022).

3.2.1.4 Synchrotron Radiation – X−Ray Fluorescence spectroscopy

The synchrotron is derived from the cyclotron, which was invented by E. O. Lawrence in 1930. In the cyclotron, acceleration is achieved by an alternating electric field between two or more electrodes immersed in a constant dipolar magnetic field. In contrast, the synchrotron, invented by E.M. McMillan and V. Veksler in 1945, is a circular and cyclic particle accelerator. In the synchrotron, both the magnetic field (necessary to bend the particle trajectory) and the variable electric field (which accelerates the particles) are synchronised with the particle beam. As the electrons move through the magnetic field, they generate brilliant beam of light called "Synchrotron Radiation" (SR), which ranges from infrared to X−rays and possess extremely useful properties. The first observation of

synchrotron radiation took place in 1947 (Elder et al., 1947) thanks to a first−generation source. Currently, more than 40 third−generation SR sources exist worldwide, which were developed mainly in the 1990s and consist of undulators. These are magnets that force electrons to travel in sinusoidal or spiral trajectories (Iida, 2013).

In 1986, Harbottle et al. first applied SR in Cultural Heritage applications (Harbottle et al., 1986). SR proves useful for all X−ray techniques, although X−ray fluorescence is the predominant method in cultural heritage, particularly in the study of ancient metal artefacts. Combining SR with XRF offers several advantages, such as:

- The use of linearly polarised light, resulting in improved detection limits (ppb);
- The ability to modulate the excitation energy, which can be selected according to the sample being analysed;
- High beam brightness, which enables the focusing of radiation on a precise spot within the sample;
- A higher sensitivity of 10^3 −10^7 compared to laboratory XRF analysis.

Thanks to these characteristics, SR−XRF can be employed for the analysis of material fingerprints to understand their origin and for studying surface degradation/alteration processes. This technique can be applied to trace−level microanalysis of organic materials (e.g., paper, pigments, inks) or silicate−rich materials such as ceramics, porcelain, and glass. In the study of ancient coins, SR−XRF is often useful for authentication studies and determining provenance. This was demonstrated in the case of Dacian gold bracelets studied by Constantinescu et al. (2008), and in the analysis of gold artefacts conducted by Guerra et al. (2008). In these works, SR−XRF played a significant role in determining the provenance of gold through the quantification of Platinum Group Elements (PGE).

However, cultural heritage objects of high historical and artistic value often cannot be moved, and they may not be allowed to cross national borders. Consequently, access to this methodology is limited, as not all countries possess a synchrotron (Radtke et al., 2009). Whenever feasible, SR−XRF is an excellent choice for the analysis of valuable ancient metal artefacts due to its inherent non−destructiveness, high sensitivity, and high spatial resolution. Since ancient materials are typically complex and heterogeneous, SR−XRF is usually used in combination with other synchrotron techniques to obtain a comprehensive insight into the sample (Bertrand et al., 2012).

3.2.1.5 Synchrotron Radiation – X−ray Absorption Near Edge Structure

In addition to XRF, synchrotron radiation can be employed for X−ray Absorption Spectroscopy (XAS). This spectroscopic method requires a high−brightness X−ray source over a broad energy range, which is characteristic of synchrotron light. XAS can be used for the analysis of amorphous or crystalline materials and provides information on oxidation states and chemical speciation in general (Cotte et al., 2010).

X−ray Absorption Spectroscopy (XAS) studies the variation in the absorption coefficient of a substance as a function of the energy of X−ray photons in a narrow region around the absorption threshold. Specifically, this variation occurs because of the absorption of an X−photon, which interacts with an electron in the nucleus. This interaction can promote an electron from a core orbital to an unoccupied electronic state or to the continuum in vacuum. To excite an electron in a specific level of the nucleus, the energy of the photon must be equal to or greater than the binding energy of this core−level electron. The energy of the incident beam can be adjusted to generate an absorption cross−section spectrum, which can be analysed to determine the density of unoccupied states (Jahrman, 2015).

The XAS spectrum is conventionally divided into the X−ray Absorption Near Edge Structure (XANES) region, which extends from pre−threshold to about 50−100 eV after the threshold, and the Extended X−ray Absorption Fine Structure (EXAFS) region, which extends to the end of the spectrum. Specifically, XANES spectroscopy is used to study the local electronic structure and molecular environment of a given atom. This include the oxidation state, coordination number, symmetry, and site distortion (Cotte et al., 2010). In contrast, the EXAFS region provides information about the local geometric structure around the absorption site (Henderson et al., 2014). The first technique is relatively recent. In 1980, A. Bianconi coined the acronym “XANES”, and in 1982, Bianconi himself published the first paper on the application of this technique for determining the local structure in organo−metallic complexes (Bianconi et al., 1982).

XANES experiments can be conducted in air, without the need of sample preparation, and are compatible with several type of samples. This makes it a highly suitable analytical technique for the analysis of cultural heritage. In fact, XAS can be performed on both hard matrix samples such as glass, ceramics, and metals, and soft samples such as bone, wood, paper, or paintings.

In the case of ancient coins, XAS can be employed to study the phenomena of corrosion and degradation of metals, which are often linked to changes in the molecular environment (Cotte et al., 2010). Studies have been conducted on archaeological iron artefacts from the 12th–16th centuries (Reguer et al., 2006), bronze samples from the 3rd millennium BC (De Ryck et al., 2003) and the late 9th century (Northover et al., 2008), as well as gold coins from the 5th century (Carlomagno et al., 2022). In these works, X−ray absorption spectroscopy has provided information on the oxidation state of some elements, which is useful for understanding the production and manufacturing procedures of ancient metal artefacts and the complex changes that affected their surfaces following exposure to the burial environment.

3.2.2 Micro−destructive techniques

In the field of cultural heritage, micro−invasive or micro−sampling techniques are not very common due to the value and rarity of the artefacts. However, in the case of ancient coins, micro−invasive techniques are often necessary to obtain quantitative information on the original alloy preserved in the bulk (Bernabale et al., 2021). Trace elements, that can provide more information about the original ore or the burial site, are also very important. Non−invasive analytical techniques frequently do not have the sensitivity and detection limits required to detect and quantify them accurately.

To optimise the sampling procedure, all steps should be considered, from sample preparation (removal, storage, and transport) to analysis and processing of results. This maximises the representativeness and reproducibility of the results (Adriaens, 2004).

The theory exploited by the analytical techniques used during the PhD project, such as ICP−AES and ICP−MS, will be briefly discussed below.

3.2.2.1 Inductively Coupled Plasma – Atomic Emission Spectroscopy

The first instruments that utilised plasma as a source of atomic excitation were developed in the mid−1960s (Greenfield et al., 1964). However, in these early instruments, the plasma was generated using direct current or induced by microwaves, which made it very unstable. Starting from 1973, ICP−AES spectrometers gained popularity and market acceptance due to their notable features such as low detection limits, the capability to

detect multiple elements simultaneously, reduced interference, and an exceptionally safe operation (Boss and Fredeen, 1997).

As the name suggests, Inductively Coupled Plasma−Atomic Emission Spectroscopy (ICP−AES, sometimes referred to as ICP−OES, Inductively Coupled Plasma−Optical Emission Spectroscopy) is an emission spectrophotometric technique, meaning it relies on the principle of atomic emission. When an atom absorbs energy, such as heat, one of its electrons can move to a higher energy level, resulting in the atom being in an excited metastable state. To return to its fundamental state, the atom emits electromagnetic radiation with a characteristic energy level, determined by the quantized energy level structure specific to each type of atom, according to Planck's equation (Figure 7).

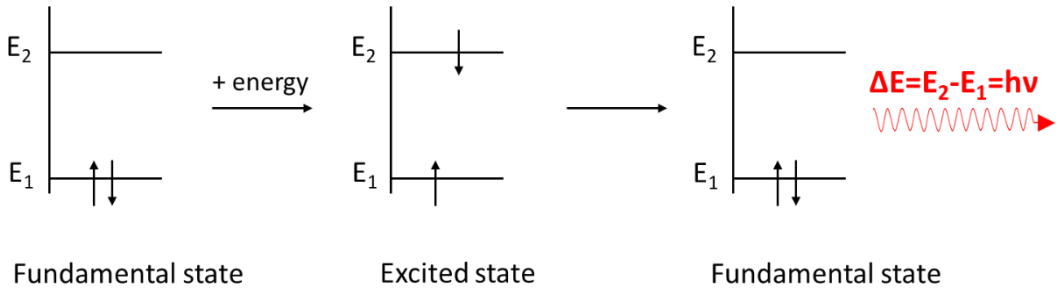

Figure 7: Atomic excitation and emission processes.

Since the transitions resulting from excitation are specific to each atom, it becomes possible to identify the atoms that constitute the sample under analysis based on the emitted wavelengths. Furthermore, the intensity of the energy emitted at the chosen wavelength for a given element is proportional to the number (concentration) of atoms of that element present in the sample.

In ICP−AES spectrometers, sample atomisation and excitation occur through the use of plasma, an ionised and overall neutral gas composed of ions and electrons. It is generated by a quartz torch and maintained in a stable state by an oscillating magnetic field generated by a radio frequency coil placed around the quartz torch. Typically, argon gas is used for the plasma, as it is an inert gas that hinders the formation of oxides and nitrides. The plasma can reach temperatures of up to 10,000 K, significantly enhancing the excitation yield of atoms (>90%) for more than 60 elements, as well as preventing the formation of polyatomic species (Dunnivant and Ginsbach, 2009).

The typical components of an ICP−AES spectrometer include:

- Autosampler
- Injection system
- Nebuliser
- ICP torch
- Monochromator
- Detector
- Computerised control system for signal processing and data acquisition.

The sample solution is introduced into the nebuliser using a peristaltic pump. The small nebuliser opening, coupled with the flow of argon, generates small sample droplets that are directed into the nebulisation chamber. Larger sample droplets collect on the chamber's walls and are removed via a drain, while the smaller particles (approximately 8 µm in diameter) are carried by the Ar flow and reach the torch. In the high−temperature plasma, the solvent evaporates, leading to atomisation and excitation of the sample. Subsequently, when the excited atoms leave the hot region of the plasma, they emit photons characteristic of their electronic transition. The emitted radiation is then dispersed by a monochromator, and the wavelengths are analysed by a detector, producing an electrical signal proportional to the intensity of the emitted electromagnetic radiation. This signal is further processed by the data processing system, typically resulting in a concentration value (Figure 8) (Hou et al., 2016).

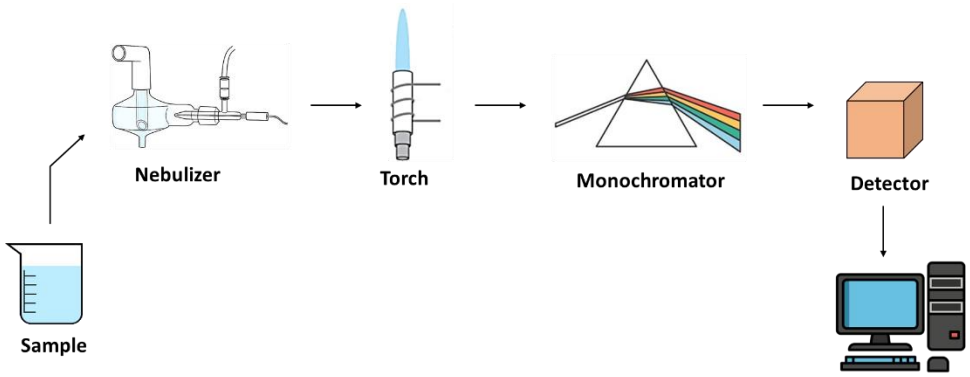

Figure 8: Schematic diagram of ICP−AES spectrometer.

The most recent generation of ICP−AES spectrometers uses a dual monochromator setup in series to enhance both resolution and optical performance. This arrangement, depicted in Figure 9, involves a prism that selectivity permits only a specific section of the spectrum containing the analyte's wavelength to pass through to an intermediate slit. This intermediate slit aligns with both the output slit of the prism and the input slit of the high−resolution Echelle monochromator. The latter monochromator is capable of dispersing the narrow spectral region that has been selected into individual wavelengths (Olesik, 1999).

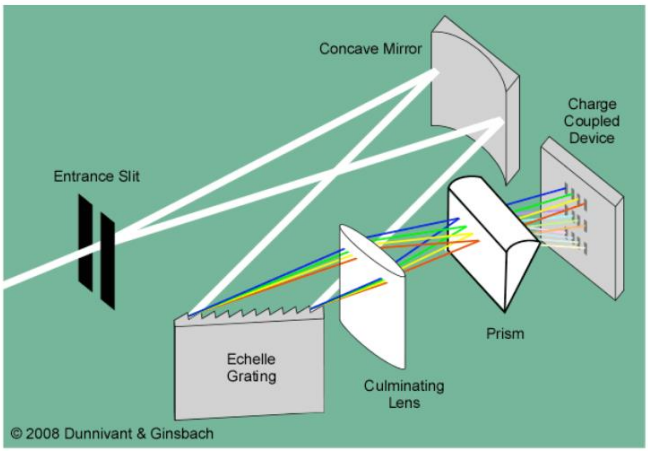

Figure 9: The multiple monochromator system in ICP−AES instruments (Dunnivant and Ginsbach, 2009).

One of the primary challenges encountered when using ICP−AES spectrometers in the field of cultural heritage is their requirement for samples to be in liquid form. Therefore, for solid matrices like ancient coins, a sampling and mineralisation step is necessary before the sample can be introduced into the instrument. Nevertheless, the ICP−AES technique remains highly sensitive, allowing for the determination of elemental composition down to concentrations at the order of part per billion (ppb), thereby making it a valuable tool for studies on the provenance of ancient metals.

3.2.2.2 Inductively Coupled Plasma – Mass Spectrometry

The first ICP−MS spectrometer was introduced in America in the 1980s by Houk et al. (1980), and in the UK by Grey and Date (1983). However, it was not until the development of the collision/reaction cell in the early 2000s that it became one of the

most important techniques for detecting over 70% of the elements in the periodic table (Chan and Caruso, 2012). Today, ICP−MS is an established technique for multi−element trace and ultra−trace analysis, and also for the determination of isotope ratios. It has several advantages, including sub−ppt (parts per trillion) detection limits (Nham, 1998), speed of analysis, and a large number of possible applications (Bulska and Wagner, 2016). An ICP−MS spectrometer usually consists of six basic compartments:

- Sample introduction
- ICP
- Interface
- Ion optics
- Mass analyser
- Detector

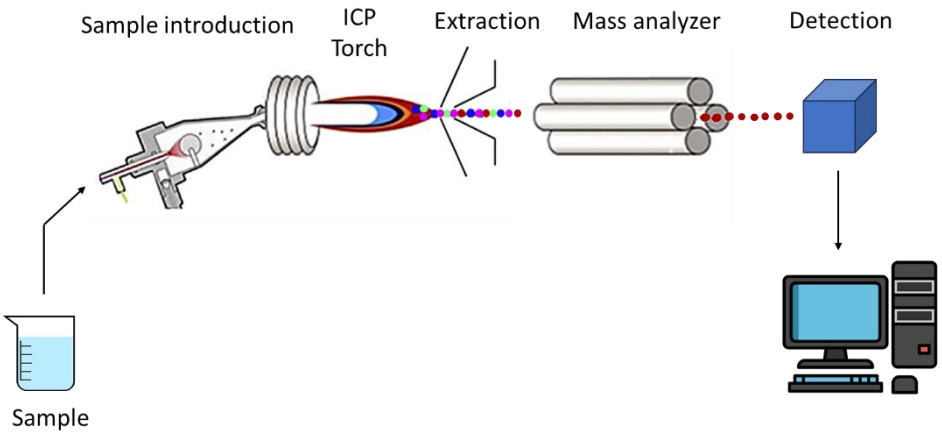

Figure 10: Schematic diagram of an ICP−MS spectrometer.

The ICP−MS instrumentation has the same sample introduction system and torch as the ICP−AES (see Chapter 3.2.2.1), with the difference that in most ICP−MS instruments, the torch is rotated by 90°. In these instruments, the ICP functions as both an atomiser and an ioniser. The ions formed in the plasma are then extracted through the interface region and introduced into electrostatic lenses, also known as “ion optics”. These lenses focus and guide the ions toward the mass analyser, which separates them according to their mass−to−charge ratio (m/z) and detects them via the detector. This is usually an

electron multiplier (EM), which converts the current of ions leaving the analyser into an electric current proportional to the abundance of the ions (Fig.10).

One of the most delicate parts of the ICP−MS setup is the interface region. Its role is to ensure that a statistically significant fraction of the ions produced is transported from the plasma − which works at atmospheric pressure (760 Torr) − to the mass analyser region − which operates in high vacuum (10^{-6} Torr). The interface consists of two coaxial cones of nickel or platinum: the first, in contact with the plasma (sampler cone), has an orifice of 0.8−1.2 mm in diameter, while the second (skimmer cone; 0.4−0.8 mm i.d.), is the one from which the ions will be extracted to the mass analyser. In some new mass spectrometers, in addition to the sampling cone and the skimmer cone, there is a third cone − hyper skimmer − by means of which the pressure is gradually decreased, ensuring less dispersion of the ions and preventing sample deposition on internal surfaces (Thomas, 2001).

Several mass analysers can be coupled to the ICP, depending on the type of analysis to be conducted. These include the magnetic sector, ion trap, time−of−flight, but the most common is definitely the quadrupole. Many modern ICP−MS are equipped with a triple quadrupole, which maximises the sensitivity for each element in each run. In this configuration, the first and third quadrupoles act as mass filters, while the central quadrupole, filled with an inert gas, acts as a collision cell to eliminate polyatomic interference.

Similar to ICP−AES spectrometers, ICP−MS spectrometers also operate in the liquid phase. Therefore, an initial sampling and solubilisation step are required for solid samples. Thanks to Gray (1985), who first developed them, ICP−MS spectrometers coupled to laser ablation have become established in recent years and are very useful in the field of cultural heritage. They do not require sample preparation but do result in a minor depletion of the sample. For quantitative analysis, appropriate matrix CRMs are required, and these can sometimes be challenging to find within the cultural heritage field (Giussani et al., 2009).

References

Adriaens, A., 2004. European actions to promote and coordinate the use of analytical techniques for cultural heritage studies. TrAC Trends in Analytical Chemistry 23, 583–586. https://doi.org/10.1016/j.trac.2004.07.001

Ager, F.J., Gómez-Tubío, B., Paúl, A., Gómez-Morón, A., Scrivano, S., Ortega-Feliu, I., Respaldiza, M.A., 2016. Combining XRF and GRT for the analysis of ancient silver coins. Microchemical Journal 126, 149–154. https://doi.org/10.1016/j.microc.2015.12.017

Ager, F.J., Moreno-Suárez, A.I., Scrivano, S., Ortega-Feliu, I., Gómez-Tubío, B., Respaldiza, M.A., 2013. Silver surface enrichment in ancient coins studied by micro-PIXE. Nuclear Instruments and Methods in Physics Research Section B: Beam Interactions with Materials and Atoms 306, 241–244. https://doi.org/10.1016/j.nimb.2012.12.037

Ben Abdelouahed, H., Gharbi, F., Roumié, M., Baccouche, S., Romdhane, K.B., Nsouli, B., Trabelsi, A., 2010. PIXE analysis of medieval silver coins. Materials Characterization 61, 59–64. https://doi.org/10.1016/j.matchar.2009.10.008

Bernabale, M., Nigro, L., Montanari, D., De Vito, C., 2021. Exploring the chemical composition and corrosion patterns of arrowheads used in the Siege of Motya (397 BC) through a multi-analytical approach. Journal of Cultural Heritage 52, 146–152. https://doi.org/10.1016/j.culher.2021.10.001

Bertrand, L., Cotte, M., Stampanoni, M., Thoury, M., Marone, F., Schöder, S., 2012. Development and trends in synchrotron studies of ancient and historical materials. Physics Reports 519, 51–96. https://doi.org/10.1016/j.physrep.2012.03.003

Bianconi, A., Dell'Ariccia, M., Durham, P.J., Pendry, J.B., 1982. Multiple-scattering resonances and structural effects in the x-ray-absorption near-edge spectra of Fe II and Fe III hexacyanide complexes. Physical Review B 26, 6502–6508. https://doi.org/10.1103/PhysRevB.26.6502

Blet-Lemarquand, M., Nieto-Pelletier, S., Téreygeol, F., Suspène, A., 2015. Are Platinum and Palladium Relevant Tracers for Ancient Gold Coins? Archaeometallurgical and Archaeometric Data to Study an Antique Numismatic Problem. Presented at the International Conference Archaeometallurgy in Europe IV, Madrid, pp. 19–28.

Boss, C.B., Fredeen, K.J., 1997. Concepts, Instrumentation and Techniques in Inductively Coupled Plasma Optical Emission Spectrometry. Perkin Elmer Corp.

Bozzini, B., Alemán, B., Amati, M., Boniardi, M., Caramia, V., Giovannelli, G., Gregoratti, L., Kazemian Abyaneh, M., 2017. Novel insight into bronze disease

gained by synchrotron-based photoelectron spectro-microscopy, in support of electrochemical treatment strategies. Studies in Conservation 62, 465–473. https://doi.org/10.1080/00393630.2016.1235339

Bulska, E., Wagner, B., 2016. Quantitative aspects of inductively coupled plasma mass spectrometry. Philosophical Transactions of the Royal Society A 374, 20150369. https://doi.org/10.1098/rsta.2015.0369

Burger, M., Glaus, R., Hubert, V., Van Willigen, S., Wörle-Soares, M., Convertini, F., Lefranc, P., Nielsen, E., Günther, D., 2017. Novel sampling techniques for trace element quantification in ancient copper artifacts using laser ablation inductively coupled plasma mass spectrometry. Journal of Archaeological Science 82, 62–71. https://doi.org/10.1016/j.jas.2017.04.009

Butcher, K., Ponting, M., 2015. The metallurgy of Roman silver coinage: from the reforms of Nero to the reform of Trajan. Cambridge University Press.

Campanella, L., Laganà, A., Pronti, L., 2011. Le indagini sui beni culturali: conoscenza, degrado e conservazione. La Chimica & L'Industria 96–100.

Carlomagno, I., Zeller, P., Amati, M., Aquilanti, G., Prenesti, E., Marussi, G., Crosera, M., Adami, G., 2022. Combining synchrotron radiation techniques for the analysis of gold coins from the Roman Empire. Scientific Reports 12, 15919. https://doi.org/10.1038/s41598-022-19682-8

Cataldo, M., Clemenza, M., Ishida, K., Hillier, A.D., 2022. A Novel Non-Destructive Technique for Cultural Heritage: Depth Profiling and Elemental Analysis Underneath the Surface with Negative Muons. Applied Sciences 12, 4237. https://doi.org/10.3390/app12094237

Chan, Q., Caruso, J.A., 2012. Plasma-Based Gas Chromatography Detectors, in: Gas Chromatography. Elsevier, pp. 355–373. https://doi.org/10.1016/B978-0-12-385540-4.00014-6

Charalambous, A., 2015. Analytical methods for the determination of the chemical composition of ancient coins [WWW Document]. Kyprios Character. History, Archaeology & Numismatics of Ancient Cyprus. URL kyprioscharacter.eie.gr/en/t/AQ (accessed 8.18.23).

Coblentz, W.W., 1911. The Reflecting Power of Various Metals. U.S. Department of Commerce and Labor, Bureau of Standards.

Colombini, M.P., 2011. Focus on analytical chemistry to illuminate the past. Analytical and Bioanalytical Chemistry 401, 1725–1726. https://doi.org/10.1007/s00216-011-5271-1

Constantinescu, B., Bugoi, R., Cojocaru, V., Radtke, M., Calligaro, T., Salomon, J., Pichon, L., Röhrs, S., Ceccato, D., Oberländer-Târnoveanu, E., 2008. Micro-SR-XRF and micro-PIXE studies for archaeological gold identification – The case of Carpathian (Transylvanian) gold and of Dacian bracelets. Nuclear Instruments and Methods in Physics Research Section B: Beam Interactions with Materials and Atoms 266, 2325–2328. https://doi.org/10.1016/j.nimb.2008.03.054

Corsi, J., Lo Giudice, A., Re, A., Agostino, A., Barello, F., 2018. Potentialities of X-ray fluorescence analysis in numismatics: the case study of pre-Roman coins from Cisalpine Gaul. Archaeological and Anthropological Sciences 10, 431–438. https://doi.org/10.1007/s12520-016-0371-7

Cotte, M., Susini, J., Dik, J., Janssens, K., 2010. Synchrotron-Based X-ray Absorption Spectroscopy for Art Conservation: Looking Back and Looking Forward. Accounts of Chemical Research 43, 705–714. https://doi.org/10.1021/ar900199m

De Castro, M.D.L., Jurado-López, A., 2019. The role of analytical chemists in the research on the cultural heritage. Talanta 205, 120106. https://doi.org/10.1016/j.talanta.2019.07.001

De Ryck, I., Adriaens, A., Pantos, E., Adams, F., 2003. A comparison of microbeam techniques for the analysis of corroded ancient bronze objects. Analyst 128, 1104. https://doi.org/10.1039/b303588c

Di Fazio, M., 2022. Multi-analytical approach for an archaeometric study on orichalcum coins. Rendiconti Online Della Società Geologica Italiana 56, 2–10. https://doi.org/10.3301/ROL.2022.01

Di Fazio, M., Felici, A.C., Catalli, F., Doménech-Carbò, A., Doménech-Carbó, M.T., De Vito, C., 2019. Roman orichalcum coins: a deep investigation from patina to core, in: Il Tempo Del Pianeta Terra e Il Tempo Dell'uomo: Le Geoscienze Fra Passato e Futuro. Presented at the SIMP-SGI-SOGEI 2019, Parma, p. 167.

Doménech, A., Doménech-Carbó, M.T., Pasies, T., del Carmen Bouzas, M., 2012. Modeling Corrosion of Archaeological Silver-Copper Coins Using the Voltammetry of Immobilized Particles. Electroanalysis 24, 1945–1955. https://doi.org/10.1002/elan.201200252

Dube, R., 2006. Interrelation between gold and tin: A historical perspective. Gold Bulletin 39, 103–113. https://doi.org/10.1007/BF03215537

Dunnivant, F.M., Ginsbach, J.W., 2009. Inductively Coupled Plasma—Atomic Emission Spectrometry [WWW Document]. http://people.whitman.edu/. URL http://people.whitman.edu/~dunnivfm/FAASICPMS_Ebook/CH3/3_1.html (accessed 9.25.23).

Egerton, R.F., 2016. An Introduction to Microscopy, in: Physical Principles of Electron Microscopy. Springer International Publishing, Switzerland, pp. 1–26. https://doi.org/10.1007/978-3-319-39877-8_1

El-Azazy, M., 2018. Introductory Chapter: Infrared Spectroscopy - A Synopsis of the Fundamentals and Applications, in: Infrared Spectroscopy - Principles, Advances, and Applications. IntechOpen. https://doi.org/10.5772/intechopen.82210

Elder, F.R., Gurewitsch, A.M., Langmuir, R.V., Pollock, H.C., 1947. Radiation from Electrons in a Synchrotron. Physical Review 71, 829–830. https://doi.org/10.1103/PhysRev.71.829.5

Fabrizi, L., Di Turo, F., Medeghini, L., Di Fazio, M., Catalli, F., De Vito, C., 2019. The application of non-destructive techniques for the study of corrosion patinas of ten Roman silver coins: The case of the medieval Grosso Romanino. Microchemical Journal 145, 419–427. https://doi.org/10.1016/j.microc.2018.10.056

Flament, C., Marchetti, P., 2004. Analysis of ancient silver coins. Nuclear Instruments and Methods in Physics Research B 226, 179–184. https:// 10.1016/j.nimb.2004.03.078

George, N.E., 2019. The Manufacture of Official Roman Silver Coinage and Blanks Between AD193 and AD270 (Thesis (Doctoral)). University of Liverpool.

Gerwin, W., Baumhauer, R., 2000. Effect of soil parameters on the corrosion of archaeological metal finds. Geoderma 96, 63–80. https://doi.org/10.1016/S0016-7061(00)00004-5

Giannossa, L.C., Loperfido, S., Caggese, M., Benedetto, G.E.D., Laviano, R., Sabbatini, L., Mangone, A., 2013. A systematic characterization of fibulae from Italy: from chemical composition to microstructure and corrosion processes. New Journal of Chemistry 37, 1238–1251. https://doi.org/10.1039/C2NJ40362E

Gitler, H., Ponting, M., Tal, O., 2008. Metallurgical Analysis of Southern Palestinian Coins of the Persian Period. Israel Numismatic Research 13–27.

Giumlia-Mair, A., 2005. Copper and copper alloys in the South Eastern Alps: an overview. Archaeometry 47, 275–292. https://doi.org/10.1111/j.1475-4754.2005.00202.x

Giussani, B., Monticelli, D., Rampazzi, L., 2009. Role of laser ablation–inductively coupled plasma–mass spectrometry in cultural heritage research: A review. Analytica Chimica Acta 635, 6–21. https://doi.org/10.1016/j.aca.2008.12.040

Glocker, R., Schreiber, H., 1928. Quantitative Röntgenspektralanalyse mit Kalterregung des Spektrums. Annalen der Physik 390, 1089–1102. https://doi.org/10.1002/andp.19283900805

Goldstein, J.I., Newbury, D.E., Michael, J.R., Ritchie, N.W.M., Scott, J.H.J., Joy, D.C., 2017. Scanning Electron Microscopy and X-Ray Microanalysis. Springer.

Gray, A.L., 1985. Solid sample introduction by laser ablation for inductively coupled plasma source mass spectrometry. Analyst 110, 551–556. https://doi.org/10.1039/AN9851000551

Gray, A.L., Date, A.R., 1983. Plasma source mass spectrometry of inorganic samples - recent developments of the technique. International Journal of Mass Spectrometry and Ion Physics 46, 7–10. https://doi.org/10.1016/0020-7381(83)80039-4

Green, G.A., Ishida, K., Hampshire, B.V., Butcher, K., Pollard, A.M., Hillier, A.D., 2021. Understanding Roman Gold Coinage Inside Out. Journal of Archaeological Science 134, 105470. https://doi.org/10.1016/j.jas.2021.105470

Greenfield, S., Jones, I.Ll., Berry, C.T., 1964. High-pressure plasmas as spectroscopic emission sources. Analyst 89, 713. https://doi.org/10.1039/an9648900713

Guerra, M.F., 2005. Trace elements fingerprinting using accelerators and ICP-MS: circulation of gold from the 6th century BC to the 12th century BC, in: Cultural Heritage Conservation and Environmental Impact Assessment by Non-Destructive Testing and Micro-Analysis. Balkema, London, pp. 223–244.

Guerra, M.F., 2004. The circulation of South American precious metals in Brazil at the end of the 17th century. Journal of Archaeological Science 31, 1225–1236. https://doi.org/10.1016/j.jas.2004.03.018

Guerra, M.F., Calligaro, T., 2004. Gold traces to trace gold. Journal of Archaeological Science 31, 1199–1208. https://doi.org/10.1016/j.jas.2002.05.001

Guerra, M.F., Radtke, M., Reiche, I., Riesemeier, H., Strub, E., 2008a. Analysis of trace elements in gold alloys by SR-XRF at high energy at the BAMline. Nuclear Instruments and Methods in Physics Research B 266, 2334–2338. https://doi.org/10.1016/j.nimb.2008.03.008

Guerra, M.F., Radtke, M., Reiche, I., Riesemeier, H., Strub, E., 2008b. Analysis of trace elements in gold alloys by SR-XRF at high energy at the BAMline. Nuclear Instruments and Methods in Physics Research Section B: Beam Interactions with Materials and Atoms 266, 2334–2338. https://doi.org/10.1016/j.nimb.2008.03.008

Guthrie, J.M., 2012. XRF Technical Overview, University of Missouri Research Reactor [WWW Document]. URL https://archaeometry.missouri.edu/xrf_technical.html (accessed 8.29.23).

Hall, E.T., 1960. X-Ray Fluorescent Analysis Applied to Archaeology. Archaeometry 3, 29–35. https://doi.org/10.1111/j.1475-4754.1960.tb00514.x

Harbottle, G., Gordon, B.M., Jones, K.W., 1986. Use of synchrotron radiation in archaeometry. Nuclear Instruments and Methods in Physics Research Section B: Beam Interactions with Materials and Atoms 14, 116–122. https://doi.org/10.1016/0168-583X(86)90431-3

Haschke, M., 2014. Laboratory Micro-X-Ray Fluorescence Spectroscopy: Instrumentation and Applications, Springer Series in Surface Sciences. Springer International Publishing, Cham. https://doi.org/10.1007/978-3-319-04864-2

He, L., Liang, J., Zhao, X., Jiang, B., 2011. Corrosion behavior and morphological features of archeological bronze coins from ancient China. Microchemical Journal 99, 203–212. https://doi.org/10.1016/j.microc.2011.05.009

Henderson, G.S., De Groot, F.M.F., Moulton, B.J.A., 2014. X-ray Absorption Near-Edge Structure (XANES) Spectroscopy. Reviews in Mineralogy and Geochemistry 78, 75–138. https://doi.org/10.2138/rmg.2014.78.3

Hou, X., Amais, R.S., Jones, B.T., Donati, G.L., 2016. Inductively Coupled Plasma Optical Emission Spectrometry, in: Meyers, R.A. (Ed.), Encyclopedia of Analytical Chemistry. Wiley, pp. 1–25. https://doi.org/10.1002/9780470027318.a5110.pub3

Houk, R.S., Fassel, V.A., Flesch, G.D., Svec, H.J., Gray, A.L., Taylor, C.E., 1980. Inductively coupled argon plasma as an ion source for mass spectrometric determination of trace elements. Analytical Chemistry 52, 2283–2289. https://doi.org/10.1021/ac50064a012

Hrnjić, M., Hagen-Peter, G.A., Birch, T., Barfod, G.H., Sindbæk, S.M., Lesher, C.E., 2020. Non-destructive identification of surface enrichment and trace element fractionation in ancient silver coins. Nuclear Instruments and Methods in Physics Research Section B: Beam Interactions with Materials and Atoms 478, 11–20. https://doi.org/10.1016/j.nimb.2020.05.019

Hrnjic, M., Röhrs, S., Denker, A., Weisser, B., Stoess, C., Matosz, M., del Hoyo-Meléndez, J.M., 2021. Multi-technical study of silver denars from medieval Poland for an improved understanding of their archaeological context and provenance. Archaeometry 63, 609–626. https://doi.org/10.1111/arcm.12624

Iida, A., 2013. Synchrotron Radiation X-Ray Fluorescence Spectrometry, in: Meyers, R.A. (Ed.), Encyclopedia of Analytical Chemistry. John Wiley & Sons, Ltd., pp. 1–23. https://doi.org/10.1002/9780470027318.a9329

Ingo, G.M., De Caro, T., Riccucci, C., Angelini, E., Grassini, S., Balbi, S., Bernardini, P., Salvi, D., Bousselmi, L., Çilingiroglu, A., Gener, M., Gouda, V.K., Al Jarrah, O., Khosroff, S., Mahdjoub, Z., Al Saad, Z., El-Saddik, W., Vassiliou, P., 2006. Large scale investigation of chemical composition, structure and corrosion mechanism

of bronze archeological artefacts from Mediterranean basin. Applied Physics A 83, 513–520. https://doi.org/10.1007/s00339-006-3550-z

Ingo, G.M., Riccucci, C., Pascucci, M., Messina, E., Giuliani, C., Fierro, G., Di Carlo, G., 2018. Integrated analytical methodologies for the study of the corrosion products naturally grown on Roman Ag-based artefacts. Applied Surface Science 446, 279–286. https://doi.org/10.1016/j.apsusc.2017.11.066

Inkson, B.J., 2016. Scanning electron microscopy (SEM) and transmission electron microscopy (TEM) for materials characterization, in: Materials Characterization Using Nondestructive Evaluation (NDE) Methods. Elsevier, pp. 17–43. https://doi.org/10.1016/B978-0-08-100040-3.00002-X

Jahrman E., 2015. Xray Absorption Near Edge Spectroscopy- XANES - Clean Energy Institute, University of Washington [WWW Document]. https://www.cei.washington.edu/. URL https://www.cei.washington.edu/education/science-of-solar/xray-absorption-near-edge-spectroscopy-xanes/ (accessed 9.15.23).

Jenkins, R., 1995. Quantitative X-Ray Spectrometry, Second Edition, CRC Press.

Kim, D.-W., 2007. Yoshio Nishina: Father of Modern Physics in Japan. CRC Press.

Klaproth, M.H., 1798. Memoires de l'academie (royale) des sciences et belles-lettres de Toulouse. Presented at the Classe de philosophie experimentale, pp. 97–113.

Knoll, M., 1935. Auftadepotential und Sekundäremission elektronenbestrahlter Körper. Zeitschrift für technische Physik 16, 467.

Linke, R., Schreiner, M., Demortier, G., 2004. The application of photon, electron and proton induced X-ray analysis for the identification and characterisation of medieval silver coins. Nuclear Instruments and Methods in Physics Research Section B: Beam Interactions with Materials and Atoms 226, 172–178. https://doi.org/10.1016/j.nimb.2004.03.084

Linke, R., Schreiner, M., Demortier, G., Alram, M., 2003. Determination of the provenance of medieval silver coins: potential and limitations of x-ray analysis using photons, electrons or protons. X-Ray Spectrometry 32, 373–380. https://doi.org/10.1002/xrs.654

Linke, Robert, Sehreiner, M., Demortier, G., Alram, M., Winter, H., 2004. Chapter 13 The provenance of medieval silver coins: analysis with EDXRF, SEM/EDX and PIXE, in: Comprehensive Analytical Chemistry. Elsevier, pp. 605–633. https://doi.org/10.1016/S0166-526X(04)80017-5

Liritzis, I., Laskaris, N., Vafiadou, A., Karapanagiotis, I., Volonakis, P., Papageorgopoulou, C., Bratitsi, M., 2020. Archaeometry: An Overview. Scientific Culture 6, 49–98. https://doi.org/10.5281/zenodo.3625220

Liu, G.-L., Kazarian, S.G., 2022. Recent advances and applications to cultural heritage using ATR-FTIR spectroscopy and ATR-FTIR spectroscopic imaging. Analyst 147, 1777–1797. https://doi.org/10.1039/D2AN00005A

Mabuchi, H., Notsu, K., Nishimatsu, S., Fuwa, K., Iyama, Hiroyuki., 1979. Chemical compositions of ancient coins. Nippon Kagaku Kaishi 1979, 586–590.

Madariaga, J.M., 2015. Analytical chemistry in the field of cultural heritage. Analytical Methods 7, 4848–4876. https://doi.org/10.1039/C5AY00072F

Martins, C.M.B., Martins, J.I., 2011. Identification of corrosion products on a medieval copper-silver coin. Protection of Metals and Physical Chemistry of Surfaces 47, 128–132. https://doi.org/10.1134/S2070205110061012

Mazzeo, R., 2017. Analytical Chemistry for Cultural Heritage. Springer.

Mazzeo, R., Roda, A., Prati, S., 2011. Analytical chemistry for cultural heritage: a key discipline in conservation research. Analytical and Bioanalytical Chemistry 399, 2885–2887. https://doi.org/10.1007/s00216-011-4672-5

Metcalf, W.E., 2011. The Oxford Handbook of Greek and Roman Coinage. Oxford University Press.

Milot, J., Malod-Dognin, C., Blichert-Toft, J., Télouk, P., Albarède, F., 2021. Sampling and combined Pb and Ag isotopic analysis of ancient silver coins and ores. Chemical Geology 564, 120028. https://doi.org/10.1016/j.chemgeo.2020.120028

Min, Y., Min, Z., Xiaobo, G., 2014. The development of X-Ray Fluorescence spectrometer based on Energy Dispersion. Presented at the Proceedings of the 16th International Conference on Mechatronics - Mechatronika 2014, pp. 543–547. https://doi.org/10.1109/MECHATRONIKA.2014.7018317

Mottner, P., 2007. Early Warning Dosimeters for Monitoring Indoor Museum Climate: Environmental Impact Sensors and LightCheck^{TM}, in: Strategies for Saving Our Cultural Heritage. Presented at the International Conference on Conservation Strategies for Saving Indoor Metallic Collections with a Satellite Meeting on Legal Issues in the Conservation of Cultural Heritage, pp. 53–57.

Mould, R.F., 1995. Röntgen and the discovery of X-rays. The British Journal of Radiology 68, 1145–1176. https://doi.org/10.1259/0007-1285-68-815-1145

Nham, T., 1998. Typical detection limits for an ICP-MS. American Laboratory 30, 17A-17D.

Nord, A.G., 2002. On the deterioration of archaeological iron artefacts in soil. Fornvännen 97, 298–300.

Nord, A.G., Mattsson, E., Tronner, K., 2005. Factors Influencing the Long-term Corrosion of Bronze Artefacts in Soil. Protection of metals 41, 309–316. https://doi.org/10.1007/s11124-005-0045-9

Northover, P., Crossley, A., Grazioli, C., Zema, N., La Rosa, S., Lozzi, L., Picozzi, P., Paparazzo, E., 2008. A multitechnique study of archeological bronzes. Surface and Interface Analysis 40, 464–468. https://doi.org/10.1002/sia.2647

Nriagu, J.O., 1985. Cupellation: The oldest quantitative chemical process. Journal of Chemical Education 62, 668. https://doi.org/10.1021/ed062p668

Olesik, J.W., 1999. Echelle Grating Spectrometers for Inductively Coupled Plasma—Optical Emission Spectrometry—A Review of Basic Equations and Operating Principles. Spectroscopy 14, 36–41.

Pagano, S., Balassone, G., Germinario, C., Grifa, C., Izzo, F., Mercurio, M., Munzi, P., Pappalardo, L., Spagnoli, E., Verde, M., De Bonis, A., 2023. Archaeometric Characterisation and Assessment of Conservation State of Coins: The Case-Study of a Selection of Antoniniani from the Hoard of Cumae (Campania Region, Southern Italy). Heritage 6, 2038–2055. https://doi.org/10.3390/heritage6020110

Pitts, K., May, C., 2023. Glass: Trace Elemental Analysis, in: Houck, M.M. (Ed.), Encyclopedia of Forensic Sciences, Third Edition (Third Edition). Elsevier, Oxford, pp. 53–62. https://doi.org/10.1016/B978-0-12-823677-2.00128-8

Pollard, A.M., Bray, P., 2014. Chemical and Isotopic Studies of Ancient Metals, in: Roberts, B.W., Thornton, C.P. (Eds.), Archaeometallurgy in Global Perspective. Springer New York, New York, NY, pp. 217–238. https://doi.org/10.1007/978-1-4614-9017-3_10

Ponting, M.J., 2012. The Substance of Coinage: The Role of Scientific Analysis in Ancient Numismatics, in: The Oxford Handbook of Greek and Roman Coinage. Oxford Handbooks.

Ponting, M.J., 1994a. Folles and forgeries: an appraisal of the composition of roman copper-alloy coinage of the mid-3rd to mid-4th centuries AD from Britain (Doctoral Thesis Doctoral). Institute of Archaeology, University College London.

Ponting, M.J., 1994b. Atomic absorption analysis and endemic coin copying in Roman Britain from the mid-third to the mid-forth centuries AD. Presented at the Symposium the Application of Scientific Methods for Investigating Coins and Coinage, British Museum, London, pp. 23–24.

Radtke, M., Reinholz, U., Riesemeier, H., 2009. Synchrotron Radiation Induced X-Ray Fluorescence for the characterization of ancient gold objects. Archeosciences 39–44. https://doi.org/10.4000/archeosciences.1969

Razani, M., Tabriz Islamic Art University, Sehati, F., Tabriz Islamic Art University, B. Kasiri, M., Tabriz Islamic Art University, 2021. Archaeometry in the Cultural Heritage Studies and Art (Definitions, Future Trends and Challenges). Journal of Roman Archaeology 7, 1–30. https://doi.org/10.52547/jra.7.1.1

Reguer, S., Dillmann, P., Mirambet, F., Susini, J., Lagarde, P., 2006. Investigation of Cl corrosion products of iron archaeological artefacts using micro-focused synchrotron X-ray absorption spectroscopy. Applied Physics A 83, 189–193. https://doi.org/10.1007/s00339-006-3506-3

Robbiola, L., Blengino, J.M., Fiaud, C., 1998. Morphology and mechanism of formation of natural patinas on archaeological Cu-Sn alloys. Corrosion Science 40, 2083–2111.

Salem, Y., Mohamed, E.H., 2019. The role of archaeometallurgical characterization of ancient coins in forgery detection. Nuclear Instruments and Methods in Physics Research Section B: Beam Interactions with Materials and Atoms 461, 247–255. https://doi.org/10.1016/j.nimb.2019.10.017

Šmit, Ž., Šemrov, A., 2006. Early medieval coinage in the territory of Slovenia. Nuclear Instruments and Methods in Physics Research Section B: Beam Interactions with Materials and Atoms 252, 290–298. https://doi.org/10.1016/j.nimb.2006.08.014

Sommer, A.J., 2020. Infrared Spectroscopy, in: Spectroscopy: Introduction to the Techniques and Recent Advances - The SciX 2020 Preview and Companion Guide. Spectroscopy, pp. 12–15.

Thomas, R., 2001. A Beginner's Guide to ICP-MS. Spectroscopy 16.

Trejos, T., Montero, S., Almirall, J.R., 2003. Analysis and comparison of glass fragments by laser ablation inductively coupled plasma mass spectrometry (LA-ICP-MS) and ICP-MS. Analytical and Bioanalytical Chemistry 376, 1255–1264. https://doi.org/10.1007/s00216-003-1968-0

Ullén, I., Nord, A.G., Fjaestad, M., Mattsson, E., Borg, G.C., Tronner, K., 2004. The degradation of archaeological bronzes underground: evidence from museum collections. Antiquity 78, 380–390. https://doi.org/10.1017/S0003598X0011302X

Volpi, V., Chiarantini, L., Cicali, C., Salvadori, B., 2023. Shedding light on the microstructure and chemical composition of rare early medieval coins from Italy (Berengario I) by combining pXRF and SEM–EDX analysis. Archaeological and Anthropological Sciences 15, 35. https://doi.org/10.1007/s12520-023-01726-3

Wells, E.C., 2014. Archaeometry: Definition, in: Smith, C. (Ed.), Encyclopedia of Global Archaeology. Springer, New York, NY, pp. 468–470. https://doi.org/10.1007/978-1-4419-0465-2_360

Zaykov, V.V., Melekestseva, I.Y., Zaykova, E.V., Fellenger, D., Motz, D., 2018. Trace Elements in Ancient Gold Products with PGE Microinclusions from Archaeological Sites of the Urals and North Black Sea Region: LA–ICP–MS Data. Archaeometry 60, 1290–1305. https://doi.org/10.1111/arcm.12381

SECTION 1

From Collection or Archaeological Finds? A Non-Destructive Analytical Approach to Distinguish between Two Sets of Bronze Coins of the Roman Empire

Giovanna Marussi[1], Matteo Crosera[1]*, Enrico Prenesti[2], Bruno Callegher[3], Elena Baracchini[1], Gianluca Turco[4], Gianpiero Adami[1]

[1] Dipartimento di Scienze Chimiche e Farmaceutiche, Università degli Studi di Trieste, 34127 Trieste, Italy

[2] Dipartimento Interateneo di Scienze, Progetto e Politiche del Territorio, Università degli Studi di Torino, 10125 Torino, Italy

[3] Dipartimento di Studi Umanistici, Università degli Studi di Trieste, 34124 Trieste, Italy

[4] Dipartimento Universitario Clinico di Scienze Mediche Chirurgiche e della Salute, Università degli Studi di Trieste, 34125 Trieste, Italy

Published on *Molecules*, https://doi.org/10.3390/molecules28052382

*Corresponding author

Matteo Crosera

Dipartimento di Scienze Chimiche e Farmaceutiche, Università degli Studi di Trieste, 34127 Trieste, Italy

Email: mcrosera@units.it

Abstract

This study stems from the need for numismatics to establish whether there may be relationships between a group of 103 bronze coins from the Roman era found in archaeological excavations on the Cesén Mountain (Treviso, Italy) and a group of 117 coins kept at the Museum of Natural History and Archaeology in Montebelluna (Treviso, Italy). The chemists were delivered six coins with neither pre–agreements nor further information on the origin of the coins. Therefore, the request was to hypothetically assign the coins to the two groups on the basis of similarities and differences in their surface composition. Only non–destructive analytical techniques were allowed to be used to characterize the surface of the six coins taken blindly from the two sets. The elemental analysis of each coins' surface was carried out by μ–XRF. To better observe the morphology of the coins' surfaces, SEM–EDS was used. Compounds covering the coins coming from both corrosion processes (patinas) and the deposition of soil encrustations were also analyzed by means of the FTIR–ATR technique. The molecular analysis confirmed the presence of silico–aluminate minerals on some coins, unequivocally indicating a provenance from clayey soil. Some soil samples, collected from the archaeological site of interest, were analyzed to verify whether the encrusted layer on coins could contain chemical components compatible with them. This result, together with the chemical and morphological investigations, led us to subdivide the six target coins into two groups. The first group is made up of two coins coming from the set of coins from excavation (found in the subsoil) and from the set from open air finds (coins found in the top layer of the soil). The second group is made up of four coins that are devoid of characteristics corresponding to exposure to soil contact for long periods of time and, moreover, their surface compounds could suggest a different provenance. The analytical results of this study made it possible to correctly assign all six coins to the two groups of finds and support numismatics, which was unconvinced in considering all coins to come from the same finding site only on the basis of archaeological documentations.

Keywords: Roman coins; numismatics; metals; alloys; bronze; patinas; micro-EDXRF; ICP-AES; FTIR-ATR; SEM-EDS

1. Introduction

Metal artefacts and, in particular, ancient coins are very important in order to obtain more information about history, the evolution of mankind, and the economy of the minting period. The critical point is that they are very sensitive to the effect of deterioration processes; in fact, their state of preservation depends on pre–burial wear and on all of the chemical and physical alterations in the burial environment. Several environmental factors contribute to the modification of the chemical composition of ancient metal artefacts, such as pH; the presence of oxygen and marine, urban, or agricultural corrosive agents; temperature cycles; and humidity (Papadopoulou et al., 2016; Reale et al., 2012). The metallographic characteristics of ancient bronze artefacts often conceal peculiar and specific corrosion behaviour, which can provide valuable tools and information to conservators and archaeologists (Quaranta et al., 2014). As a result of burial and corrosion, on the surface of artefacts, especially copper–based artefacts, several insoluble compounds can form, usually as successive, irregular, and disintegrated layers. From the analysis of these, it is possible to trace the burial site of the samples. Various works have focused on the study of bronze artefacts and their burial environments, such as some Cu–based archaeological artefacts found during archaeological excavations in Turkey, Jordan, and Italy (Ingo et al., 2006) and Montefortino helmets found in the Mediterranean seabed (Armetta et al., 2021). Among the most widely used analytical techniques for this purpose is X–Ray Fluorescence (XRF), which allows a semi–quantitative elemental analysis of the surface of samples (Caponetti et al., 2017; Estalayo et al., 2019).

With reference to this case study, the elemental composition of an archaeological patina of ancient bronze coins found in the subsoil is usually very complex and results from the deterioration processes, generically named corrosion, that occur during centuries of burial. The corrosion products covering the coins are strictly correlated to the environmental characteristics of the recovery site (Pronti et al., 2015; Reale et al., 2012). Thus, the chemical analysis of the coins' surfaces can be a useful tool for numismatists to obtain clues and information on the history of finds (Paolillo and Giudicianni, 2009). A different surface composition of materials that are similar in bulk, in fact, could likely be due to different micro–environmental conditions of the archaeological site of recovery (Armetta et al., 2021; Caponetti et al., 2017; Estalayo et al., 2019; Ingo et al., 2006; Pronti et al., 2015; Quaranta et al., 2014; Reale et al., 2012; Robbiola et al., 1998).

This type of research is inscribed in the line of studies on bronze artefacts of archaeological origin aimed at determining the chemical characteristics and structure of the patinas formed on them following their existence for centuries in corrosive environments (Sandu et al., 2006).

In 2012, an excavation led to the discovery of a possible place of worship visited by migrant people on the pass of the Cesén Mountain, a massif of the Venetian Pre–Alps located at the north–western edge of the province of Treviso, Italy (see the map in Figure 1); the highest peak is 1570 m AMSL (Callegher et al., 2018). In contrast to what normally happens in archaeological sites, the ceramic findings were small in amount, having probably been destroyed by harsh winters; nevertheless, the numismatic finds are noteworthy and deserve attention for the purpose of obtaining information. The archaeological area under study has similarities with other sanctuaries found in Venetia et Histria (north–eastern Italy). The findings of bronze coins dated from the first to the fourth centuries AD suggest the discovery of a possible votive deposit visited by transhumant shepherds, located on the transhumance paths from the alpine region to plane pasturelands. To outline the hypothesis of the votive character of the place, there is also the discovery of some blocks of limestone connected to the collapse of a low wall, which, in all probability, delimited the cult area where the coins were laid down in small dimples covered with scales of biancone (a local name to indicate a limestone lithological formation). The coins were found in multiple cavities around the cult area.

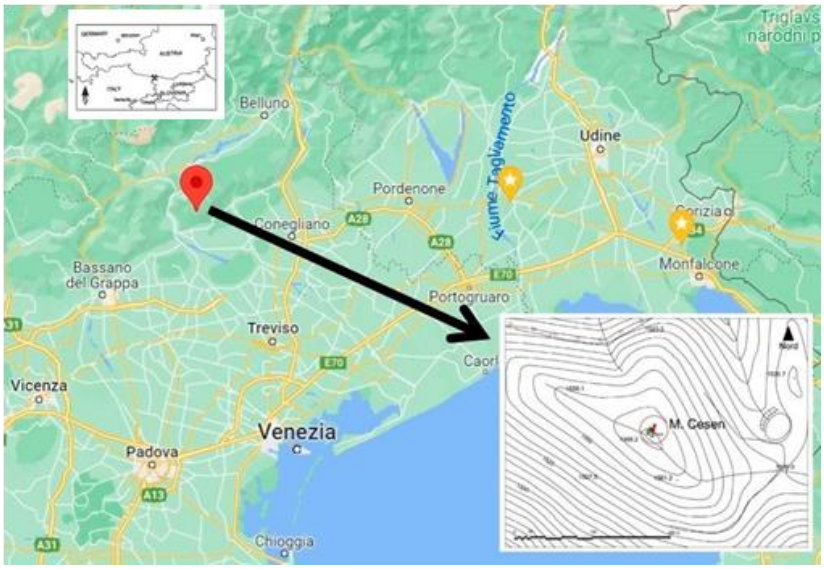

Figure 1: Location of Cesén Mountain, the survey site.

This study stems from the need for numismatics to establish whether there may be relationships between (i) bronze coins (117 specimens that date back between the first and fourth centuries AD) kept at the Museum of Natural History and Archaeology in the municipality of Montebelluna (Treviso, Italy), found during various archaeological surveys on Cesén Mountain before 2012 (the first discovery dates back to 1996), and (ii) bronze coins (103 specimens from the Roman imperial era) found in 2012 during some archaeological excavations on Cesén Mountain (Callegher et al., 2018).

Six target coins were blindly taken from the two sets of specimens in order to highlight similarities and differences between the groups. The chemists were delivered six coins (see Figure 2) with neither pre–agreements nor further information; the task was to identify if it was a compositionally homogeneous set or if the coins were attributable to two different groups of finds. The limited availability of coins' specimens usable for the analyses is a constraint established by the institutional body who commissioned the study (Janssens et al., 2000a; Mantler and Schreiner, 2000; Van Grieken and Markowicz, 2001). As the analysts did not know the size of the two groups of coins until the end of the study, six coins were considered sufficient to test the method. In fact, the probability of correctly assigning the six coins to the two groups of finds in a random manner is 1.56%.

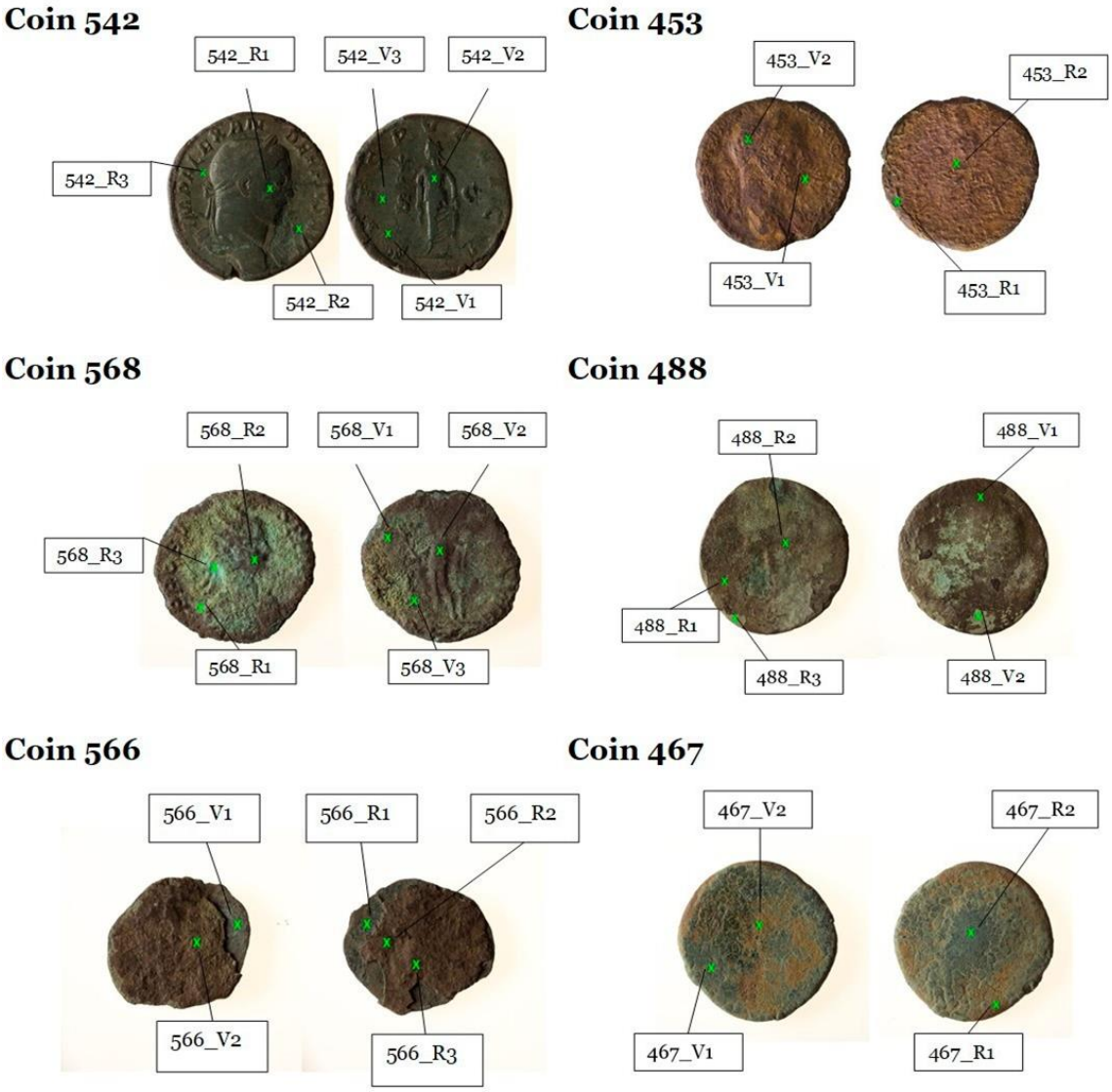

Figure 2: Sampling points for the six target coins analysed by μ–XRF (R = recto; V = verso).

To avoid damage to the numismatic finds, only non–destructive analytical techniques were allowed to be used in order to characterize the surface of the coins (Carlomagno et al., 2022; Marussi et al., 2022). The elemental analysis of each coins' surface was carried out by μ–X–Ray Fluorescence spectroscopy (μ–XRF) (Baldassarri et al., 2014). To better observe the morphology of the coins' surfaces, Scanning Electron Microscopy coupled to Energy Dispersive Spectroscopy (SEM–EDS) was used (Torrisi et al., 2008).

The μ–XRF technique was first employed to identify the presence of elements other than the major element, copper, which is often used as the reference element (Crosera et al., 2019; del Hoyo-Meléndez et al., 2015). This technique is useful to gather information about the surface composition of a material, as only low depths can be reached by the

analytical ray. On the other hand, no treatment of the sample was required. Compounds covering the coins coming from both corrosion processes (patinas) and depositions of soil encrustations were also analyzed by means of the FTIR–ATR (Fourier Transform Infrared spectroscopy–Attenuated Total Reflection) technique. To strengthen the investigation, three soil samples, collected from the archaeological site of interest, were analyzed to verify whether the encrusted layer of coins could contain chemical components compatible with the elemental composition of the soil.

It is important to point out that, until the end of the study, analysts had no information regarding the origin of the coins, the issue period, or the composition, nor was any reference to the historical-numismatic hypotheses made.

2. Results and discussion

The SEM–EDX investigation was carried out on three coins, namely, 488, 542, and 566. This preliminary analysis was useful to observe the morphology of the coins' surfaces. In Figure 3a, the results for coin 566, obtained on a clean area, show the presence of copper (about 33%) and lead (about 25%) in the bulk of the coin. Figure 3b shows the SEM–EDX spectrum on the area covered by the soil concretions, which consist essentially of Ca (4%), Si (about 7%), Al (about 3%), and Fe (about 3%), while Pb % decreases a lot and Cu % remains at previous levels of about 35.

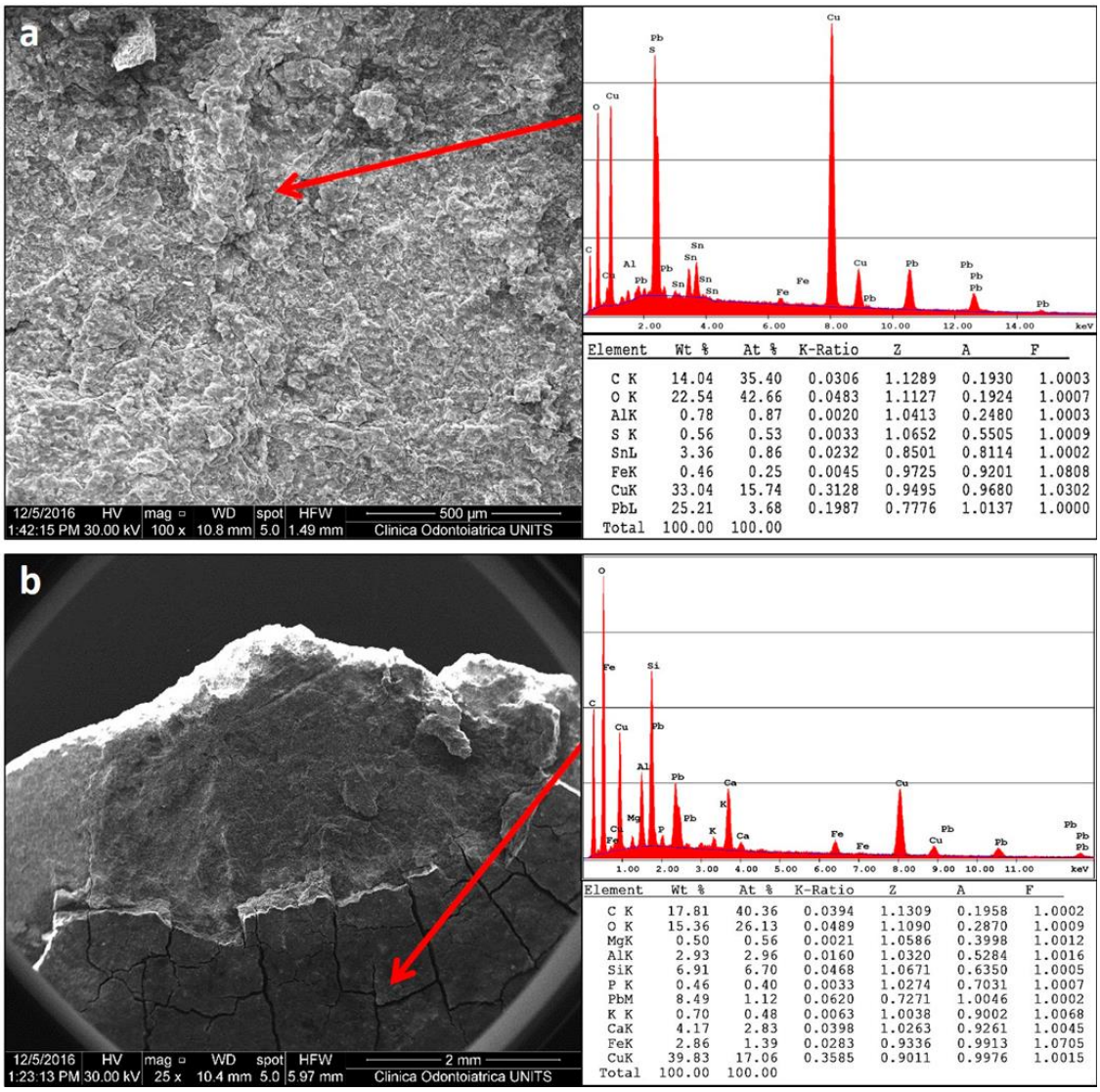

Figure 3(a,b): Representative SEM micrographs and relative EDX spectra with standardless quantification (element normalized) of coin 566: (a) bulk and (b) soil concretions.

µ–XRF measurements were performed on both the clean and altered (corroded or encrusted) areas and at least two spectra were collected on the recto and two on the verso of each coin in order to obtain representative data of the entire specimen (see Figure 4).

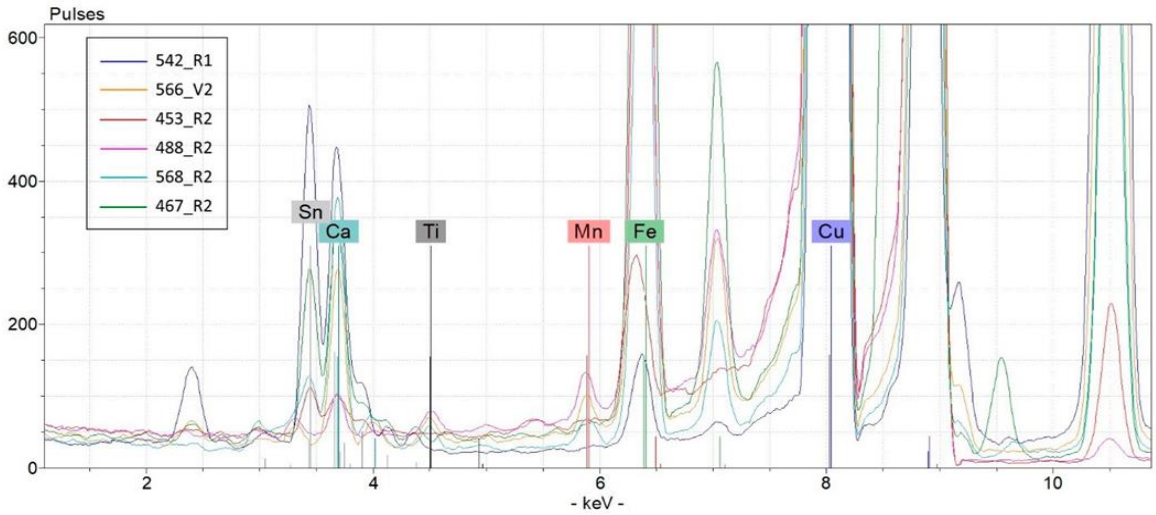

Figure 4: Representative μ-XRF spectra of the six coins.

The signal counts of the elements of interest are shown in Table 1. By calculating the area subtended by the peaks relative to the copper Kα1 line and to the lead Lα1 line and tin Kα2 line, it was possible to calculate the ratios Pb/Cu and Sn/Cu in order to delineate the trend of these metals at the surface (see Table 1).

Table 1: μ–XRF signals (counts) of selected elements (average of versus and recto analysis) and Pb/Cu and Sn/Cu ratios obtained for all six coins analysed.

Coin number	Counts	Cu	Pb	Sn	Ca	Fe	Ag	Ti	Mn	Zn	Pb/Cu	Sn/Cu
542	**Average**	**228,719**	**92,501**	**25,335**	**5523**	**2307**	**<100**	**<20**	**<100**	**<100**	**0.41**	**0.11**
	SD	11,079	12,348	2132	441	482	*	*	*	*	0.07	0.01
568	**Average**	**518,505**	**17,656**	**17,602**	**2012**	**16,793**	**23,636**	**199**	**585**	**<100**	**0.04**	**0.04**
	SD	202,308	4266	2216	1123	4628	6189	228	152	*	0.02	0.02
566	**Average**	**492,103**	**95,768**	**1362**	**2285**	**9918**	**<100**	**72**	**310**	**<100**	**0.21**	**0.003**
	SD	115,653	41,448	442	1,353	8,146	*	67	249	*	0.14	0.001
453	**Average**	**1,086,044**	**6004**	**2,113**	**960**	**2318**	**<100**	**<20**	**<100**	**<100**	**0.006**	**0.002**
	SD	44,968	2332	194	563	305	*	*	*	*	0.002	0.000
488	**Average**	**1,083,968**	**869**	**664**	**424**	**12,607**	**<100**	**<20**	**323**	**<100**	**0.001**	**0.001**
	SD	92,111	449	161	324	7318	*	*	318	*	0.000	0.000
467	Average	**882,254**	**10,367**	**2,837**	**2,197**	**25,950**	**<100**	**<20**	**<100**	**59,741**	**0.014**	**0.004**
	SD	197,141	6387	1,376	1157	12,715	*	*	*	15,645	0.011	0.003
soil	Average	**206**	**239**	**<100**	**906**	**78,768**	**<100**	**1520**	**2489**	**851**	*	*
	SD	51	95	*	61	11,639	*	187	309	48	*	*

* Not determinable.

To obtain more interpretable data of the element surface composition of the six coins, for each spectrum, the percentage ratio of the peak intensities (expressed in counts) of each element to the sum of the peak intensities of all the elements considered and measurable by the μ–XRF spectrum was calculated. The values obtained for the different points of the same coin were averaged (see Table 2); a high coefficient of variation expressed as a percentage relative standard deviation indicates a non–homogeneous distribution of the elements on the surface of the coin. This may be indicative of a different environmental history for the coins.

Table 2: Peak area vs. total peak area (in %) of the coins obtained by the μ-XRF technique expressed as the average, standard deviation, and percentage relative standard deviation for the nine elements detected.

Coin #	Peak Area vs. Total Peaks Area (%)	Cu	Pb	Sn	Ca	Fe	Ag	Ti	Mn	Zn
542	**average**	**64.5**	**26.0**	**7.14**	**1.56**	**0.65**	**<0.03**	**0.006**	**<0.03**	**<0.03**
	SD	2.8	3.0	0.42	0.14	0.12	*	0.000	*	*
	RSD%	4.4	11	5.8	8.9	18		4.4		
568	**average**	**85.1**	**3.3**	**3.24**	**0.39**	**3.29**	**4.6**	**0.049**	**0.113**	**<0.03**
	SD	7.1	1.3	1.18	0.27	2.00	2.7	0.060	0.070	*
	RSD%	8.4	39	37	68	61	58	123	62	
566	**average**	**81**	**16.5**	**0.23**	**0.40**	**1.69**	**<0.03**	**0.013**	**0.056**	**<0.03**
	SD	7.8	8.7	0.09	0.26	1.34	*	0.010	0.037	*
	RSD%	9.7	52	37	65	79		78	66	
453	**average**	**98.9**	**0.6**	**0.19**	**0.09**	**0.21**	**<0.03**	**<0.006**	**<0.03**	**<0.03**
	SD	0.3	0.2	0.02	0.05	0.03	*	*	*	*
	RSD%	0.3	42	9.5	62	12				
488	**average**	**98.6**	**0.1**	**0.06**	**0.04**	**1.18**	**<0.03**	**<0.006**	**0.033**	**<0.03**
	SD	0.8	0.0	0.02	0.03	0.73	*	*	0.029	*
	RSD%	0.8	48	28	80	62			90	
467	**average**	**89.3**	**1.2**	**0.32**	**0.25**	**2.92**	**<0.03**	**<0.006**	**<0.03**	**6.01**
	SD	2.9	0.9	0.21	0.17	1.95	*	*	*	0.43
	RSD%	3.2	79	67	70	67				7.1

On the basis of these μ–XRF data, we can affirm the following:

1. coin 542 differs from the others owing to its lower Cu content and highest content of Pb and Sn;

2. coin 467 contains Zn, an element that is under the limit of detection in the other specimens; Roman bronze was a typical alloy made of Cu, Sn, Pb, and Zn, and the Romans manufactured copper alloys by combining variable percentages of alloys containing Sn and Zn; the result was an alloy with a composition ranging between that of common bronzes and brass;
3. coin 568 contains Ag, an element that is under the limit of detection in the other specimens;
4. coins 568 and 566 are related by the presence of Ti and Mn, which are typical elements of the ground;
5. coins 453 and 488 are similar to each other in terms of their Cu content, which, for both coins, is close to the totality.

These results indicate a wide chemical heterogeneity of these finds – even within the substantial common tin bronze alloy identity – revealing different histories. This outcome allows to sustain the hypothesis that the coins under study were found in a place visited by migrant people on Cesén Mountain.

Conventional bronze alloy is usually based on Cu and Sn as the main alloy elements, even though arsenical bronze (probably the first alloy of the wide bronze family) and Roman bronze are known to have Zn. We found some unexpected elements in various combinations, often fortuitous and mirroring the variability of raw materials. Ti and Mn were found only on the surface of two coins (namely 566 and 568). In particular, Ti, Mn, Fe, and Ca are typical terrigenous elements and were in fact also found in the soil sampled in this archeological site (see Table 3). The surface of coins 566 and 568 bears a covering of brown earthy crust, indicating a discovery of the finds in the subsoil, probably after being underground for a long time. Specifically, regarding coin 488, the Ti signal is present only in the μ-XRF spectrum acquired in point 488_R1. This fact can be considered as a simple fortuitous contamination, and it sharply discourages the inclusion of this coin in the small group of specimens found in the subsoil.

Table 3: Elemental composition of the soil sampled in the archaeological site obtained by the ICP-AES technique (% dw = percentage calculated on the dry weight of the sample).

	Ca	**Fe**	**Al**	**Mg**	**K**	**Ti**	**Mn**
average (% dw)	0.228	2.743	3.49	0.229	0.66	0.235	0.119

SD	0.016	0.067	0.46	0.07	0.055	0.003	0.003

For the sake of example, Figure 5 shows the comparison between the µ-XRF spectrum related to a representative point (566_V2) of the superficial patina of coin 566 and a point (542_R1) of coin 542 that shows the presence of Ti and Mn signals in the first case and their absence in the second case. The same comparison can be made between the spectra of the most indicative points of all of the coins.

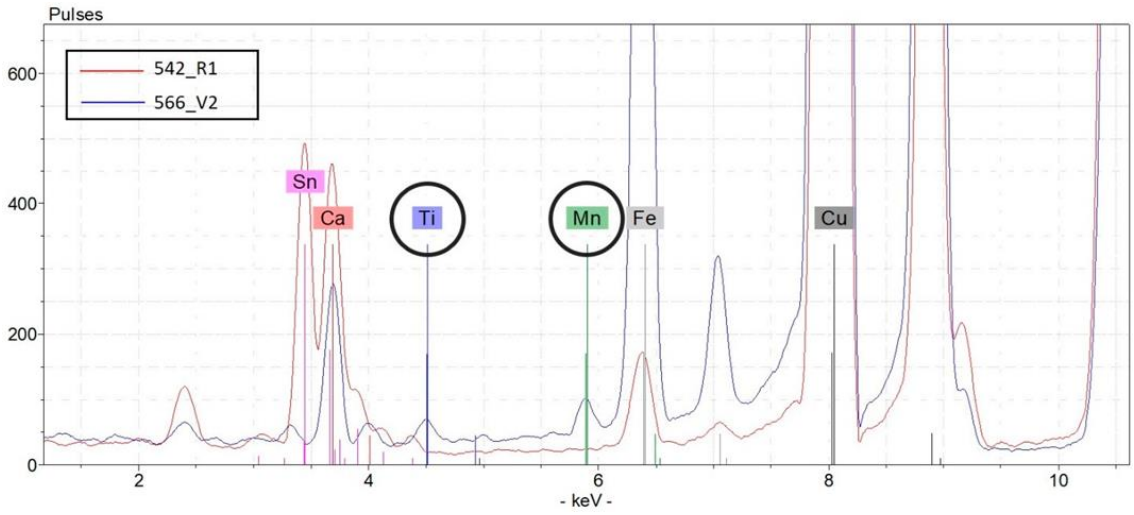

Figure 5: µ–XRF spectra comparison between a representative point (566_V2) of the superficial patina of coin 566 and a point (542_R1) of coin 542.

From the µ–XRF spectra of soil samples (Table 1) coming from the excavation site (see also the quantitative concentration results collected in Table 3), one can note that (Figure 6), limited to the presence of Ti and Mn, only the profiles relating to coins 566 and 568 seem to be compatible with that of the local soil.

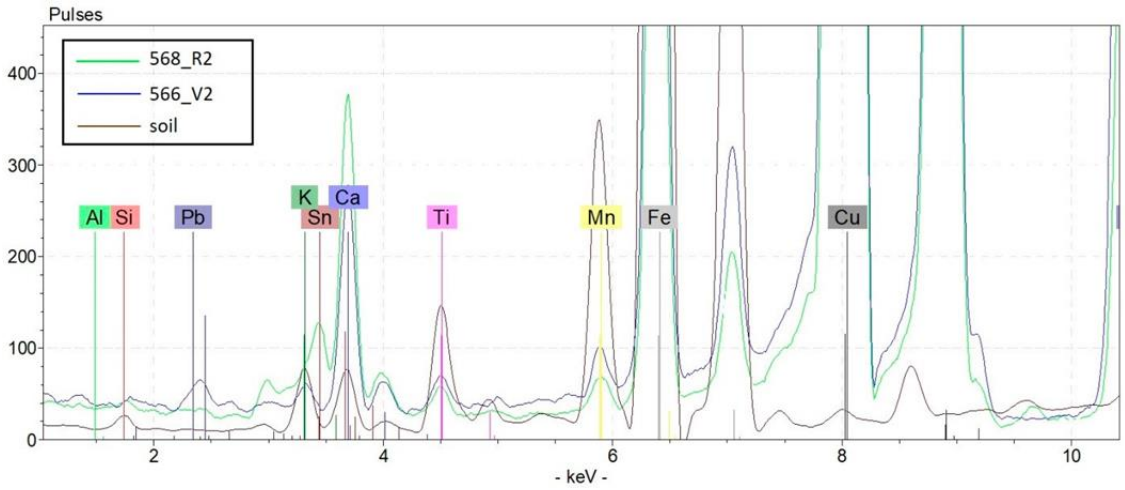

Figure 6: μ–XRF spectra comparison between points 566_V2 (blue line), 568_R2 (green line), and the soil sample (brown).

A fairly good correlation (correlation coefficient > 0.7) between Ti and Mn signal peaks was found, thus fortifying the hypothesis of soil attribution of these exogenous elements as to those conventionally foreseeable for a common bronze (even beyond any minor metals present in the raw materials). The μ–XRF signal ratio Ti/Mn was 0.62 for soils and has a very similar value of 0.60 for coin 568 (average of spectra 568_R1, 568_R2, and 568_V2).

FTIR–ATR analyses on coins 488 and 566, carried out in both cleaned areas and encrusted areas, confirmed the presence of silico–aluminate minerals, unequivocally indicating a provenance from clayey soil (at least to the depth of the find).

Carbonates (calcareous soils) show (see Figure 7) strong absorption bands near 1400 and 870 cm^{-1}, and we can observe a peak for coin 566 at 1392 cm^{-1} due to calcite and/or dolomite minerals (Udvardi et al., 2014).

For both coins, we can observe the presence of the typical peak of kaolinite ($Al_2(OH)_4Si_2O_5$) in the range of 1000–1100 cm^{-1} due to asymmetric stretching of silicates. Silico-aluminates (clayey soils) also show IR absorption bands around 630, 800, and 850 cm^{-1} (Böke et al., 2004; Gorassini et al., 2016; Manso and Carvalho, 2009; Sandu et al., 2006; Udvardi et al., 2014).

Sulphates ($CaSO_4$ and related hydrated salts) are not detectable in all IR spectra; the characteristic corrugated absorption bands in the range of 3600–3300 cm^{-1} and a typical small band at about 1620 cm^{-1} are in fact absent.

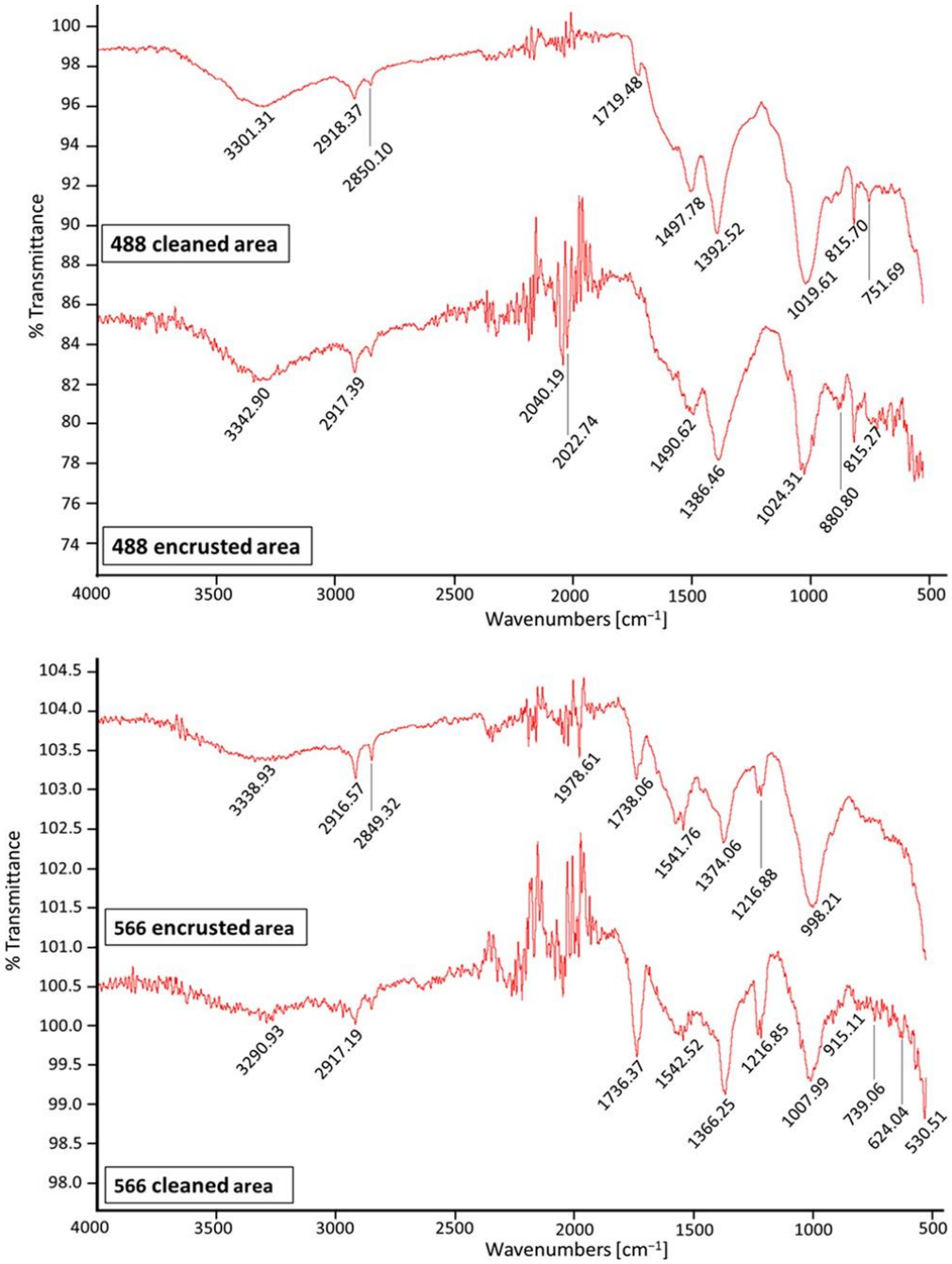

Figure 7: FTIR–ATR spectra of coins 488 and 566, carried out in both cleaned and encrusted areas.

3. Material and Methods

3.1 Chemical and apparatuses

All chemicals used were of analytical grade. Nitric acid (69% w/w), hydrochloric acid (37% w/w), hydrofluoric acid (48%), boric acid (99.99%), and hydrogen peroxide (30%) were purchased from Sigma Aldrich (Milan, Italy). Water of reagent grade was produced with a Millipore purification pack system (MilliQ water). Standards of Ca, Fe, Al, Mg, K, Ti, and Mn used for the calibration curves related to ICP-AES analyses were obtained by dilution (in 2.5% HNO_3 aqueous solution) of SPECTRASCAN® 1000 mg L^{-1} standard solutions purchased from Teknolab (Drøbak, Norway).

3.2 Elemental analyses

3.2.1 Sample acquisition

Coins

As the study was carried out blindly, information on the group to which each coin belongs was disclosed only at the end of the investigations. Both groups of specimens are declared as being found in the same area during archaeological excavations carried out at different times.

The six specimens of coins provided for analyses were identified with a general inventory (GI) number (marked “IG” in Italian language with the same meaning) as follows:

IG369542 = appendix n. 57: coin #542

IG369568 = catalogue n. 102: coin #568

IG369566 = catalogue n. 103: coin#566

IG369453 = appendix n. 59: coin #453

IG369488 = appendix n. 20: coin #488

IG369467 = appendix n. 102: coin #467

The term “appendix” indicates the coins from recent archaeological surveys, while the term “catalogue” indicates the coins from the quoted museum collection.

The chemical analyses were performed at least on two points per coin on both sides. The measurement points are evidenced in pictures shown in Figure 2 (where R = recto and V = verso).

Soils

Soil samples were collected by means of a plastic spoon and a plastic bag in the archaeological site of the find, and then dried for two days before undergoing chemical analysis. Soil samples were analyzed according to two techniques: (i) without pretreatment by means of μ–XRF (a non-destructive technique) and (ii) after acid digestion, by means of destructive inductively coupled plasma–atomic emission spectroscopy (ICP-AES).

3.2.2 μ-XRF Qualitative Measurements

The elemental analysis of each coin's surface was carried out by micro-Energy Dispersive X–Ray Fluorescence spectrometry (μ–EDXRF, briefly μ–XRF). An ARTAX 200 μ–XRF spectrometer (supplied by Bruker Nano GmbH) was used. The instrument was setup with the following test parameters: X–ray tube, 30 W, Mo target U = 50 kV, I = 700 μA, acquisition time: 60 s (live time), and collimator: 650 μm (air environment). The instrument consists of an air–cooled Mo X–ray fine focus tube (max 50 kV, 1 mA, 40 W) controlled by a compact high voltage generator unit and equipped with a 650 mm collimator. It is equipped with a Peltier cooled XFlash® silicon drift detector (10 mm^2 of active area and energy resolution <150 eV for Mn–Ka at 100 kcps) and a color CCD camera (500 x 582 pixels) for sample positioning. The focal spot is 1.2·0.1 mm^2, with a 0.2 mm lateral resolution and a 100 μm beryllium window.

The Spectra ARTAX software was used for hardware control and analytical data evaluation (version 5.3.14.0, license of Bruker AXS Microanalysis GmbH, Berlin, Germany). For each acquired spectrum, the percentage ratio of the peak intensities (counts) of each element to the sum of the peak intensities of all the elements was calculated. Data are plotted as counts versus energy (keV).

The following elements were examined: Cu (line: Kα1 8.0463 keV), Pb (line: Lα1 10.551 keV), Sn (line: Kα2 25.044 keV), Fe (line: Kα1 6.4052 keV), Ca (line: Kα2 3.6888 keV),

Zn (line: Kα2 8.6141 keV), Ag (line: Kα2 21.99 keV), Ti (line: Kα2 4.5058 keV), and Mn (line: Kα1 5.9003 keV).

3.2.3 ICP-AES Quantitative Measurements

After the collection in the archaeological site of the find, soil samples were transferred to the laboratory, where they were dried for two days until a constant weight. Each dried soil sample was powdered and homogenized in an agate mortar and then an aliquot was digested in a closed microwave system (Multiwave PRO, Anton Paar GmbH, Graz, Austria) following the method EPA 3052 (USEPA, 1996); that is, 250 mg of homogenized dried samples was transferred to PTFE vessels and mineralized using two heating steps. In the first step, nitric acid, hydrochloric acid, hydrofluoric acid, and hydrogen peroxide were used. In the second step, a solution of boric acid (6%) was added to buffer the excess HF. After mineralization, the solutions were diluted to a volume of 25 mL by adding Milli–Q water and stored at 4°C until analysis.

Solutions were then analyzed with an ICP–AES spectrometer (Optima 8000, PerkinElmer with S10 autosampler, Waltham, MA, USA). The analyses were conducted using a calibration curve obtained by dilution (range: 0–100 mg L^{-1}) of certified standard solutions (1000 mg L^{-1}) for ICP analyses. Blanks, laboratory–fortified blanks, and laboratory–fortified samples were analyzed before and after sample solutions in order to evaluate the procedure accuracy. The limit of detection (LOD) in the solution sample at the working wavelength for each element was as follows: 0.025 mg L^{-1} for Ca at 317.933 nm, 0.050 mg L^{-1} for Fe at 238.204 nm, 0.025 mg L^{-1} for Al at 396.153 nm, 0.025 mg L^{-1} for Mg at 285.213 nm, 0.025 mg L^{-1} for K at 766.490 nm, 0.025 mg L^{-1} for Ti at 334.940 nm, and 0.025 mg L^{-1} for Mn at 257.610 nm. The repeatability of the measurements expressed as relative standard deviation (RSD%) was always lower than 5%. The concentrations of all other measured elements (Pb, As, Cu, Cd, Zn, Cr, V, Co, and Ni) are always low in sampled soil (lower than 0.01%) and not significant.

3.2.4 FTIR-ATR Spectra

The infrared analysis of coin surfaces was carried out by means of a Perkin–Elmer Spectrum 100 FT–IR spectrophotometer equipped with a universal attenuated total

reflectance (ATR) sampling accessory (ZnSe cell) with a diamond window (about 2 mm in diameter). Spectral analyses were performed at a resolution of 4 cm^{-1} in the range of 4000–550 cm^{-1}, scanned eight times, at room temperature and humidity. The number of scans was chosen to maximize the signal-to-noise ratio.

3.2.5 SEM–EDS

Morphological analyses and microanalyses were performed using SEM (Scanning Electron Microscope) Quanta250 (FEI, Hillsboro, OR, USA), in high vacuum, in secondary electron mode. The working distance was adjusted in order to obtain a suitable magnification and the accelerating voltage was 30 kV. In order to detail the state of eventual patinas or encrustations, microanalysis was performed in full-frame acquisition by EDS (energy–dispersive spectroscopy) using an Apollo X EDAX probe (EDAX, Mawah, NJ, USA) coupled with SEM.

3.3 Data processing

Data analysis was performed with Excel for Windows, release 2016, and Stata Software, version 11.0 (StataCorp LP, College Station, TX, USA).

4. Conclusions

It is important to remember that, at the time of coins' delivery, the analyst was not given any information regarding the origin of the specimens, the issue period, or the composition of the alloy, nor was any reference made to the hypotheses based on historical–numismatic considerations.

The non–destructive analyses carried out allowed us, despite the scarcity of complementary information, to achieve the goal of assigning the six coins to the two groups in the correct way as requested by the public institution. First, two elements were found only on the surface of two coins, that is, Ti and Mn, that were also found in soil samples appositely picked up in the archaeological area. Chemical and morphological outcomes allowed us to subdivide the six target coins into two groups that were well

characterized and, therefore, well distinguishable from each other. This grouping corresponds to the set of coins from excavation (coins found in the subsoil) and to the set coming from open–air finds (coins found in the top layer of the soil). The chemical composition allows to characterize the six target coins delivered to the study with respect to the following: (i) the finding conditions: two coins were buried (566 and 568), found encrusted with earth and with oxidation patinas, while four coins, found clean, with oxidation patinas, existed mainly in the open–air (in the top soil) over centuries (542, 453, 488, and 467); and (ii) the marked chemical heterogeneity of the alloys – mostly the wide difference in copper percentage – indicates a multiplicity of provenances (and, therefore, of raw materials and workmanship) of bronze coins found in this rather popular votive site.

The archaeological site located on a mountain pass – evidence has been found to support the hypothesis of the votive character of the place – probably welcomed transhumant shepherds and/or migrants passing of different origins, and thus with different currencies as well as different travel aims and destinations. People with different origins, itineraries, and travel purposes bring coins of different composition according to their origins, rather than collected in trades during travel.

The results indicate a wide chemical heterogeneity of these finds as well as a different history and modality of findings. It is likely that the minor elements found in the specimens analyzed reveal that different raw minerals, or melted again alloys (like old coins that have gone out of circulation), were used to manufacture the various coins.

Specimens of the group containing four coins are devoid of characteristics of coins exposed to subsoil for long periods of time; this could suggest a different provenance.

In conclusion, this study demonstrated the possibility of attributing a small subset of coins to the two groups based on their chemical and morphological characteristics, using only non-destructive methods. The findings support numismatists who were not convinced about considering all coins to come from the same site on the basis of archaeological documentations. For this reason, they will not consider all of the coins to have interpretive hypotheses, but only those coming from archaeological excavations. In the future, the public institution will decide whether to continue the analyses on a greater number of coins to reinforce the information acquired.

References

Armetta, F., Saladino, M.L., Scherillo, A., Caponetti, E., 2021. Microstructure and phase composition of bronze Montefortino helmets discovered Mediterranean seabed to explain an unusual corrosion. Scientific Reports 11, 23022. https://doi.org/10.1038/s41598-021-02425-6

Baldassarri, M., Cavalcanti, G.D.H., Ferretti, M., Gorghinian, A., Grifoni, E., Legnaioli, S., Lorenzetti, G., Pagnotta, S., Marras, L., Violano, E., Lezzerini, M., Palleschi, V., 2014. X-Ray Fluorescence Analysis of XII–XIV Century Italian Gold Coins. Journal of Archaeology 2014, 1–6. https://doi.org/10.1155/2014/519218

Böke, H., Akkurt, S., Özdemir, S., Göktürk, E.H., Caner Saltik, E.N., 2004. Quantification of $CaCO_3$–$CaSO_3 \cdot 0.5\ H_2O$–$CaSO_4 \cdot 2\ H_2O$ mixtures by FTIR analysis and its ANN model. Materials Letters 58, 723–726. https://doi.org/10.1016/j.matlet.2003.07.008

Callegher, B., Larese, A.M., Rinaldi, L., Baracchini, E., Crosera, M., Prenesti, E., Adami, G., 2018. Un deposito votivo sul crinale delle Prealpi Trevigiane-Bellunesi: lo scavo archeologico del Monte Cesén, reperti numismatici e analisi archeometriche. Journal of Archaeological Numismatics 8, 69–124.

Caponetti, E., Armetta, F., Martino, D.C., Saladino, M.L., Ridolfi, S., Chirco, G., Berrettoni, M., Conti, P., Bruno, N., Tusa, S., 2017. First Discovery of Orichalcum Ingots from the Remains of A 6^{th} Century BC Shipwreck near Gela (Sicily) Seabed. Mediterranean Archaeology and Archaeometry 17, 11–18. https://doi.org/10.5281/ZENODO.581716

Carlomagno, I., Zeller, P., Amati, M., Aquilanti, G., Prenesti, E., Marussi, G., Crosera, M., Adami, G., 2022. Combining synchrotron radiation techniques for the analysis of gold coins from the Roman Empire. Scientific Reports 12, 15919. https://doi.org/10.1038/s41598-022-19682-8

Crosera, M., Baracchini, E., Prenesti, E., Giacomello, A., Callegher, B., Oliveri, P., Adami, G., 2019. Elemental characterization of surface and bulk of copper-based coins from the Byzantine-period by means of spectroscopic techniques. Microchemical Journal 147, 422–428. https://doi.org/10.1016/j.microc.2019.03.025

del Hoyo-Meléndez, J.M., Świt, P., Matosz, M., Woźniak, M., Klisińska-Kopacz, A., Bratasz, Ł., 2015. Micro-XRF analysis of silver coins from medieval Poland. Nucl. Instrum. Nuclear Instruments and Methods in Physics Research Section B: Beam Interactions with Materials and Atoms 349, 6–16. https://doi.org/10.1016/j.nimb.2015.02.018

Estalayo, E., Aramendia, J., Matés Luque, J.M., Madariaga, J.M., 2019. Chemical study of degradation processes in ancient metallic materials rescued from underwater

medium. Journal of Raman Spectroscopy 50, 289–298. https://doi.org/10.1002/jrs.5553

Gorassini, A., Adami, G., Calvini, P., Giacomello, A., 2016. ATR-FTIR characterization of old pressure sensitive adhesive tapes in historic papers. Journal of Cultural Heritage 21, 775–785. https://doi.org/10.1016/j.culher.2016.03.005

Ingo, G.M., De Caro, T., Riccucci, C., Angelini, E., Grassini, S., Balbi, S., Bernardini, P., Salvi, D., Bousselmi, L., Çilingiroglu, A., Gener, M., Gouda, V.K., Al Jarrah, O., Khosroff, S., Mahdjoub, Z., Al Saad, Z., El-Saddik, W., Vassiliou, P., 2006. Large scale investigation of chemical composition, structure and corrosion mechanism of bronze archeological artefacts from Mediterranean basin. Applied Physics A 83, 513–520. https://doi.org/10.1007/s00339-006-3550-z

Janssens, K., Vittiglio, G., Deraedt, I., Aerts, A., Vekemans, B., Vincze, L., Wei, F., De Ryck, I., Schalm, O., Adams, F., Rindby, A., Knöchel, A., Simionovici, A., Snigirev, A., 2000. Use of microscopic XRF for non-destructive analysis in art and archaeometry. X-Ray Spectrometry 29, 73–91. https://doi.org/10.1002/(SICI)1097-4539(200001/02)29:1<73::AID-XRS416>3.0.CO;2-M

Manso, M., Carvalho, M.L., 2009. Application of spectroscopic techniques for the study of paper documents: A survey. Spectrochimica Acta Part B: Atomic Spectroscopy, 10th Rio Symposium on Atomic Spectrometry 64, 482–490. https://doi.org/10.1016/j.sab.2009.01.009

Mantler, M., Schreiner, M., 2000. X-ray fluorescence spectrometry in art and archaeology. X-Ray Spectrometry 29, 3–17. https://doi.org/10.1002/(SICI)1097-4539(200001/02)29:1<3::AID-XRS398>3.0.CO;2-O

Marussi, G., Crosera, M., Prenesti, E., Cristofori, D., Callegher, B., Adami, G., 2022. A Multi-Analytical Approach on Silver-Copper Coins of the Roman Empire to Elucidate the Economy of the 3rd Century A.D. Molecules 27, 6903. https://doi.org/10.3390/molecules27206903

Paolillo, L., Giudicianni, I., 2009. La Diagnostica nei Beni Culturali-Moderni Metodi di Indagine. Loghia Publishing & Research, Napoli, Italy.

Papadopoulou, O., Vassiliou, P., Grassini, S., Angelini, E., Gouda, V., 2016. Soil-induced corrosion of ancient Roman brass – A case study. Materials and Corrosion 67, 160–169. https://doi.org/10.1002/maco.201408115

Pronti, L., Felici, A.C., Alesiani, M., Tarquini, O., Bracciale, M.P., Santarelli, M.L., Pardini, G., Piacentini, M., 2015. Characterisation of corrosion layers formed under burial environment of copper-based Greek and Roman coins from Pompeii. Applied Physics A 121, 59–68. https://doi.org/10.1007/s00339-015-9351-5

Quaranta, M., Catelli, E., Prati, S., Sciutto, G., Mazzeo, R., 2014. Chinese archaeological artefacts: Microstructure and corrosion behaviour of high-leaded bronzes. Journal of Cultural Heritage 15, 283–291. https://doi.org/10.1016/j.culher.2013.07.007

Reale, R., Plattner, S.H., Guida, G., Sammartino, M.P., Visco, G., 2012. Ancient coins: cluster analysis applied to find a correlation between corrosion process and burial soil characteristics. Chemistry Central Journal 6, S9. https://doi.org/10.1186/1752-153X-6-S2-S9

Robbiola, L., Blengino, J.M., Fiaud, C., 1998. Morphology and mechanism of formation of natural patinas on archaeological Cu-Sn alloys. Corrosion Science 40, 2083–2111.

Sandu, I., Marutoiu, C., Alexandru, A., Sandu, A.V., 2006. Authentication of Old Bronze Coins I. Study on Archaeological Patina. Acta Universitatis Cibiniensis Seria F Chemia 9, 39–53.

Torrisi, L., Mondio, G., Serafino, T., Caridi, F., Borrielli, A., Margarone, D., Giuffrida, L., Torrisi, A., 2008. LAMQS, EDXRF and SEM analyses of old coins. Presented at the I Workshop about Plasma Physics, Sources, Biophysics and Applications, University of Salento, Lecce, Italy.

Udvardi, B., Kovács, I.J., Kónya, P., Földvári, M., Füri, J., Budai, F., Falus, G., Fancsik, T., Szabó, C., Szalai, Z., Mihály, J., 2014. Application of attenuated total reflectance Fourier transform infrared spectroscopy in the mineralogical study of a landslide area, Hungary. Sedimentary Geology 313, 1–14. https://doi.org/10.1016/j.sedgeo.2014.08.005

USEPA, 1996. EPA Method 3052: Microwave assisted acid digestion of siliceous and organically based matrices. Test methods for evaluating solid waste.

Van Grieken, R., Markowicz, A., 2001. Handbook of X-Ray Spectrometry. CRC Press.

SECTION 2

Non−destructive and micro−destructive chemical analysis of Late Antique gold solidi (4th–6th century) from Balkan hoards

The study of ancient metal artefacts, in particular coins, yields valuable insights into minting technologies, economic history, and the materials employed. This helps in comprehending the sources of raw materials and the locations of the mines from which they were extracted. Understanding the composition of alloys makes it possible to reconstruct monetary policies and to comprehend the relationship between political and economic events. Additionally, the examination of corrosion products can reveal the burial place of artefacts, providing important information on their preservation and potential restoration (Guerra, 1995).

Gold, with its characteristics of malleability, elasticity, and tensile strength, was one of the earliest metals utilised by humans. The Varna Treasure in Bulgaria serves as proof of this, comprising a diverse range of gold objects, including bracelets, pendants, and beads produced during the Copper Age (4,600 BC − 4,200 BC).

The earliest evidence of coinage dates back to the period between 700 and 550 BC in the ancient kingdom of Lydia, situated in the western part of Anatolia, which is present−day Turkey (Guerra and Calligaro, 2003). The invention of coins marked a fundamental shift in human history, as it played a crucial role in the evolution of trade between different cultures. Initially, these coins were minted using a natural alloy of approximately 80−90% gold and 10−20% silver. As metallurgical knowledge progressed, ancient civilizations learned to partially removed silver from gold and begun producing almost pure gold coins.

By the end of the 4th century AD, gold had become the most valuable asset in the Roman Empire. Its value was partly due to its intrinsic rarity and partly to its cultural significance. Gold, being pure and incorruptible, was often associated with the sacred nature of the emperor.

In this section, two studies on the analysis of Late Antique gold solidi are presented. The solidus was initially introduced by Diocletian in small issues and later widely reintroduced by Constantine in 312 AD. It became the standard gold coin issued in the Late Roman period, and its production was one of the primary responsibilities of the Count of the Sacred Largesses (*Comes Sacrarum Largitionum*). The solidus was minted at 72 cents of a Roman pound and, since its introduction in the early 4th century, was produced using the purest gold. During the reigns of Valentinian I and Valens, its purity was increased from 95% to 99%, and the new coins bore the letters "OB" in the mintmark (an abbreviation of *obryzum*) to indicate their higher purity (Guest, 2008).

The literature on chemical analyses of Late Antique solidi is limited. With a substantial batch of specimens available (49 gold coins minted between 367 and 565 AD), the primary aim was to identify a trend in the noble metal content across all coin specimens, aiming to detect possible devaluations or forgeries.

The first study focused precisely on this issue: the coins were analysed using readily available laboratory techniques such as μ−EDXRF, ICP−AES, and ICP−MS in liquid phase. In addition to the determination of the gold content, trace metals were also identified and quantified, which proved helpful in formulating hypotheses about the gold's origin, whether primary or secondary, and the place where the coins were buried.

The second study, published in 2022 in the journal Scientific Reports, involved a collaboration between the Department of Chemical and Pharmaceutical Sciences at the University of Trieste and Elettra Sincrotrone Trieste. Using techniques that exploit synchrotron light (SR−XRF and SR−XANES), four coins were thoroughly examined. Even we are aware that this is a limited sample, it serves as the first step towards extending similar investigations to the dozens of 4th– and 5th–century solidi available at the Department of Humanities at the University of Trieste. Thanks to the very low detection limits, the SR−XRF technique provided insights into the alloy composition and surface patina found in one of the four coins selected for analysis. In addition, certain regions of interest were analysed using the XANES technique. The results of this investigation provided information on the site where the coins were unearthed, offering further understanding of their history over the centuries.

1. A multi−technique preliminary study of 49 gold solidi from the Late Antique period (4th–6th century AD)

Abstract

The aim of this study is to investigate 49 gold solidi issued between the 4th– and 6th–century AD in order to determine their overall chemical composition. Since this was a preliminary study, readily available laboratory techniques were employed. Initially, the coins were catalogued, measuring their mass, diameter, and thickness. Subsequently, all 49 specimens underwent non−destructive analysis using μ−EDXRF to identify the main elements, upon which more sensitive analyses were performed for their quantification. Leveraging the availability of a gold standard, a semi−quantitative fineness analysis of the coins was performed. To validate these results, six coins were randomly selected and micro−sampled. The obtained material was dissolved in aqua regia (3:1 HCl:HNO_3), heated, and sonicated to facilitate dissolution. The resulting solutions were then analysed using ICP−AES to determine the gold percentage, and ICP−MS for trace elements quantification. The non−destructive analysis revealed consistently high average gold percentages in all 49 solidi, and no forgeries were detected, confirming the widespread use of this noble metal during the studied period. Two distinct groups were identified based on the Pt/Pd ratio, which likely have different sources of gold. A comparison of the results obtained from the two techniques used for gold content quantification showed that XRF produced higher values than ICP−AES, except for coin No. 5. An analysis of variance conducted on the two sets of data led to the conclusion that the results are significantly different, indicating that the surface of the six micro−sampled coins does not represent the bulk composition. Trace elements analysis revealed low concentrations of Cu, Sn, and Pb, suggesting that the gold used to mint the studied coins was likely alluvial gold. Furthermore, the relative amounts of the terrigenous elements and their correlation imply that the burial site of the coins is soil, ruling out metallic or ceramic canisters.

1.1 Introduction

One of the first metals used by man in antiquity was gold. Due to its ductility and easy availability, the earliest gold artefacts can be dated to 4,400−4,100 BC. The "Golden Treasure of Varna" in Bulgaria is considered the oldest processed gold object in the world, dating back to the period of the Varna Culture of the Chalcolithic (Eneolithic, Copper Age). This extraordinary discovery has also allowed us to learn more about the development of gold metallurgy, which, along with copper metallurgy, can be dated to the beginning of the 5th century BC (Leusch et al., 2015).

Gold can be extracted from quartz veins or found in secondary deposits (placers) formed as a result of natural phenomena. The latter were widely exploited by humans, as alluvial gold could be easily obtained by panning and washing (Guerra and Calligaro, 2003).

In the Western world, the earliest evidence of coinage seems to date back to the beginning of the 8th century BC in the eastern Mediterranean. Due to the ancients' difficulties in separating gold from silver, the first coins were made of electrum – a natural alloy composed of three parts of gold and one part of silver (Kemmerer, 2009). The composition of the archaeological finds from the Sardis excavations and the Lydian gold coins struck by Croesus (561−546 BC) suggest that gold purification was already known and adopted around the 6th century BC (Guerra and Calligaro, 2003).

Therefore, the study of ancient coins is important for gathering information on their place and period of minting, the historical context, and trade. In particular, the determination of the gold content provides the fineness of the coins, while the identification and quantification of major and minor elements can indicate their debasement (Guerra, 1995). Furthermore, trace elements associated with gold can be used as fingerprint of its original source. As metallurgy evolved, the ancients developed new techniques for separating and purifying gold, resulting in the loss or oxidation of the major contaminating elements. Among the elements affected by these processes, platinum and palladium may still be characteristic of gold ores due to their very high melting points (Guerra and Calligaro, 2004). In particular, platinum is associated with native gold and, for this reason, is commonly used as tracer for the provenance and manufacture of the precious metal (Van Loon et al., 2018).

In this work, 49 Late Antique gold coins issued in the mints of Constantinople, Thessaloniki, and Ravenna were analysed non−destructively and micro−invasively.

The term solidus, which was already in common use in the Republican and Late Antiquity periods, meant “pure”, mainly in reference to precious metals. Solidus was introduced by the emperor Constantine in 312 AD. It was minted at 1/72 of a Roman pound (i.e., an individual weight of about 4.55 g) and served as the primary gold coin of the late Roman Empire, leading to the regularisation and rationalisation of gold circulation in the Empire (Carlà, 2009). The shape and weight of this coin remained essentially unchanged at the main mint of Constantinople until the reign of Nicephorus (963−969 AD) (Oddy and La Niece, 1986). From 317 AD onwards, there was a decline in the gold content, followed by a rapid increase between 364 and 367 AD to a maximum of 94.7%. In parallel with the decrease in fineness, there was an increase in platinum content occurred in the 4th century: in Constantinian coins, its content was 45 ppm, which increased to 900 ppm after 368 AD and stabilised at 400 ppm in the 5th century. In addition to platinum, the amounts of silver and copper also changed, although the fineness remained the same. This is evident in the first issue of Anastasius (491−492 AD), which contained 99.2% gold, 0.73% silver, and 0.04% copper, but the following two issues (492−507 AD and 507−518 AD), as well as those of Justinian and his successors, contained about 1.4% silver and up to 0.5% copper (Morrisson, 1982).

In this preliminary work, the aim is to determine the quantity of the main metal in order to highlight any changes over time, as well as to identify minor and trace elements. Several analytical techniques can be used for this purpose in the case of gold coins. Non−destructive techniques are always preferred, although micro−destructive chemical analysis offers better precision and reproducibility. Given the high historical and economic value of the coin specimens under study, the visual appearance of the sample must not be altered in any way. Therefore, micro−sampling was carried out on the edge of six coins, selected using the blind method to avoid investigator’s bias.

Moreover, since corrosion processes are not prominent in gold alloys with a high gold content, it can be stated that the composition of the surface does not differ much from that of the bulk, and the surface methods provide information on the entire sample (Sándor et al., 2003). By comparing the results obtained with the two techniques, we will try to confirm this hypothesis.

This study, made possible thanks to the collaboration between the Department of Chemical and Pharmaceutical Sciences and the Department of Humanities at the University of Trieste, concerns 49 gold coins − 47 solidi and 2 tremisses – allegedly found

in a hoard in the Balkan area. First, the physical parameters of each coin − weight, diameter, and thickness − were measured. Then, all coins were analysed using the non−destructive technique (μ−EDXRF) to identify the main elements upon which the subsequent micro−destructive analysis could be focused. The latter was conducted on only six specimens (see Table 1) and was based on acquiring a bulk sample by removing a few milligrams of material from the edge of the coins (Crosera et al., 2019; Marussi et al., 2022). Subsequently, the micro−sampled material was dissolved in aqua regia, made with ultra−pure hydrochloric acid (3 vol) and ultra−pure nitric acid (1 vol). Inductively Coupled Plasma−Atomic Emission Spectroscopy (ICP−AES) was used to quantify the main metal, while Inductively Coupled Plasma−Mass Spectrometry (ICP−MS) was employed in the quantification of minor elements – all of which were less than 1% of the total mass.

Table 1: The six coins micro−sampled with their respective codes and issuing emperors.

		
Solidus no.1, Arcadius (395 – 408 AD)	Solidus no.5, Theodosius II (408 – 450 AD)	Solidus no.12, Arcadius (395 – 408 AD)
		
Solidus no.36, Valentinian III (425 – 455 AD)	Tremisses no.42, Theodosius II (408 – 450 AD)	Solidus no.45, Theodosius II (408 – 450 AD)

1.2 Results and discussion

1.2.1 Preliminary non−invasive investigation by μ−EDXRF

The measurement of the physical characteristics showed good uniformity and conservation of the samples. The measured masses ranged from 4.22 to 4.54 g, with an average of 4.39 g, which is very close to the theoretical value of 4.50 g (Carlà, 2009). The

two tremisses also had an average mass of 1.49 g and 1.50 g, exactly one−third of the value found in the solidi, confirming the data in the literature (Gennari, 2018).

The 49 gold solidi investigated were qualitatively analysed by μ−EDXRF spectroscopy to determine the elements present, which guided the subsequent micro−destructive analysis. For each solidus analysed, four measurements were performed, two on the recto, presenting the emperor's face, and two on the verso.

The spectra obtained were almost all superimposable, except for the coins with evident surface concretions. These, in fact, exhibited a distinct calcium Kα peak (3.69 keV) and a lower intensity of the characteristic gold lines. Other elements, probably related to the burial site, were identified in some coins: K, Mn, Ti, V, and Zn (Marussi et al., 2023).

Thanks to the availability of a 99.9% pure gold standard that had undergone satin−finishing and pickling processes, it was also possible to perform a semi−quantitative analysis of the fineness of the coins. As these gold coins are well−preserved, it can be assumed that the surface is representative of the entire sample (Cataldo et al., 2022). We only considered the Lα line of Au at 9.67 keV, as it is more intense and better resolved.

By comparing the peak areas of the coins with those of the standard, we gained the results shown in Figure 1. The solidi are grouped according to emitter. The gold content for all 49 coins remains very high (>97%), confirming previous studies that until the end of the 9th century, the gold coinage of Constantinople was not debased and consisted of almost pure gold (Oddy, 1988).

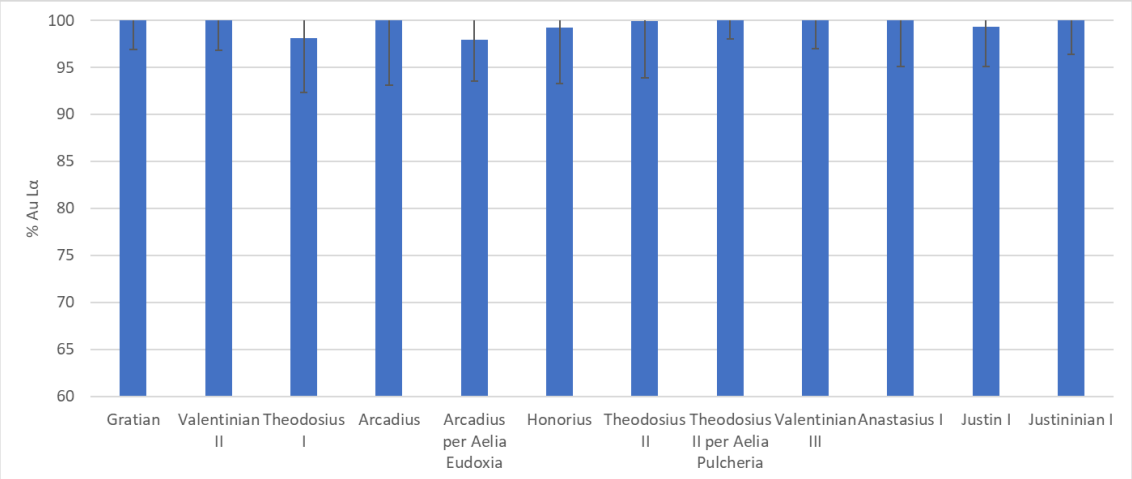

Figure 1: The gold content obtained from the ratio of the Lα gold peaks of the coins and the standard. Percentages greater than 100% are reported equal to 100%. Standard deviations are expressed as error bars.

The peak areas of copper, silver, palladium, and platinum, as well as the ratios between these elements, were also calculated.

Archaeometallurgical experiments have shown that the Pt/Au and Pd/Au ratios remain unchanged when the gold−based alloy is melted, cupeled, and then cemented. For this reason, platinum and palladium can serve as relevant tracers for studying the provenance of gold (Blet−Lemarquand et al., 2017). Considering the Pt/Pd ratio, two distinct groups were observed: one consisting of 36 coins with an average ratio of 3.1±0.4, and the other group with an average Pt/Pd ratio of 7.5±0.5, consisting of 10 solidi. Three coins (No. 13, 36 and 46) were not considered in this discussion, as they exhibited comparable Pd peaks within the background noise of the instrument. The result obtained is quite interesting because it suggests that the two batches of coins, although they came to us together, might have different origins. Graphically, these two groups are shown in Figure 2. Unfortunately, apart from the Pt/Pd ratio, there is no further information available to classify the coins.

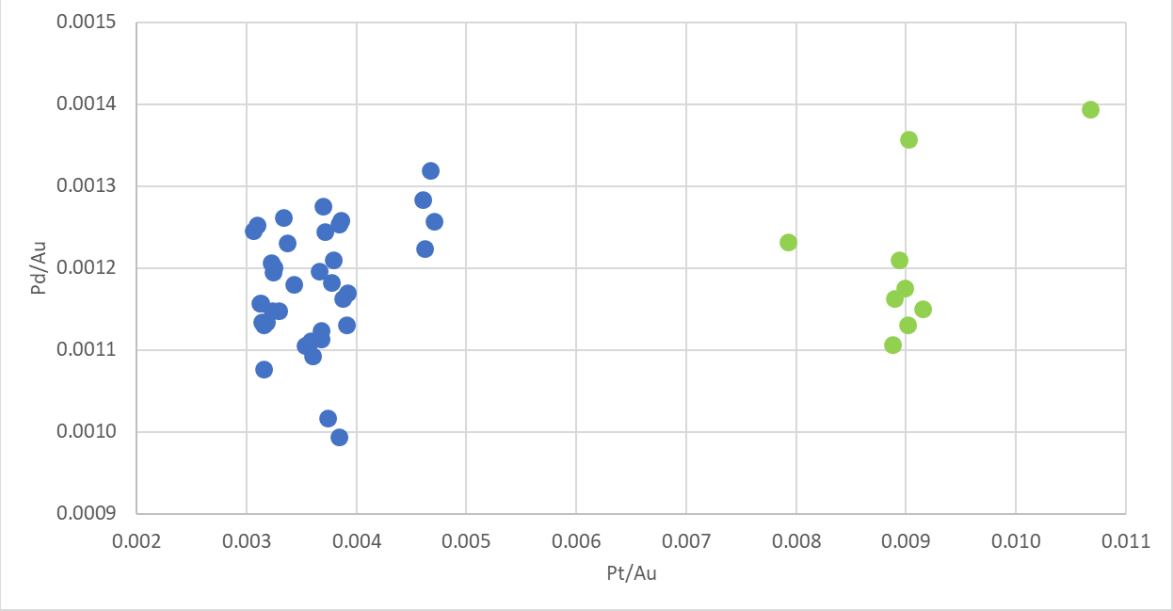

Figure 2: Platinum and palladium contents normalised to gold for all the 49 coins under study. In blue are highlighted the solidi with an average Pt/Pd ratio of 7.5, while in green those with an average ratio between the two elements of 3.1.

1.2.2 Determination of the fineness of solidi by means of ICP−AES

Six randomly selected coins were micro−sampled by cutting their edge with a professional cutter and taking a few mg of sample. The fragments obtained were dissolved

in aqua regia and analysed with Inductively Coupled Plasma−Atomic Emission Spectroscopy to quantify the gold content of these coins. Specifically, these were five solidi and one tremissis. The results obtained from this analysis are shown in Table 2. As can be seen, the fineness of the investigated coins is generally very high, as also suggested by the inscription "OB" engraved on the verso next to the mintmark. The inscription "OB" was introduced as early as 368 AD, during the reigns of Valentinian I and Valens, to indicate that the solidi were made of pure gold, precisely "obryzum" (Sear, 2014).

Table 2: The average gold percentage for the six coins subjected to micro−sampling.

Coin	Emperor	Period of issue	Mint	Dissolved mass (mg)	% Au ICP−AES	RSD%
No. 1	Arcadius	395−408	Ravenna	7.4	97.5	0.5
No. 12	Arcadius	395−408	Constantinople	7.8	94.6	0.6
No. 5	Theodosius II	408−450	Thessaloniki	7.2	100	0.5
No. 42	Theodosius II	408−450	Constantinople	8.3	96.9	1.5
No. 45	Theodosius II	408−450	Constantinople	8.1	96.3	2.8
No. 36	Valentinian III	425−455	Ravenna	5.8	97.8	0.6

Analysing the values presented in Table 2, one can clearly deduce that the gold percentages obtained for the Constantinople mint are the lowest. This contrasts with the findings of Miškec (2021), who stated that solidi minted in the western mints contained slightly less gold than those in the eastern ones, which were nearly 99% pure gold. Unfortunately, there are not many studies in the literature on coins of this type and age. Biborski and Biborski (2019) studied a solidus of Theodosius II, revealing a gold content of 99.16% on the recto and 99.20% on the verso, along with a silver content of 0.65% and 0.62%, respectively. Regarding Valentinian III's solidus, Kent (1994) indicated that his later coins contained just over 96% pure gold. Therefore, it could be assumed that the specimen analysed in this study may be one of Valentinian III's earliest issues.

1.2.3 Determination of trace elements with ICP−MS

In order to quantify trace elements, an analysis using Inductively Coupled Plasma−Mass Spectrometry was also carried out. The concentrations obtained, expressed in mg kg^{-1},

are provided in Table 3. Concentrations are reported concerning the mass of material sampled and dissolved. The fact that copper is present in percentages lower than 2% may suggest that the gold used to make the coins in this study is natural gold, a notion further supported by the low concentrations of tin. As indicated by Dube (2006), the presence of Sn should be related to cassiterite (SnO_2), which is often found alongside gold in placers. Indeed, during the atmospheric melting of the nugget containing cassiterite, the latter is reduced to metallic tin, which becomes part of the liquid phase of the primary gold (Morteani and Northover, 2013). Therefore, the presence of small amounts of this element could be considered indicative of alluvial gold (Constantinescu et al., 2010). Further evidence for the origin of the gold is provided by the low concentrations of lead found (Schlosser et al., 2012).

Table 3: Average content of trace metals expressed in mg kg^{-1} for the six coins selected for the ICP−MS analysis.

Coin number	Emperor	Ag	Cu	Pt	Pd	Hg	Pb	Sn	Ni	Al	Ca	Ti	Cr	Mn	Fe	Zn	Sr
1	Arcadius	1162	99.1	39.4	2.53	60.0	3.94	137	276	4.16	54.0	2.50	471	39.6	2539	1.44	<0.64
12	Arcadius	1627	134	449	14.4	1.06	30.8	50.8	23.0	4.26	35.3	2.44	<1.24	2.58	266	3.66	<0.64
5	Theodosius II	11514	2219	151	23.1	5.30	81.3	19.7	47.4	61.2	1854	3.07	30.5	12.6	879	50.2	11.2
42	Theodosius II	2077	514	261	8.32	0.61	153	35.0	10.6	2.87	32.7	2.22	<1.24	13.9	1734	15.1	<0.64
45	Theodosius II	5479	422	384	21.2	4.79	31.6	41.8	20.8	54.3	2104	2.42	24.6	21.6	1589	32.3	12.8
36	Valentinian III	2235	1190	248	28.9	1.18	25.3	10.1	1298	<1.72	77.6	1.07	1822	144	9660	4.28	0.992

The concentration of mercury was found to be around 60 mg kg^{-1} in coin No. 1. However, the high gold content found in this coin by ICP−AES and its proximity to theoretical mass rule out surface gilding and confirm that coin No. 1 is not a forgery (Habashi, 2016; Reiff et al., 2001).

While XRF analysis identified two distinct groups of coins based on the Pt/Au and Pd/Au ratios, suggesting two different origins for the main metal, destructive analysis did not reveal any significant trends in the quantification of these elements. This is likely because the sample size chosen for the micro−destructive analysis (six coins) may be too small to draw conclusions and identify a trend for these two elements. Nevertheless, it can be stated that the Pt content consistently exceeds the Pd content.

Ancient coins are typically buried in the ground for extended periods before discovery. Consequently, some characteristic elements of the soil have also been quantified: Al, Ca, Ti, Cr, Mn, Fe, Ni, Zn, and Sr. Iron and nickel, in particular, can be related to the coin alloy or surface contamination, given their abundance in nature (Allouch et al., 2022). Bivariate analysis was performed on these elements (Table 4). The correlations observed between Cr, Mn, Fe, and Ni confirm that iron and nickel have a terrigenous origin, as well as Zn, which positively correlates with Ca, Al, and Sr. The case of titanium, which exhibited a negative correlation with calcium and strontium, is noteworthy.

Table 4: Correlation matrix for the bulk data set (bivariate analysis) for the terrigenous elements. Values greater than 0.5 or lower than −0.5 are in bold.

	Ni	*Al*	*Ca*	*Ti*	*Cr*	*Mn*	*Fe*	*Zn*	*Sr*
Ni	1.000								
Al	– 0.415	1.000							
Ca	– 0.359	**0.986**	1.000						
Ti	**– 0.879**	**0.597**	0.498	1.000					
Cr	**0.998**	– 0.431	– 0.374	**– 0.873**	1.000				
Mn	**0.993**	– 0.371	– 0.302	**– 0.885**	**0.993**	1.000			
Fe	**0.986**	– 0.397	– 0.325	**– 0.909**	**0.985**	**0.996**	1.000		
Zn	– 0.413	**0.943**	**0.898**	**0.587**	– 0.438	– 0.377	– 0.382	1.000	
Sr	– 0.335	**0.983**	**1.000**	0.476	– 0.350	– 0.277	– 0.301	**0.894**	1.000

1.2.4 Comparison of surface and bulk results obtained with the two different techniques

In their study, Cruz et al. (2013) analysed a single gold solidus minted by Valentinian I. Their primary aim was to investigate the potential enrichment of gold on the coin's surface. Employing electrical conductivity measurements, Cruz et al. demonstrated that the core of the coin had a lower gold content than its surface.

This finding prompted us to compare the results obtained from the two analytical techniques employed in our study, μ−EDXRF and ICP−AES, to determine if the surface could be considered representative of the entire sample. It is worth noting that in the case of gold, XRF has a penetration depth ranging from 8 to 60 μm (Guerra, 2018), while ICP−AES provides a more comprehensive analysis encompassing both the bulk and surface of the coin.

Figure 3 shows the main results of this comparison for the six coins subjected to micro−sampling. Specifically, when calculating the gold content based on the Lα emission line, it becomes evident that the assumption of Cruz et al. holds true, with one exception: coin No. 5. Remarkably, this coin exhibited an inverse behaviour, displaying a higher gold content with ICP−AES analysis compared to XRF analysis. Furthermore, coin No. 5 also has the highest silver content and a notable concentration of copper. This observation raises the possibility that the dissolution of these more reactive metals in the burial environment did not occur, and thus, the surface depletion of silver and copper, which contributed to an overestimation of the surface gold content, did not take place.

One-way analysis of variance (ANOVA) was employed to compare the results obtained from the two techniques. By considering the ICP−AES results more reliable, given the robustness of the technique compared to X−ray Fluorescence, ANOVA led us to conclude that the information provided by the non−destructive technique slightly differed ($p=0.093$) from that obtained through the micro−destructive technique. The Bland-Atman analysis also showed a mean difference of 2.64% and a 95% limit of agreement in the –5.11∼10.39 %. Accordingly, we can conclude that X−ray Fluorescence overestimated the Au % with respect to ICP−AES. However, based solely on the analysis of the six samples examined using both techniques, it cannot be definitively asserted that the surface is representative of the entire bulk.

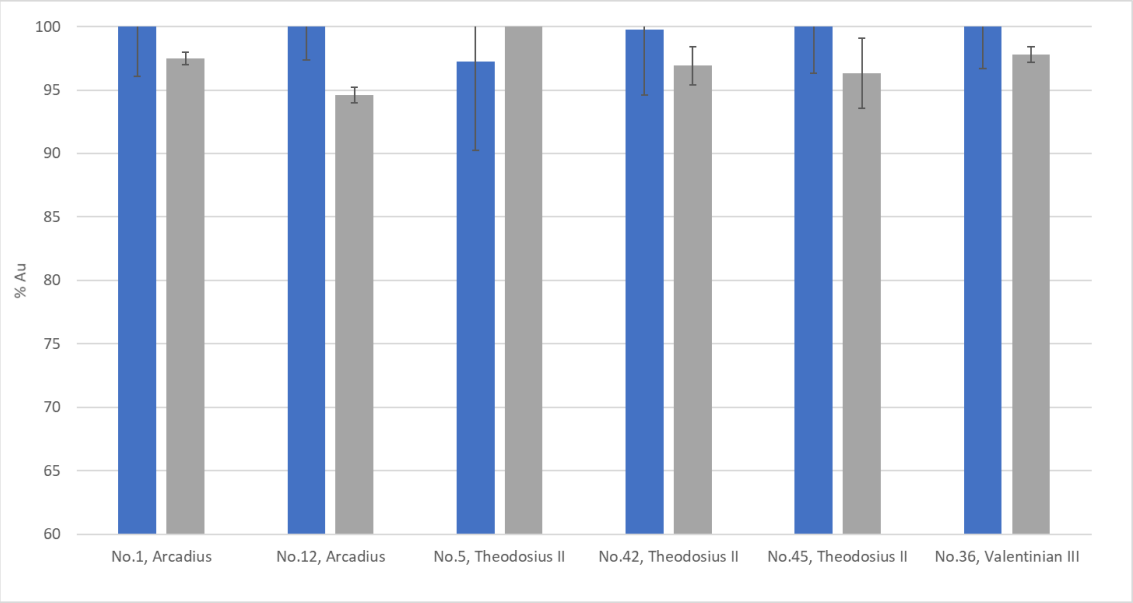

Figure 3: Average gold percentage obtained by μ−EDXRF in blue and by ICP−AES in grey. Percentages greater than 100% are reported equal to 100%. Standard deviations are expressed as error bars.

1.3 Material and Methods

1.3.1 Chemicals and Apparatuses

All chemicals utilised were of analytical quality. Nitric acid (with a concentration of 67–69% v/v) and hydrochloric acid (with a concentration of 30% v/v) were sourced from VWR (Milan, Italy). Water conforming to reagent grade standards was generated using a Millipore purification pack system (MilliQ water from Millipore, Burlington, MA, USA). To establish calibration curves for ICP−AES and ICP−MS analyses, it was necessary to dilute multi−standard solutions (initially at 10 mg L^{-1}) for ICP analyses. These multi−standard solutions were supplied by Sigma−Aldrich (Saint−Louis, MO, USA), and included Periodic Table MIX 1 and Periodic Table MIX 2. The elements subject to examination included Au, Ag, Cu, Pt, Pd, Sn, Pb, Hg, Al, Ca, Fe, Ti, Sr, Cr, Mn, Ni, and Zn.

For micro−destructive analysis, small flakes were taken from the edge of the coins using a professional cutter. The collected material was weighed using an analytical weigh scale (Sartorius Series CPA225D) with a capacity of 220 g, a readability of 0.01 mg, linearity ≤0.03 mg, standard deviation ≤0.02 mg, and a stabilization time of ≤6 s. Furthermore, with the assistance of Vernier callipers, the diameter and thickness of each coin were measured at three different points.

The semi-quantitative analysis was carried out using a gold sample of 99.9% purity, measuring 4.0 x 4.0 x 0.52 mm, weighing 0.2 g and subjected to satin-finishing and pickling processes. It was prepared especially for this study by a goldsmith technician.

1.3.2 µ−EDXRF

For non−invasive analysis, we employed an ARTAX 200 micro−XRF spectrometer (provided by Bruker Nano GmbH in Berlin, Germany). This instrument is equipped with an air−cooled Mo X-ray fine focus tube (maximum 50 kV, 1 mA, 40 W), which is controlled by a compact high−voltage generator unit and features a 650 µm collimator. Additionally, it has a Peltier−cooled XFlash® silicon drift detector with 10 mm^2 of active area and an energy resolution of <150 eV for Mn–Kα at 100 kcps. A CCD camera with 500 × 582 pixels is integrated for sample positioning. The instrument's focal spot measures 1.2 × 0.1 mm^2, offering a lateral resolution of 0.2 mm, and it includes a 100 µm beryllium window.

We utilised the ARTAX control semi−quantitative XRF software (version 5.3.14.0, licensed by Bruker AXS Microanalysis GmbH, Berlin, Germany) for both hardware control and the evaluation of analytical data. Data were represented in the form of counts per second (cps) versus energy (keV). In our analyses, the instrumental settings were configured as follows: X-ray tube = 30 W, Mo target voltage U = 50 kV, current I = 700 µA, and an acquisition time of 60 s (live time). The collimator was set at 650 µm in an air environment. The elements examined included Au (line: Lα1 9.71 keV), Ag (line: Kα1 22.16 keV), Cu (line: Kα1 8.05 keV), Pd (line: Kα1 21.18 keV), Pt (line: Lγ1 12.93 keV), Fe (line: Kα1 6.40 keV), Ni (line: Kα1 7.48 keV), Sr (line: Kα1 14.16 keV), and Ca (line: Kα1 3.69 keV).

Four spectra were acquired for each coin, consisting of two on the obverse (recto) and two on the reverse (verso).

1.3.3 Sample Preparation

Since ICP−AES and ICP−MS analyses are in liquid phase, sampling is necessary. The material was removed with a professional cutter along the edge of the coin to prevent damage to the coin faces (Crosera et al., 2019; Marussi et al., 2022). The flakes obtained

(about 7 mg) were collected in weighing boats in polystyrene and weighed, dissolved in aqua regia (3:1 HCl:HNO_3 mixture), and heated overnight to facilitate the dissolution. The solutions were then appropriately diluted in a 100 mL volumetric flask (class A) with MilliQ water for subsequent analyses.

1.3.4 ICP−AES

The primary alloy element, gold (Au), was quantified by analysing sample solutions using an ICP−AES spectrometer (PerkinElmer® Optima™ 8000, Waltham, MA, USA).
Calibration, which was linear within the concentration range of 0.1–10 mg L^{-1}, was conducted following the dilution of a multi−standard solution with an initial concentration of 10 mg L^{-1} for ICP analysis (Periodic Table Mix 2 for ICP TraceCERT®, Sigma−Aldrich). The limit of detection (LOD) for the solution samples at the operating wavelength (242.795 nm) was 0.02 mg L^{-1}. The coefficients of variation for repeatability (RSD %) were determined to be less than 5%.

1.3.5 ICP−MS

Trace metal concentrations were determined using Inductively Coupled Plasma−Mass Spectrometry (ICP-MS). The NexION 350x Spectrometer from PerkinElmer (Waltham, MA, USA) equipped with an ESI SC autosampler, was employed to quantify the amounts of Ag, Cu, Pt, Pd, Sn, Pb, Hg, Al, Ca, Fe, Ti, Sr, Cr, Mn, Ni, and Zn. The analysis was conducted in KED mode (Kinetic Energy Discrimination), with ultra−high purity helium (at a flow rate of 4.8 mL min^{-1}) used to prevent interference caused by cell−formed polyatomic ions.
Calibration of the instrument, which was linear within the concentration range of 0.5–100 µg L^{-1}, was carried out following the dilution of a multi−standard solutions initially at a concentration of 10 mg L^{-1} for ICP analysis (Periodic Table Mix 1 for ICP TraceCERT® and Periodic Table Mix 2 for ICP TraceCERT®, Sigma−Aldrich). The composition of the samples was determined using the calibration curve method obtained by analysing standard solutions. The limits of detection (LOD) for each element were as follows: Ag 0.02 µg L^{-1}, Cu 0.20 µg L^{-1}, Pt 0.005 µg L^{-1}, Pd 0.005 µg L^{-1}, Sn 0.07 µg L^{-1}, Pb 0.06

μg L^{-1}, Hg 0.01 μg L^{-1}, Al 0.10 μg L^{-1}, Ca 1.2 μg L^{-1}, Fe 1.5 μg L^{-1}, Ti 0.05 μg L^{-1}, Sr 0.05 μg L^{-1}, Cr 0.10 μg L^{-1}, Mn 0.03 μg L^{-1}, Ni 0.20 μg L^{-1}, and Zn 0.09 μg L^{-1}.

1.3.6 Data analysis

The analytical similarity and possible systematic differences between the two methods were estimated statistically. One-way Analysis of Variance (ANOVA) for repeated measurements and Bland-Altman analysis were performed within the R software environment for statistical computing and graphics (R version 4.1.2 "Bird Hippie"), on a commercially available workstation (x86_64-apple-darwin17.0 64-bit).

1.4 Conclusions

Thanks to the availability of a gold standard, it was possible to semi−quantitatively determine the gold content in all 49 Late Antique gold solidi. The results obtained from non−invasive analysis with μ−EDXRF showed that no minting debasement occurred during the period when the coins under study were issued (367−565 AD). Furthermore, no forgeries were found, confirming that in the 4^{th}–6^{th} centuries, the Roman Empire had a high availability of gold for minting coins. The Pt/Pd ratio is indicative for obtaining more information about the origin of gold, as these two elements are not affected by the metallurgical processes used in coins production. By comparing the area of the non−interfering peaks Lγ1 of Pt and Kα1 of Pd, two groups of coins, consisting of 36 and 10 coins, respectively, were distinguished. Out of the total of 49 solidi, three coins did not show the characteristic palladium peaks.

The specimens of this study held high historical value, which is why micro−destructive analyses were performed on only six coins, selected using a blind method to avoid experimenter's bias. A few milligrams of samples were collected from the edges of the coins. Although the sampling method used had some limitations due to the scarcity of material obtained, it provided representative samples of the gold solidi under study for the purpose of quantifying the principal metal and trace elements.

Inductively Coupled Plasma−Atomic Emission Spectroscopy provided the gold content of the six coins subjected to micro−sampling. Although very high, the gold contents found for the coins minted in the Constantinople mint were the lowest.

The ANOVA test applied to the results obtained from the investigation with μ−EDXRF and ICP−AES showed that the information achieved by the two techniques was not equal. In particular, the semi−quantification carried out with X−Ray Fluorescence was consistently higher (except for coin No. 5) than that obtained with ICP−AES, suggesting that surface enrichment may have occurred in the six specimens analysed using the two techniques.

Regarding trace elements, quantified by ICP−MS, the presence of tin and the low concentrations of copper and lead suggest that the gold used to produce the six analysed coins had alluvial origin. The Pt/Pd ratios obtained by the micro−destructive technique did not show any particular trend, perhaps due to the limited number of samples chosen for sampling. In any case, the analysis and quantification of the main terrigenous elements showed positive correlations between Cr, Mn, Fe, Ni, and between Ca, Al, Sr, leading to the conclusion that the burial site of the coins was the soil.

2. Combining synchrotron radiation techniques for the analysis of gold coins from the Roman Empire

Ilaria Carlomagno[1]*, Patrick Zeller[1,4,5], Matteo Amati[1], Giuliana Aquilanti[1], Enrico Prenesti[2], Giovanna Marussi[3], Matteo Crosera[3], Gianpiero Adami[3]

[1] Elettra − Sincrotrone Trieste, Trieste 34149, Italy

[2] Dipartimento di Chimica, Università di Torino, Torino, Italy

[3] Dipartimento di Scienze Chimiche e Farmaceutiche, Università di Trieste, Trieste, Italy

[4] Present address: Helmholtz−Zentrum Berlin für Materialien and Energie GmbH, BESSY II, Berlin, Germany

[5] Present address: Dept. Inorganic Chemistry, Fritz−Haber−Institut der Max−Planck−Gesellschaft, Berlin, Germany

Published on *Scientific Reports*, https://doi.org/10.1038/s41598-022-19682-8

*Corresponding author:

Ilaria Carlomagno

Elettra−Sincrotrone Trieste S.C.p.A., Basovizza, 34149 Trieste, Italy

email: ilaria.carlomagno@elettra.eu

Abstract

Four gold coins minted in the V century have been studied with non−destructive synchrotron radiation techniques, namely X−Ray Fluorescence (XRF) and X−ray Absorption Near Edge Spectroscopy (XANES). XRF data analysed coupling standard and statistical methods were used to distinguish the composition of the alloy constituting the coins from that of successive deposits processes. Our analysis presents a quantification of the trace elements present in the metallic alloy providing interesting details for historical insight. Furthermore, on the basis of the XRF maps, some regions of interest were selected for XANES at the K−edge of Fe. Our analysis of the Fe spectra points out two main phases which can be related to Fe oxides naturally present in soil. From the relative abundance of these oxides, information on the site where the coins were found can be obtained, providing additional information on their fate across the centuries.

2.1 Introduction

X−rays, being a non−destructive probe, are an excellent tool for the investigation of delicate, fragile, and valuable samples. This is certainly the case of ancient gold coins which, besides the intrinsic value due to the precious materials they are made of, have also a high historical worth.

Among the X−ray based techniques, X−Ray Fluorescence (XRF) is widely known in the cultural heritage community as an efficient way to analyse elements distribution and quantification (Janssens et al., 2000b). Synchrotron Radiation (SR) sources, offering high photon flux and energy tunability, are suitable for achieving a superior degree of accuracy in XRF trace elements analysis with respect to laboratory sources (Adams et al., 1998). However, this hardly compensates for the relatively difficult access to the facilities (long proposal preparation process and low acceptance rates) and for the limited time available for measurements, which prevents from analysing a high number of pieces typically involved in numismatics studies. On the other hand, SR offers the possibility of carrying out XRF at different energies, which can be useful to enhance the sensitivity to certain elements and to shed light on identifying the presence of a given element in case of emission lines overlap. A far more interesting advantage of SR is that many beamlines are capable of applying different techniques at once permitting a multimodal and full characterization of the samples in the same conditions. This is the case of the XRF beamline at Elettra synchrotron in Trieste, Italy (Jark et al., 2014), where we have performed not only XRF, but also X−ray Absorption Near Edge Spectroscopy (XANES) measurements. XANES, among other information, assesses the local chemical environment and oxidation states of the elements which has been proven relevant for a wide variety of applications in cultural heritage (Farges and Cotte, 2016).

The aim of this work is to describe a methodological strategy based on advanced analytical synchrotron techniques coupled with a statistical data analysis approach to find minor differences and give useful information to the historians on several aspects of ancient civilizations. On the XRF maps, collected with a spatial resolution of 100 µm, we apply a statistical analysis to disentangle the contributions coming from the metallic alloy from those due to the overlayer. In that way, not only do we obtain information on the metallic alloy, but we also have an insight on the accumulated debris, yielding details ranging from the Au minting process to the source of the gold, to the area of conservation of the artefacts. On the basis of the XRF maps, a few areas of the coins were selected for

XANES measurements at the Fe K−edge. From the investigation of the dirt accumulated in the hollow regions, we could characterise the Fe compounds deposited during the burial period. Through the identification and quantification of Fe oxides present in the sample, the burial area could be hypothesized based on the environmental conditions corresponding to the oxides presence in soils (Bigham et al., 2002).

2.2 Results

2.2.1 XRF analysis

In this section, we present the results obtained on one sample, but the same procedure described here was applied to all of them.

The XRF measurements were collected in a small region (about $2 \times 2 mm^2$) of the obverse of the coins (for a detailed description of the samples, see "Samples" section, for the XRF maps of the coins, see the Supplementary materials, Fig. S1). For each coin, the area selected for the XRF map was raster scanned collecting the total fluorescence emission for each pixel (See Fig. 1a, b and c). The cumulative XRF spectrum is obtained by summing up the contribution of all the pixels. From the XRF cumulative spectrum of each coin, we could identify the emission peaks of several elements reported in Table 1.

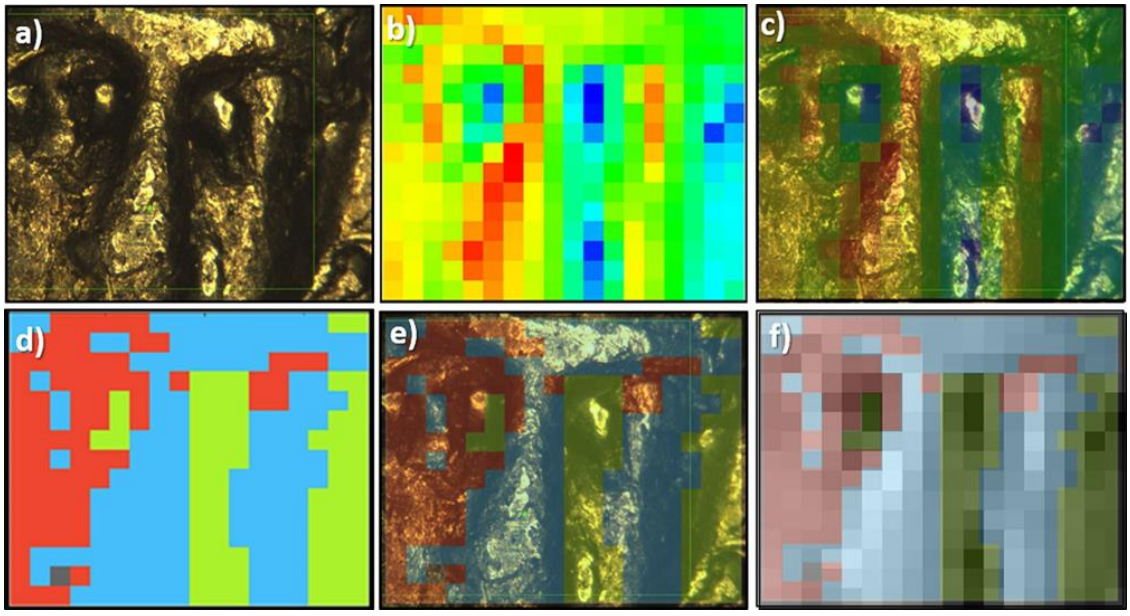

Figure 1: (a) Optical image of coin B, where the XRF map was collected, (b) fluorescence emission induced with an exciting beam of 10 keV in the area shown in panel a: the emission energy range corresponds to the Au M lines, the intensity follows a temperature scale, (c) superposition of panels (a) and (b), (d) the three groups found in the t−SNE analysis: blue for G1, red for G2, green for G3, (e) superposition of panel (a) and (d), and (f) superposition of panel d and a grey scale version of (b).

Table 1: Elements identified by XRF analysis divided between metallic alloy and dirt.

Alloy	Dirt
Pd, Ag, Pt	Mg, Al, Si
Au, Hg, Pb	P, S, Cl, K
	Ca, Ti, V
	Cr, Mn, Fe
	Ni, Cu, Zn

The beam size with which the XRF maps were collected 100 x 100 μm^2 is a good compromise to achieve fast measurements with a spatial resolution being good enough to correlate the elements distribution with the topography of the coin. In addition, their spatial distribution contains the key information to distinguish the evenly distributed components of the metal alloy from the materials deposited on the coin surface during the burial period, accumulated in indented areas. To classify each element in one of the two categories based on the topography, we used the t−distributed stochastic neighbour embedding (t−SNE) algorithm (Mihalić et al., 2021) available in the Orange software (Demšar et al., 2013) (see "t−SNE" section).

The t−SNE analysis returned the plot shown in Fig. 2a in which three distinct groups could be identified: G1 (blue points), G2 (red points), and G3 (green points). G1 and G2 are both located in the top left part of the plot and are closer to each other than to G3, lying in the bottom right part of the plot instead. The fluorescence spectra corresponding to the pixels of the same group were summed up and are shown upon normalization to the Au emission peak at 2.1 keV in Fig. 2b. Noticeably, two of the three spectra (G1 and G2) are rather similar to each other, suggesting that they could be considered as a single group.

As a further element to validate this choice, their spatial distribution was considered. It is presented in Fig. 1d and for sake of comparison it is shown overlapped with the optical image (Fig. 1e) and with a grey scale version of the XRF map (Fig. 1f). The different morphology of the three groups is evident: while G1 and G2 are associated with mostly flat areas (red and blue pixels), the other covers mostly indented areas (green, G3).

This is consistent with the different spectral features in Fig. 2b: the G3 group (green) presents a particularly high intensity in the region of K, Ca, Ti, Fe, Ni, Zn peaks. These elements, compatible with soil composition, can be attributed to the debris accumulated

in the hollows, therefore the spectra in this group were not considered for the evaluation of the alloy composition.

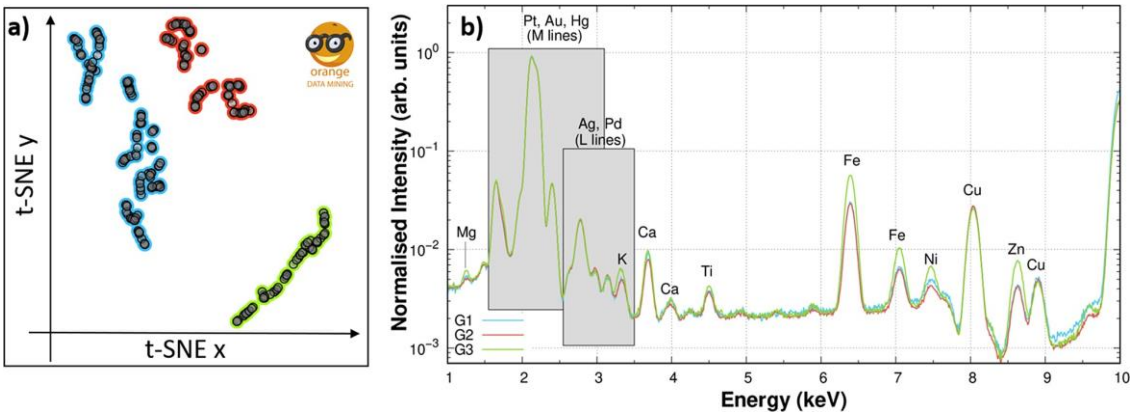

Figure 2: (a) t−SNE plot of the XRF map obtained with 10 keV on coin B. Three groups are identified: blue G1, red G2, and green G3. (b) The spectra of the three groups collected with an incident energy of 10 keV are shown upon normalisation to the Au emission peak at 2.1 keV. Each peak is identified with the element giving rise to that spectral feature.

The advantage of using t−SNE analysis with respect to an arbitrary manual selection of the pixels evaluated as the best representation of the metallic alloy is that a higher number of pixels is selected on the basis of their spectral similarity. Conversely, one would have to rely only on position−based discrimination, assuming that the safest choice includes only the pixels in the flat, even regions. The t−SNE algorithm, based on statistic−evaluated similarity, groups together a higher amount of pixels, providing better resolved spectral features and, hence, higher accuracy results.

Once the pixels distinction was done, the same pixels were selected in the 11.6 keV map and a single spectrum was obtained summing up the contribution of the "gold alloy" groups, G1+G2. This spectrum was then analysed using PyMCA (see "PyMCA" section) obtaining the results reported in Table 2.

Table 2: Average date of coinage, and concentrations (%) obtained from the best fit parameters for XRF spectra at 11.6 keV relative to the G1+G2 regions of the four coins.

Sample	A	B	C	D
Period (AD)	409	409	417	440
Au	97.8	96.2	96.2	96.1
Ag	0.1	0.4	0.3	0.8
Pt	0.1	1.0	0.9	0.7

Hg	0.1	0.5	0.6	0.5
Pd	0.2	0.2	0.2	0.2
Pb	1.0	1.1	1.1	1.2

We have to stress here that due to the large uncertainty associated with the parameters of L and M emission lines (Cohen et al., 2015; Kolbe et al., 2012), our analysis is to be considered as a semi−quantitative one. This implies that, while our results do provide insightful details on the variations among the pieces, a direct comparison with data available in literature should be avoided. This approach, far from being unreliable, is already known in literature (Calparsoro et al., 2019) and represents a viable option to compare samples characterized in the same conditions. In particular, although the absolute values cannot be directly compared to those obtained in other experiments (i.e., under different conditions), the purity of the pieces can be reliably compared below 0.5%. The main limitation of our analysis is due to the fact that the database available for L−shells calculations is affected by large uncertainties: this affects the absolute concentrations which might be off by 0.2−0.5%. However, even within this broader range, our results of Au concentrations are in agreement with the available literature (Gorghinian et al., 2013).

2.2.2 Coins fineness

One of the most studied parameters of ancient coins is their fineness, as this can provide information on economic inflation or debasement dynamics in the ancient coinage (Suspène et al., 2020). However, preliminary XRF analysis carried out with laboratory sources showed no significant differences among the pieces. This agrees with the fair amount of literature already demonstrating how the Au fineness in Roman coins was around 98% (Guest, 2008; Suspène et al., 2020). Our results show that, except sample A, which is 97.8% pure, the others have a fineness around 96%, with slightly higher amounts of Hg, Ag, and Pt compensating for the missing Au. Considering the uncertainty of the absolute value around 2% (as discussed in “XRF analysis” section), we can say that the true value is in the range 94−98%. This range was already discussed in literature and is unlikely due to any intentional debasement but, most probably, is related to lose control on the gold sources. Such sources could be old coins or jewellery, resulting into similar

fineness values (like the aurei issued by Cornificius in I century BC (Suspène et al., 2020)). Once again, we stress that although we have analysed a limited number of samples, our analysis is aimed at presenting the potentiality of a new approach based on the combination of different, complementary techniques. In particular, we combine XRF with a fine statistical analysis, trace elements evaluation, and XANES−based oxidation state study.

The quantification of trace elements can represent evidence for different supplies of gold (Gondonneau and Guerra, 2002). Identifying sources of contaminants containing these fingerprints elements is crucial for an archaeometric analysis and cannot be overlooked, however, the analysis of elements like Pt, Hg, and Pb, requires some additional care. As the fluorescence lines of these elements overlap with Au M−lines, in the case of Pt, the L emission lines are found at 2050 eV, i.e., very close to the M emission lines of Au at 2122 eV. Alternatively, to address the issue regarding the other elements, a reference spectrum collected on a pure Au foil was used. This spectrum was subtracted from the spectra of each coin. As shown in the study of Guerra et al. (2008) for the case of Pt traces in Au, upon the subtraction, the spectra were showing the "hidden" features, i.e., peaks which were previously unresolved due to the high intensity of the Au peaks, supporting the presence of these elements. The three spectra (coin, Au reference, subtraction) are shown in the Supplementary materials, in Fig.S2.

The presence of Pt can be interpreted as a fingerprint of the Au source (Gondonneau and Guerra, 2002; Hinds et al., 2014). In fact, Au can be extracted from the so−called primary deposits (i.e., naturally found within rock formations) or from secondary deposits, produced via weathering from the primary ones (Bendall, 2003). Pt is very rare in primary deposits and is commonly associated with secondary deposits as a result of fluvial transport (Meeks and Tite, 1980). Hence, the Pt/Au correlation can be used to identify different sources of gold in ancient artefacts (Bendall et al., 2009). Our results, in agreement with literature (Gondonneau and Guerra, 2002), the amount of Pt was found to be < 0.5% in coin A, and between 0.5% and 1.0% for all the others coins, suggesting a different origin of the gold used to struck coin A with respect to the others (Bendall et al., 2009). The fact that Au used for coin A might have a different origin is compatible with the higher purity of this sample: in fact, the small variation observed in the fineness ($\simeq$ 2%) is typically explained with better sources of Au (Suspène et al., 2020). Interestingly, coins A and B show differences on the basis of both the fineness and the Pt/Au correlation.

These two coins were issued in the same period but in two different mints. Coin A presents an engraving “COM”, standing for Comes Sacrarum Largitionum which was the comitatus responsible for issuing solidi of fixed weight and fineness (Guest, 2008). Coin B, on the other hand, presents another mint mark on its reverse, “CON”, which refers to the Constantinople mint.

2.2.3 Debris analysis

XRF analysis can also be employed to assess information about the debris composition. This can be useful to shed light on the nature of some encrustations found the artefacts (Haller, 2013), or, like in our case, when dealing with dirt accumulated during burial periods. To understand the nature of such deposit, we collected a spectrum in a debris−rich area. The spectrum, shown in Fig. 3, was fitted using the multilayer algorithm implemented in PyMCA which allows to determine the thickness of the layers. Two layers were considered to represent the dirt and the coin. The coin composition was obtained from the above−mentioned analysis and the same values of Table 2 were used. On the contrary, the debris composition was allowed to vary, as the deeper layer accumulated in the hollow area could be different from the shallower patina present on the even region. The initial guess, however, was considered to be equal to the contaminants found in the clean area. From this starting point, the thickness of the debris layer and its composition were varied until a good agreement with the experimental data was reached. The final result is shown in Fig. 3. The concentrations of the elements > 1% are reported in Table 3; traces of Ni, Cr, Mn, Ti, Cl, Cu, P, Zn were also found. The debris layer is found to be approximately 4.3 μm thick. The light elements (like O and C) are not reported because the cross section of their X−ray absorption is fairly low at 10 keV, and their fluorescence is easily shielded by the other elements before reaching the detector.

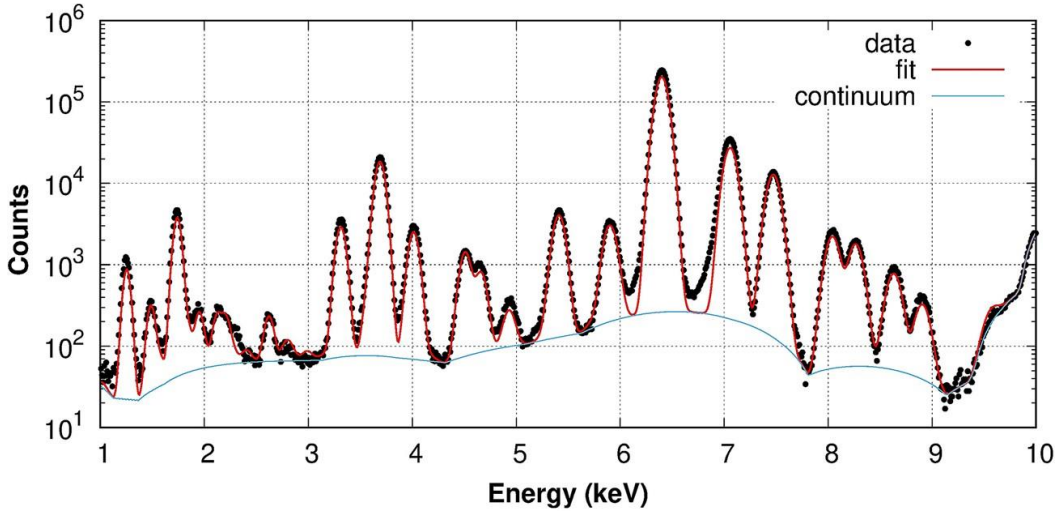

Figure 3: XRF spectrum collected using an incident beam of 10 keV (points) collected over 300 s in a hollow region of coin D, best−fit (thick red line) and continuum baseline used for the fit (thin blue line).

Table 3: Concentrations (%) of the main elements making up the debris accumulated in the hollow region of coin D. The values were obtained from the best fit of a single XRF spectrum collected on the same spot for 300s. Uncertainties are ±0.5%.

Element	Concentration (%)
Si	31.0
Fe	26.6
Mg	23.0
Ca	9.0
Al	5.0
K	2.0

2.2.4 XANES analysis

To gain further insight on the nature of the dirt, the elemental selectivity and chemical sensitivity of XANES were exploited. In particular, we used this technique on coin D to show the possibility of identifying the mineral nature of dirt accumulated on the coin surface. The measurements were carried out at the Fe K−edge in two different areas of the coin: in the cheek area, having an even and rather flat surface, and in a hollow part where some dirt is accumulated; the two positions are shown in Fig. 4.

Figure 4: Image of coin D and magnified area showing the two positions where the XANES measurementswere carried out.

The dirt composition was evaluated through the Linear Combination Fitting (LCF) tool available in the Athena software (Ravel and Newville, 2005). LCF consists in combining spectra of Fe references to reproduce the experimental spectrum of the sample. The spectra of both regions were satisfactorily reproduced using two contributions: magnetite and hematite, as reported in Table 4. The addition of other phases to our combination (e.g., goethite and wüstite), did not improve significantly the agreement between fit and data shown in Fig. 5. The reference spectra considered are shown in the Supplementary Materials (Fig. S3). We must stress here that in our first attempts of fitting some goethite was found (< 5%). However, this amount is lower than the uncertainty of the analysis and, therefore, this minor contribution was excluded.

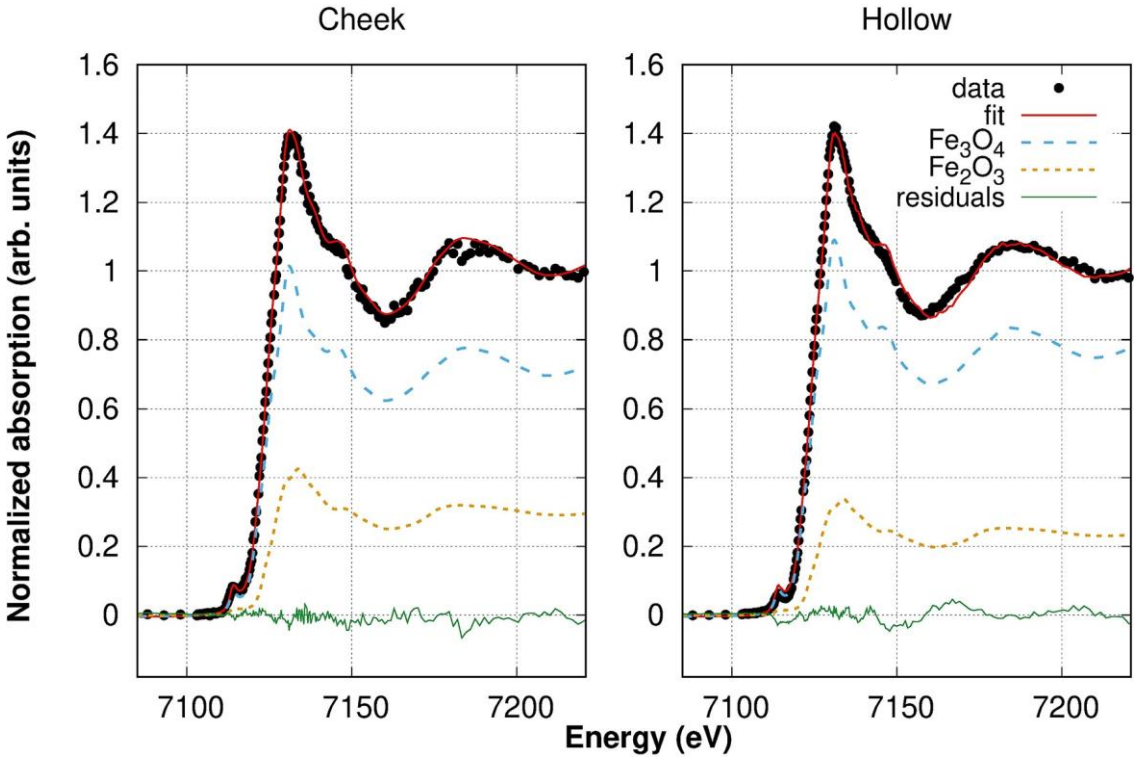

Figure 5: LCF analysis of the Fe K−edge spectra collected on the cheek area (left) and on the hollow area (right) of coin D. In both cases, the contributions needed for the best fit are magnetite (Fe_3O_4) and hematite (Fe_2O_3).

Table 4: Relative amount of Fe oxides in the two regions, calculated through LCF analysis of the XANES data. Uncertainties are ±5%.

Fe oxide	Cheek (%)	Hollow (%)
Magnetite (Fe_3O_4)	71	77
Hematite (Fe_2O_3)	29	23

The small differences between the two regions can be explained considering that the dirt on the flat, more regular surface of the cheek area is expected to be more recent than that found in the hollow region. In facts, the latter, due to its morphology, facilitates the dirt accumulation. The hollow region hosts debris of different times, with the oldest being deeper and the newest being closer to the surface. The outermost layer is expected to be very similar to the clean area, hosting recent debris. Any additional component found in the hollow spectrum and not in the clean one, could be due to a deeper layer of dirt, i.e., to the debris accumulated less recently.

The composition of the soil varies depending on the geographical area: for instance, hematite, magnetite, and goethite prevail in tropical and subtropical soils (Alleoni and

Camargo, 1995). Typically, the presence of goethite is favoured by the high content of organic matter and by the acid pH of the soils (Cornell and Schwertmann, 2003), which usually exhibit a higher affinity for this mineral than for hematite (Guzman et al., 1994). Higher temperature or lower water activity are probably the most important factors favouring the formation of hematite over goethite (Schwertmann, 1988). Such conditions are commonly met in tropical environments but might be found also in temperate regions presenting a well−drained calcareous gravel (Schwertmann et al., 1982).

According to Bigham et al. (2002), the composition of the dirt found on the coin − i.e., magnetite (Fe_3O_4, with Fe^{2+} and Fe^{3+}) and hematite (Fe_2O_3 with Fe^{3+}) − can be related to warm climates (favouring Fe higher oxidation states) and to sandy and silty soils.

This suggests that the burial soil belongs to the Mediterranean region, possibly in the coastal area. Although the exact location where the coins where found is unknown, the pieces come from the Balkan area, in agreement with our results. Comparing the compositions of the two different area, a lower concentration of hematite is observed in the hollow region. As the presence of hematite increases with the mean annual temperature of the environment (Schwertmann et al., 1982), this finding can indicate that the outermost layer of dirt comes from a more temperate area than the outer layer, i.e., closer to the coastal region.

2.3 Methods

2.3.1 Samples

The four specimens were selected from the collection available at the Department of Humanities (DiSU) of the University of Trieste. At the best of our knowledge, the coins were retrieved in the Balkan area. Throughout the text, they are referred to as Coins A, B, C, and D, as given in Table 5.

Table 5: Details of the four coins analysed in this work. The estimated year is the one marking the middle of the reign period of the emperor pictured on the obverse of the artefact.

Sample	Period (AD)	Coin	Mint (mark)	Emperor
A	409	Solidus	Ravenna (COM OB)	Arcadius

B	409	Solidus	Constantinople (CON OB)	Arcadius
C	417	Tremissis	Constantinople (CON OB)	Theodosius II
D	440	Solidus	Ravenna (COM OB)	Valentinianus III

The coins were dated on the basis of the emperor pictured on their obverse: the estimated year is the one marking the middle of the reign period of that emperor. The dating was carried out upon comparison with information by one of the main references of the field (Kent, 2018). The dating is reported in the first row of Table 2. Samples A and B are dated the same, but A was minted in Ravenna (mintmark COM), B in Constantinople (mintmark CON) ("Roman Numismatic Gallery," 2022). Sample C was minted under emperor Theodosius II and is a tremissis, i.e., worth 1/3 of a solidus. Finally, sample D was chosen to represent a later production, roughly 30 years after the first two coins.

Before the measurements, the samples were gently brushed to remove dust and coarse dirt deposited on the surface, no chemicals were used in this process. The coins were then mounted on a sample holder using Teflon stripes, as shown in Fig. 6. This rough cleaning was aimed at avoiding that coarse dirt fall in the UHV chamber during the measurements. The debris accumulated in the indentations is resistant to gentle brushing using a soft brush, as shown by the magnified images of the samples showing the dirt in the hollow parts even after the brushing. This allowed us to carry out analysis on the accumulated debris and to propose hypotheses on the provenance of the soil.

Figure 6: The four gold coins analysed in this work, inside the UHV chamber at the XRF beamline at Elettra Synchrotron.

2.3.2 Synchrotron radiation characterization

XRF and XANES measurements were carried out in a UHV chamber (Karydas et al., 2018) at the XRF beamline (Jark et al., 2014) with a beam size of 100 × 100 μm^2. The beam intensity before the sample, I0, was monitored using an AH501B diamond detector developed by the detector group of Elettra Sincrotrone Trieste. The system is based on a 4−channel solid state sensor composed of a 12 μm−thick, free−standing, polycrystalline diamond plate (Dectris, Rigi). Its total active area is 9 mm x 3 mm subdivided into four electrodes of 4.5 mm x 1.5 mm area each. The individual currents from the four sensors are registered by a 4−channel picoammeter. Every step of the analysis described in this work was carried out after normalizing the raw data for the I0. XRF maps were collected using two exciting energies: below and above the Pt L3 edge, at 10 and 11.6 keV, respectively. The 11.6 keV beam provides an optimal sensitivity to the Pt L lines but the tails of these peak attenuate the signal of the Zn K alpha line, hindering a reliable topography assessment of this element. For this reason, the 10 keV maps were collected. In the analysis, they were used whenever the elemental analysis of the debris was involved. Once the Zn absence in the alloy was proven, the 11.6 keV spectra could be used in the quantification analysis of the gold alloy, taking advantage of the high sensitivity to Pt. Furthermore, XRF measurements carried out on imprinted surfaces of ancient coins at 11.6 keV were proven to be highly reliable and comparable to the same measurements carried out on a polished flat side of the coins (Van Loon et al., 2018). Both energies result into a penetration depth of about 10 μm but we stress here that the probed depth, limited by the low penetration depth of low−energy X−rays emitted from the sample, is around 1 μm. The samples were raster scanned using a motorized sample holder and the fluorescence yield was recorded by a single element Silicon Drift Detector (XFlash 5030, Bruker Nano GmbH, Germany) in 45°/45° geometry. Reference metallic foils (purity 99.97%) from Goodfellow were measured in the same conditions and served as calibration standards for the analysis: these included Au, Cu, Fe, Pt, Zn.

XANES spectra were collected at the K−edge of Fe in fluorescence geometry using the same experimental set−up described for XRF measurements. The monochromator was calibrated on the Zn K edge measured on a metallic Zn foil. The data was normalised

using standard methods for XANES and using the Athena software (Ravel and Newville, 2005).

2.3.3 t−SNE

The t−SNE algorithm is a multivariate analysis which evaluates independently each pixel in a given XRF map and returns a 2D plot in which each point represents a pixel of the map. This allows to obtain a simpler representation of high−dimensional data in 2D. The raw data was normalised to the I0, then, the t−SNE algorithm was applied to the 10 keV maps: Fig. 2a shows the 2D plot obtained for coin B. The distance between the different points in the 2D plot is an indicator of the spectral similarity of the different pixels, with a shorter distance denoting a higher similarity. However, as density in high dimension is not preserved in the t−SNE plot, data segmentation should be carried out not only on the distribution of the pixels in the 2D plot, but also, simultaneously, on the basis of the average raw spectra of each group and the position of the relative pixels in the original XRF map.

2.3.4 PyMCA

The spectra were analysed using PyMCA, choosing the SNIP algorithm for background subtraction and the Pseudo−Voigt function for fitting the experimental curve. The fit procedure relied on the fundamental parameters approach, whose values were first refined on the reference compounds and then applied to the specimens. In particular, fundamental parameters were optimised on reference spectra collected on metallic foils of Fe, Co, Cu, Zn, Au, Ag. The relative amount of elements present in the alloys was calculated excluding those elements whose signal was stronger in the “indentation” group.

2.4 Conclusions

We characterised four gold coins dated back to the V century A.D. using a non−invasive approach combining complementary investigation techniques coupled with statistical analysis tools.

Applying the t−SNE algorithm to spatially resolved XRF data sets, we could identify the elements used in the minting of each piece, disentangling the fluorescence emission of the dirt accumulated on the surface from the signal of the elements making up the original coin.

A semi−quantitative fitting of the XRF spectra relative to the metallic alloy evaluated the Au fineness and the presence of minority alloy elements. Our data shows a variation in the alloy purity of about 2% among the pieces analysed, which is in agreement with the available literature. The lower fineness of some of the coins can be explained with the use of Au alloys probably coming from tax collection as heterogeneous source material of minting. The fine evaluation of the trace elements highlighted a different Pt content in one of the coins (sample A) with respect to the others. This suggests that a different gold source was used to strike this coin with respect to the other samples.

The same quantitative analysis was used to shed light on the nature of the dirt accumulated in an indented area of one coin. In this area, XANES measurements were carried out at the K−edge of Fe, one of the major elements present in the compound. The XANES spectrum collected in a flat, even region showed a weaker signal compared to that collected in a hollow area. What is more, we were able to reproduce the spectral features using LCF with two Fe oxides: hematite and magnetite. From the quantification of these contributions, we could identify the environmental conditions compatible with the terrigenous debris accumulated at the very surface (flat, even surface) and in deeper regions (indented part). Our results suggest that both deposits are consistent with the Mediterranean area, and that the most recent deposits are from warmer, more temperate regions (likely closer to the coastal region) compared to the soil accumulated deeper.

Our approach could be easily and efficiently applied when dealing with encrustation, corrosion, and conservation in general, which are common topics in the field of archaeometry, including numismatics (Haller, 2013).

Supplementary material

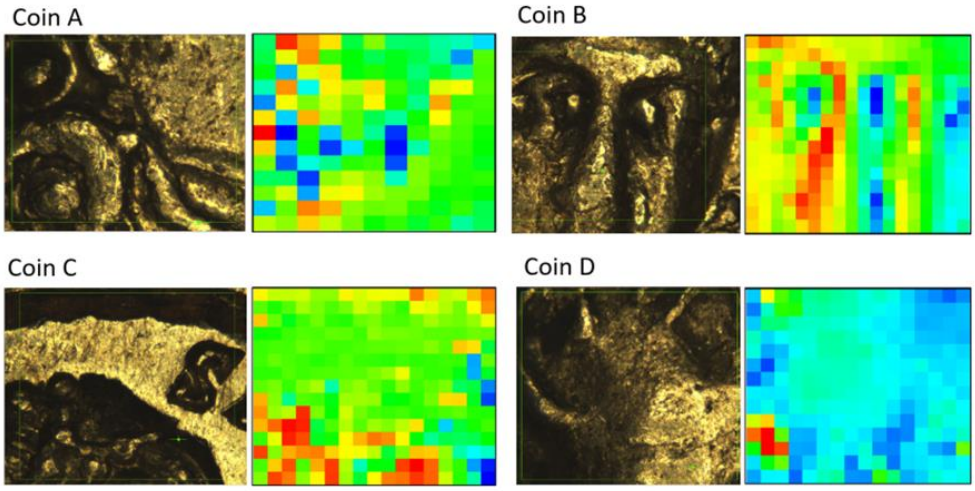

Figure S1: XRF maps collected on the four coins under investigation.

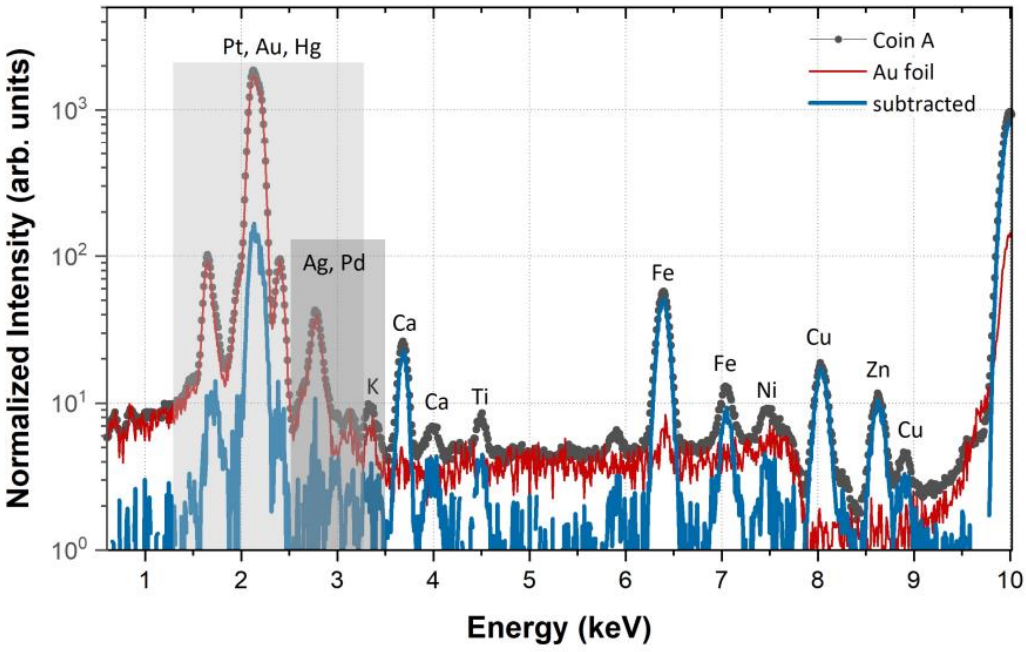

Figure S2: XRF spectra collected at 10 keV on Coin A (black points) and on an Au foil (thin red line). The difference of the spectra is reported as thick blue line. Labels identify the fluorescence emission of the elements: the elements reported twice refer to Kα and Kβ lines.

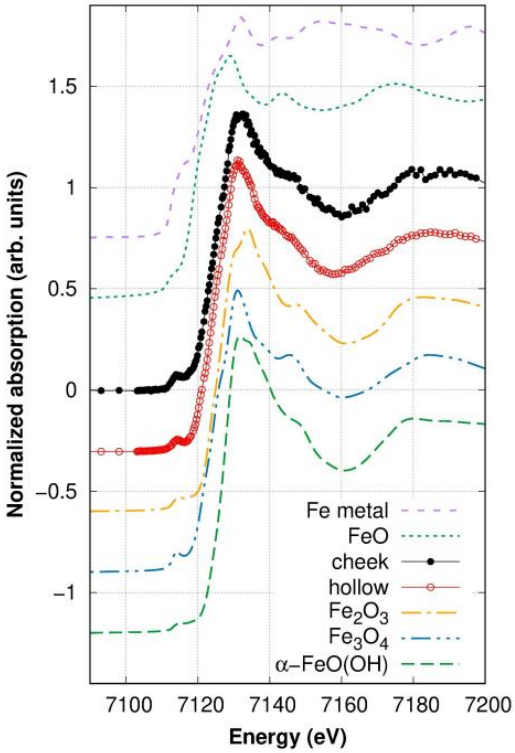

Figure S3: The points show experimental XANES spectra collected in the cheek and hollow areas of sample D (solid and hollow points, respectively). Dashed lines present the reference spectra used for the linear combination fitting (LCF) as discussed in Sec. 1.4, and additional reference spectra of a Fe foil and of the wüstite phase (FeO). The spectra are shifted for clarity.

References

Adams, F., Janssens, K., Snigirev, A., 1998. Microscopic X-ray Fluorescence Analysis and Related Methods with Laboratory and Synchrotron Radiation Sources. Journal of Analytical Atomic Spectrometry 13. https://doi.org/10.1039/A707100K

Alleoni, L.R.F., Camargo, O.A., 1995. Iron and aluminium oxides and the mineralogy of iron free clay fraction of acric oxisols. Scientia Agricola 52, 416–421. https://doi.org/10.1590/S0103-90161995000300002

Allouch, A., Lamrhari, M., Benyaich, F., 2022. Physico-Chemical, Archaeological and Numismatic Analysis of Almoravid Gold Coins (XIth to XIIth Century). Journal of Hunan University Natural Sciences 49, 227–234. https://doi.org/10.55463/issn.1674-2974.49.12.23

Bendall, C., 2003. The Application of Trace Element and Isotopic Analyses to the Study of Celtic Gold Coins and their Metal Sources. Johann Wolfgang Goethe University, Frankfurt.

Bendall, C., Wigg-Wolf, D., Lahaye, Y., Von Kaenel, H.-M., Brey, G.P., 2009. Detecting changes of Celtic gold sources through the application of trace element and Pb isotope laser ablation analysis of Celtic gold coins. Archaeometry 51, 598–625. https://doi.org/10.1111/j.1475-4754.2008.00423.x

Biborski, Marcin, Biborski, Mateusz, 2019. Theodosius II's solidus from Prełuki, Sanok County in material and traseological examinations. Acta Archaeologica Carpathica 54, 285–292. https://doi.org/10.4467/00015229AAC.19.016.11893

Bigham, J.M., Fitzpatrick, R.W., Schulze, D.G., 2002. Iron Oxides, in: Soil Mineralogy with Environmental Applications. John Wiley & Sons, Ltd, pp. 323–366. https://doi.org/10.2136/sssabookser7.c10

Blet-Lemarquand, M., Nieto-Pelletier, S., Téreygeol, F., Suspène, A., 2017. Are platinum and palladium relevant tracers for ancient gold coins? Archaeometallurgical and archaeometric data to study an antique numismatic problem, in: Montero-Ruiz, I., Perea, A. (Eds.), Archaeometallurgy in Europe IV. Consejo Superior de Investigaciones Cientificas, Madrid, pp. 19–28.

Calparsoro, E., Maguregui, M., Morillas, H., Arana, G., Iñañez, J.G., 2019. Non-destructive screening methodology based on ED-XRF for the classification of medieval and post-medieval archaeological ceramics. Ceramics International 45, 10672–10683. https://doi.org/10.1016/j.ceramint.2019.02.138

Carlà, F., 2009. L'oro nella tarda antichità: aspetti economici e sociali, Collana del Dipartimento di storia dell'Università di Torino. S. Zamorani, Torino.

Cataldo, M., Clemenza, M., Ishida, K., Hillier, A.D., 2022. A Novel Non-Destructive Technique for Cultural Heritage: Depth Profiling and Elemental Analysis Underneath the Surface with Negative Muons. Applied Sciences 12, 4237. https://doi.org/10.3390/app12094237

Cohen, D.D., Crawford, J., Siegele, R., 2015. K, L, and M shell datasets for PIXE spectrum fitting and analysis. Nucl. Instrum. Nuclear Instruments and Methods in Physics Research Section B: Beam Interactions with Materials and Atoms 363, 7–18. https://doi.org/10.1016/j.nimb.2015.08.012

Constantinescu, B., Vasilescu, A., Radtke, M., Reinholz, U., 2010. Micro-SR-XRF studies for archaeological gold identification—the case of Carpathian gold and Romanian museal objects. Journal of Applied Physics A 99, 383–389. https://doi.org/10.1007/s00339-010-5624-1

Cornell, R.M., Schwertmann, U., 2003. The Iron Oxides: Structure, Properties, Reactions, Occurrences and Uses. John Wiley & Sons.

Crosera, M., Baracchini, E., Prenesti, E., Giacomello, A., Callegher, B., Oliveri, P., Adami, G., 2019. Elemental characterization of surface and bulk of copper-based coins from the Byzantine-period by means of spectroscopic techniques. Microchemical Journal 147, 422–428. https://doi.org/10.1016/j.microc.2019.03.025

Cruz, J., Corregidor, V., Alves, L.C., Carvalho, P.A., Fonseca, M., 2013. Analysis of a gold solidus of roman emperor Valentinian I. Microscopy and Microanalysis 19, 139–140. https://doi.org/10.1017/S1431927613001311

Demšar, J., Curk, T., Erjavec, A., Gorup, Č., Hočevar, T., Milutinovič, M., Možina, M., Polajnar, M., Toplak, M., Starič, A., Štajdohar, M., Umek, L., Žagar, L., Žbontar, J., Žitnik, M., Zupan, B., 2013. Orange: Data Mining Toolbox in Python. Journal of Machine Learning Research 14, 2349–2353.

Dube, R., 2006. Interrelation between gold and tin: A historical perspective. Gold Bulletin 39, 103–113. https://doi.org/10.1007/BF03215537

Farges, F., Cotte, M., 2016. X-Ray Absorption Spectroscopy and Cultural Heritage: Highlights and Perspectives, in: Van Bokhoven, J.A., Lamberti, C. (Eds.), X-Ray Absorption and X-Ray Emission Spectroscopy. Wiley, pp. 609–636. https://doi.org/10.1002/9781118844243.ch21

Gennari, A., 2018. Un mezzo tremisse inedito di Eraclio I (610-641). Con annesso un catalogo dei mezzi tremissi ad oggi noti. Revista Numismática Hécate 5, 55–63.

Gondonneau, A., Guerra, M.F., 2002. The circulation of precious metals in the Arab Empire: the case of the near and the Middle East. Archaeometry 44, 573–599. https://doi.org/10.1111/1475-4754.t01-1-00087

Gorghinian, A., Esposito, A., Ferretti, M., Catalli, F., 2013. XRF analysis of Roman Imperial coins. Nuclear Instruments and Methods in Physics Research Section B: Beam Interactions with Materials and Atoms 309, 268–271. https://doi.org/10.1016/j.nimb.2013.02.022

Guerra, M.F., 2018. Physicochemical approaches to gold and silver work: an overview, in: Sabbatini, L., van der Werf, D. (Eds.), Chemical Analysis in Cultural Heritage. W. de Gruyter, Berlin.

Guerra, M.F., 1995. Elemental analysis of coins and glasses. Applied Radiation and Isotopes 46, 583–588. https://doi.org/10.1016/0969-8043(95)00095-X

Guerra, M.F., Calligaro, T., 2004. Gold traces to trace gold. Journal of Archaeological Science 31, 1199–1208. https://doi.org/10.1016/j.jas.2002.05.001

Guerra, M.F., Calligaro, T., 2003. Gold cultural heritage objects: a review of studies of provenance and manufacturing technologies. Measurement Science and Technology 14, 1527–1537. https://doi.org/10.1088/0957-0233/14/9/305

Guest, P., 2008. Roman Gold and Hun Kings: the use and hoarding of solidi in the late fourth and fifth centuries, in: Roman Coins Outside the Empire. Ways and Phases, Contexts and Functions. Collection Moneta 82, Wetteren, pp. 295–307.

Guzman, G., Alcantara, E., Barron, V., Torrent, J., 1994. Phytoavailability of phosphate adsorbed on ferrihydrite, hematite, and goethite. Plant Soil 159, 219–225. https://doi.org/10.1007/BF00009284

Habashi, F., 2016. Gold – An Historical Introduction, in: Adams, M.D. (Ed.), Gold Ore Processing: Project Development and Operations. Elsevier, pp. 1–20. https://doi.org/10.1016/B978-0-444-63658-4.00001-3

Haller, E., 2013. The Nature of Encrustation on Coins from the Wreck of the Republic (1865). Odyssey Marine Exploration 31.

Hinds, M.W., Bevan, G., Burgess, R.W., 2014. The non-destructive determination of Pt in ancient Roman gold coins by XRF spectrometry. Journal of Analytical Atomic Spectrometry 29, 1799–1805. https://doi.org/10.1039/C4JA00170B

Janssens, K., Vittiglio, G., Deraedt, I., Aerts, A., Vekemans, B., Vincze, L., Wei, F., De Ryck, I., Schalm, O., Adams, F., Rindby, A., Knöchel, A., Simionovici, A., Snigirev, A., 2000. Use of microscopic XRF for non-destructive analysis in art and archaeometry. X-Ray Spectrometry 29, 73–91. https://doi.org/10.1002/(SICI)1097-4539(200001/02)29:1<73::AID-XRS416>3.0.CO;2-M

Jark, W., Eichert, D., Luehl, L., Gambitta, A., 2014. Optimisation of a compact optical system for the beamtransport at the x-ray fluorescence beamline at Elettra for experiments with small spots, in: Morawe, C., Khounsary, A.M., Goto, S. (Eds.),

. Presented at the SPIE Optical Engineering + Applications, San Diego, California, United States, p. 92070G. https://doi.org/10.1117/12.2063009

Karydas, A.G., Czyzycki, M., Leani, J.J., Migliori, A., Osan, J., Bogovac, M., Wrobel, P., Vakula, N., Padilla-Alvarez, R., Menk, R.H., Gol, M.G., Antonelli, M., Tiwari, M.K., Caliri, C., Vogel-Mikuš, K., Darby, I., Kaiser, R.B., 2018. An IAEA multi-technique X-ray spectrometry endstation at Elettra Sincrotrone Trieste: benchmarking results and interdisciplinary applications. Journal of Synchrotron Radiation 25, 189–203. https://doi.org/10.1107/S1600577517016332

Kemmerer, E.W., 2009. Gold and the Gold Standard. Ludwig von Mises Institute.

Kent, J.P.C., 2018. THE ROMAN IMPERIAL COINAGE - The Divided Empire and the Fall of the Western Parts 395-491. Spink and Son Ltd, London.

Kolbe, M., Hönicke, P., Müller, M., Beckhoff, B., 2012. L-subshell fluorescence yields and Coster-Kronig transition probabilities with a reliable uncertainty budget for selected high- and medium- Z elements. Physical Review A 86, 042512. https://doi.org/10.1103/PhysRevA.86.042512

Leusch, V., Armbruster, B., Pernicka, E., Slavčev, V., 2015. On the Invention of Gold Metallurgy: The Gold Objects from the Varna I Cemetery (Bulgaria)—Technological Consequence and Inventive Creativity. Cambridge Archaeological Journal 25, 353–376. https://doi.org/10.1017/S0959774314001140

Marussi, G., Crosera, M., Prenesti, E., Callegher, B., Baracchini, E., Turco, G., Adami, G., 2023. From Collection or Archaeological Finds? A Non-Destructive Analytical Approach to Distinguish between Two Sets of Bronze Coins of the Roman Empire. Molecules 28, 2382. https://doi.org/10.3390/molecules28052382

Marussi, G., Crosera, M., Prenesti, E., Cristofori, D., Callegher, B., Adami, G., 2022. A Multi-Analytical Approach on Silver-Copper Coins of the Roman Empire to Elucidate the Economy of the 3rd Century A.D. Molecules 27, 6903. https://doi.org/10.3390/molecules27206903

Meeks, N.D., Tite, M.S., 1980. The analysis of platinum-group element inclusions in gold antiquities. Journal of Archaeological Science 7, 267–275. https://doi.org/10.1016/S0305-4403(80)80029-X

Mihalić, I.B., Fazinić, S., Barac, M., Karydas, A.G., Migliori, A., Doračić, D., Desnica, V., Mudronja, D., Krstić, D., 2021. Multivariate analysis of PIXE + XRF and PIXE spectral images. Journal of Analytical Atomic Spectrometry 36, 654–667. https://doi.org/10.1039/D0JA00529K

Miškec, A., 2021. A gold coin of the Roman emperor Anthemius (467 – 472 AD) from Črnomelj. Vjesnik Arheološkog muzeja u Zagrebu 54, 99–110. https://doi.org/10.52064/vamz.54.1.4

Morrisson, C., 1982. Numismatique et histoire, l'or monnayé de Rome à Byzance : purification et altérations. Comptes rendus des séances de l'Académie des Inscriptions et Belles-Lettres 126, 203–223. https://doi.org/10.3406/crai.1982.13935

Morteani, G., Northover, J.P., 2013. Prehistoric Gold in Europe: Mines, Metallurgy and Manufacture. Springer Science & Business Media.

Oddy, A., 1988. Studies in Early Byzatine Gold Coinage, Numismatic Studies. American Numismatic Society, New York, NY.

Oddy, A., La Niece, S., 1986. Byzantine gold coins and jewellery: A study of gold contents. Gold Bulletin 19, 19–27. https://doi.org/10.1007/BF03214640

Ravel, B., Newville, M., 2005. ATHENA, ARTEMIS, HEPHAESTUS: data analysis for X-ray absorption spectroscopy using IFEFFIT. Journal of Synchrotron Radiation 12, 537–541. https://doi.org/10.1107/S0909049505012719

Reiff, F., Bartels, M., Gastel, M., Ortner, H., 2001. Investigation of contemporary gilded forgeries of ancient coins. Fresenius' Journal of Analytical Chemistry 371, 1146–1153. https://doi.org/10.1007/s002160101082

Roman Numismatic Gallery [WWW Document], n.d. . Roman Numis. Gallery - Roman Coins Sculpt. Mil. Equip. URL http://www.romancoins.info/Content.html (accessed 10.4.23).

Sándor, Z., Gresits, I., Juhász, M.K., 2003. X-ray fluorescence analysis of medieval gold coins and jewellery. Journal of Radioanalytical and Nuclear Chemistry 256, 283–288.

Schlosser, S., Reinecke, A., Schwab, R., Pernicka, E., Sonetra, S., Laychour, V., 2012. Early Cambodian gold and silver from Prohear: composition, trace elements and gilding. Journal of Archaeological Science 39, 2877–2887. https://doi.org/10.1016/j.jas.2012.04.045

Schwertmann, U., 1988. Occurrence and Formation of Iron Oxides in Various Pedoenvironments, in: Stucki, J.W., Goodman, B.A., Schwertmann, U. (Eds.), Iron in Soils and Clay Minerals, NATO ASI Series. Springer Netherlands, Dordrecht, pp. 267–308. https://doi.org/10.1007/978-94-009-4007-9_11

Schwertmann, U., Murad, E., Schulze, D.G., 1982. Is there holocene reddening (hematite formation) in soils of axeric temperate areas? Geoderma 27, 209–223. https://doi.org/10.1016/0016-7061(82)90031-3

Sear, D., 2014. Roman Coins and Their Values Volume 5. Spink & Son, Ltd.

Suspène, A., Bocciarelli, D., Blet-Lemarquand, M., Gehres, B., 2020. Gold coinage and debasement. A preliminary examination of the fineness of Roman gold coinage

from the Republic and early Empire, in: Debasement. Manipulation of Coins Standards in Pre-Modern Monetary Systems. Oxbow Books, pp. 53–62.

Van Loon, L.L., Banerjee, N.R., Hinds, M.W., Gordon, R., Bevan, G., Burgess, R.W., 2018. Rapid, quantitative, and non-destructive SR-WD-XRF mapping of trace platinum in Byzantine Roman Empire gold coins. Journal of Analytical Atomic Spectrometry 33, 1763–1769. https://doi.org/10.1039/C8JA00227D

SECTION 3

A Multi−Analytical Approach on Silver−Copper Coins of the Roman Empire to Elucidate the Economy of the 3rd Century A.D.

Giovanna Marussi[1]*, Matteo Crosera[1], Enrico Prenesti[2], Davide Cristofori[3,4], Bruno Callegher[5] and Gianpiero Adami[1]*

[1] Dipartimento di Scienze Chimiche e Farmaceutiche, Università degli Studi di Trieste, 34127 Trieste, Italy

[2] Dipartimento di Chimica, Università degli Studi di Torino, 10125 Torino, Italy

[3] Centro di Microscopia Elettronica "Giovanni Stevanato", Campus Scientifico, Università Ca' Foscari Venezia, 30172 Venezia Mestre, Italy

[4] Dipartimento di Scienze Molecolari e Nanosistemi, Università Ca' Foscari Venezia, 30172 Venezia Mestre, Italy

[5] Dipartimento di Studi Umanistici, Università degli Studi di Trieste, 34124 Trieste, Italy

Published in *Molecules*, https://doi.org/10.3390/molecules2720690

*Corresponding author

Giovanna Marussi, Dipartimento di Scienze Chimiche e Farmaceutiche, Università degli Studi di Trieste

Email: giovanna.marussi@phd.units.it

Gianpiero Adami, Dipartimento di Scienze Chimiche e Farmaceutiche, Università degli Studi di Trieste

Email: gadami@units.it

Abstract

In this study, 160 silver−copper alloy denarii and antoniniani from the 3rd century A.D. were studied to obtain their overall chemical composition. The approach used for their characterisation is based on a combination of physical, chemical, and chemometric techniques. The aim is to identify and quantify major and trace elements in Roman silver−copper coins in order to assess changes in composition and to confirm the devaluation of the currency. After a first cataloguing step, μ−EDXRF and SEM−EDX techniques were performed to identify the elements on the coins' surface. A micro−destructive sampling method was employed on a representative sample of the coins to quantify the elements present in the bulk. The powder obtained from drilling 12 coins (keeping the two categories of coins separate) was dissolved in an acidic medium; heated and sonicated to facilitate dissolution; and then analysed by ICP−AES and ICP−MS. The two currencies had different average alloy percentages; in particular, the % difference of Ag was about 8%. The other elements were found in concentrations <1 wt%. Of these, the element highest in concentration were Pb and Sn, which is in agreement with the literature. The multivariate analysis performed on the data acquired revealed two groups of coins, corresponding to the two currencies.

Keywords: archaeometry; roman coins; μ−EDXRF; ICP−MS; silver alloys; trace elements

1. Introduction

The investigation of the chemical composition provides the fineness of ancient coins that allows to gain information on the evolution of coinage over the centuries (if samples from various periods are available and can be analysed) (Beck et al., 2004). Coinage, in turn, can reveal politically, socially, and economically relevant facts. Moreover, it can help to understand the economic choices of the imperial authorities, especially the military ones, in times of crisis resulting from conflicts between legions, but also from the reduced supply of metal in contrast to a greater demand for metal to be minted, especially silver during the period in which the coins were issued.

The aim of this study is to identify and quantify major and trace elements in Roman silver−copper coins of the 3rd century A.D., in order to assess changes in composition between denarii and antoniniani (introduced by emperor Caracalla in 214 A.D.) and to confirm the devaluation of the currency during the "Military Anarchy" or "Imperial Crisis" (A.D. 235−284). The later 3rd and early 4th centuries A.D. were signed by a deep political and military crisis, which strongly affected the entire administrative and military organisation of the Roman Empire. From the monetary reform of Augustus (23 B.C.) and Nero (54 A.D.) to at least the reform of Caracalla (ca. 214 A.D.), the silver coin, i.e., the denarius, had played a central role in the monetary system of the Roman Empire. Its stability, however, had been weakening overtime. The silver coin adulteration, in fact, had become the remedy to which the emperors resorted in cases of increased expenses (especially military). In other words, they increased public expenditure by increasing the production of the monetary stock; they decreased the silver fineness, but the nominal value of the coin remained unchanged. In fact, from the denarius by Nero with a silver fineness of about 93.5% and a weight of 3.4 g, it came to the denarius minted between Septimius Severus and Caracalla with a silver fineness even lower than 50% and a weight lower than 3.4 g (Caley and McBride, 1956; Gitler and Ponting, 2007; Manukyan et al., 2019).

This devaluation led to increasing in the alloy the copper content, or lead and tin in some cases (base metals), and to developing new metallurgical techniques of surface silvering (a trick to mask reality of the bulk) (Manukyan et al., 2019). As a consequence, the emperor Caracalla introduced a new currency, the antoninianus. This coin has been valued at 2 denarii, as indicated by the radiated crown on the recto, although it was equal to 11

denarii in weight (5.11 g) and contained about the same percentage of silver as only one denarius. It was introduced in 214 A.D., but its continuous and massive production began only in 238 A.D., when it replaced the denarius definitely. Starting from the year 238 A.D., the antoninianus shows a deterioration in comparison to the similar currencies minted during the empire of Caracalla; indeed, the silver content dropped from about 50% to 42% and remained almost constant until about 250 A.D. The devaluation reached its peak with the last issues of the emperors Gallienus (260−268 A.D.) and Claudius II Gothicus (268–270 A.D.) when the antoninianus was coined with an alloy of argentiferous bronze containing less than 5% silver (Caley and McBride, 1956; King and Hedges, 1974).

The analytical determination of the composition of ancient coins can give a reliable documentation for historical, numismatic, and archaeological studies, providing information on ancient minting methods and contaminations introduced during manufacture but, above all, the intentional adulteration of the metal alloy of monetary issues. In addition, it allows the identification of possible corrosive processes affecting the surface, especially in the case of silver−copper alloy coins, and such information is crucial to identify conservation and restoration treatments of ancient coins (Linke et al., 2003; Pardini et al., 2012).

As this type of specimen is usually very rare, maybe unique, and of great historical and economic value, non−destructive analysis is preferred. The most common non−destructive techniques for elemental determination are μ−EDXRF (micro−Energy Dispersive X−Ray Fluorescence, henceforth μ−XRF) spectroscopy, Energy Dispersive X−ray microanalysis in a Scanning Electron Microscope (SEM−EDX), Neutron Activation Analysis (NAA), and the X−ray Emission Induced by Particles (PIXE) (Linke et al., 2003; Tanasi et al., 2017). The most widely used non−destructive technique for the analysis of ancient metal alloys is undoubtedly μ−XRF, as it is rapid, inexpensive, reproducible, and semi−quantitative, at least for non−corroded and well−preserved samples (Callu, 1984).

Depending on the production criteria and environmental conditions to which silver−copper alloy coins are subjected, alterations to the alloy and the formation of surface concretions can occur (Borges et al., 2017). As highlighted by Hrnjić et al. (2020), copper diffusion at the surface can take place, resulting in the formation of insoluble oxidized compounds such as cuprite (Cu_2O) and tenorite (CuO), or original intentional or

post−depositional enrichment of silver at the surface may occur. In these cases, the coins' surface is not representative of the bulk, therefore surface analysis of Ag and Cu concentrations would lead to inaccurate results, thus necessitating micro−destructive analysis to determine the alloy composition in the bulk.

In this study, resulting from a collaboration of various public research bodies, a total of 160 silver−copper based coins from a hoard found allegedly in the Balkan area, now kept in the Numismatics Laboratory of Department of Humanities (University of Trieste, Italy), was studied. In particular, they were 138 denarii and 22 antoniniani from the 3rd century A.D. (Roman emperors from Septimius Severus to Marcus Aurelius Probus) (Table 1).

Table 1: List of coins under study. Each coin is associated with a code where A = antoninianus, D = denarius, followed by a progressive number from 1 to 160. Coins marked with a star (*) are sampled for ICP-AES and ICP-MS analyses, while coins marked with a cross (†) are those analysed with SEM-EDX.

Emperor	**Period of Issue**	**Number of Samples**	**Sample Code**
Antoninus Pius	138-161	1	D144
Antoninus Pius for Diva Faustina I	141-161	1	D35
Marcus Aurelius for Faustina II	145-161	3	D43; D65; D137
Marcus Aurelius	161-180	3	D38; D112; D116
Commodus	177-192	7	D2; D15; D54; D67; D78; D93; D108
Didius Julianus-Manlia Scantilla	193	1	D121
Septimius Severus	193-211	54	D1; D3; D4; D9; D11; D13; D14; D29; D30; D31 †; D33; D37; D40; D42; D45; D46; D50; D51; D52; D53; D55; D57; D58; D59*; D60; D61; D63; D64; D66; D71; D72; D73; D74; D76; D80; D82; D84; D86;

			D87; D97; D98; D99; D100; D110; D113; D118; D119; D122; D128*; D129; D138; D140; D143; D151*
Septimius Severus for Julia Domna	193–211	24	D5; D8; D17; D19; D21; D27*; D28; D34; D41; D47; D49; D56; D70; D77; D95; D106; D114; D115; D123; D125*; D131; D132; D141; D142
Septimius Severus for Caracalla	198–209	13	D6; D23*; D25; D39; D44; D62; D75; D85; D89; D117*; D130*; D134; D149
Septimius Severus for Caesar	198	1	D7
Septimius Severus for Geta	209-212	2	D10; D96
Caracalla	198-217	8	D12; D18; D68; D79; D94; D102; D107; D145
Trebonianus Gallus	215-253	1	A150
Macrinus	217-218	1	D32
Elagabalus	218-222	13	D36; D69; D83; D92; D104; D105; D126†; D133; D136; D139; A147; A152; A155*
Severus Alexander	221-235	3	D26; D90; D120
Maximinus Thrax	230–235	3	D103; D157; A20
Gordian III	238–244	6	D91; D153; A48*,†; A158; A159*; A160*
Philip the Arab	244–249	4	A81; A109; A111; A154
Philip the Arab–Marcia Otacilia Severa	244–249	1	D127
Trajan Decius	249–251	2	A101; A135

Trajan Decius for Herenia Etruscilla	249–251	2	A22; A24
Valerian	253–260	3	A88; A146; A156
Gallienus	260–268	1	A148†
Gallienus for Salonina	260–268	1	A16
Aurelian	270–275	1	A124

First, weight, diameter, and thickness of each coin were determined. Then, non−destructive techniques μ−XRF and SEM−EDX were used to identify the elements on the surface of the coins (Ag, Cu, Pb, Sn, Ni, Zn, Bi, Fe, and Ca). A micro−destructive sampling method − based on acquiring a bulk sample by mechanically drilling the edge of each coin (Crosera et al., 2019) − was then used. Subsequently, Inductively Coupled Plasma−Atomic Emission Spectroscopy (ICP−AES) and Inductively Coupled Plasma−Mass Spectrometry (ICP−MS) were employed in the determination of Ag and Cu (the two alloying elements), as well as of Pb, Sn, Ni, Zn, Bi, Fe, and Ca (minor elements, overall lower than 1% of the mass), in the powder resulting from the drilling of 12 coins (see Table 2), previously dissolved in a concentrated nitric acid aqueous solution, heated, and sonicated to facilitate the dissolution. The samples for the micro−destructive analyses were chosen because they had greater average thickness, also paying attention to currency, so that the different compositions could be compared.

Table 2: Recto and verso of the 12 coins micro-sampled.

D27, Septimius Severus for Julia Domna

D59, Septimius Severus

D125, Septimius Severus for Julia Domna

D128, Septimius Severus

D151, Septimius Severus

D23, Septimius Severus for Caracalla

D117, Septimius Severus for Caracalla

D130, Septimius Severus for Caracalla

A155, Elagabalus

A48, Gordian III

A159, Gordian III

A160, Gordian III

2. Results and Discussion

2.1 Qualitative Analyses

2.1.1 μ−EDXRF Results

As the depth analysed is in the order of hundreds of μm (Hrnjić et al., 2020), micro−Energy Dispersive X−Ray Fluorescence spectrometry (μ−EDXRF) was used to investigate only the surface composition of the coins. Moreover, since no treatment of the sample was required, it was used to study the corrosion phenomena that may have occurred on their surface. All coins were analysed qualitatively by μ−EDXRF spectroscopy that allowed the identification of the main elements present on the surface of the denarii and antoniniani under study.

Although the spectra were not entirely overlapping in terms of peak intensity, all were confirmed on the presence of Ag, Cu, Sn, Ca, Fe, Pb, Au, Zn, Bi, and Ni (Figure 1).

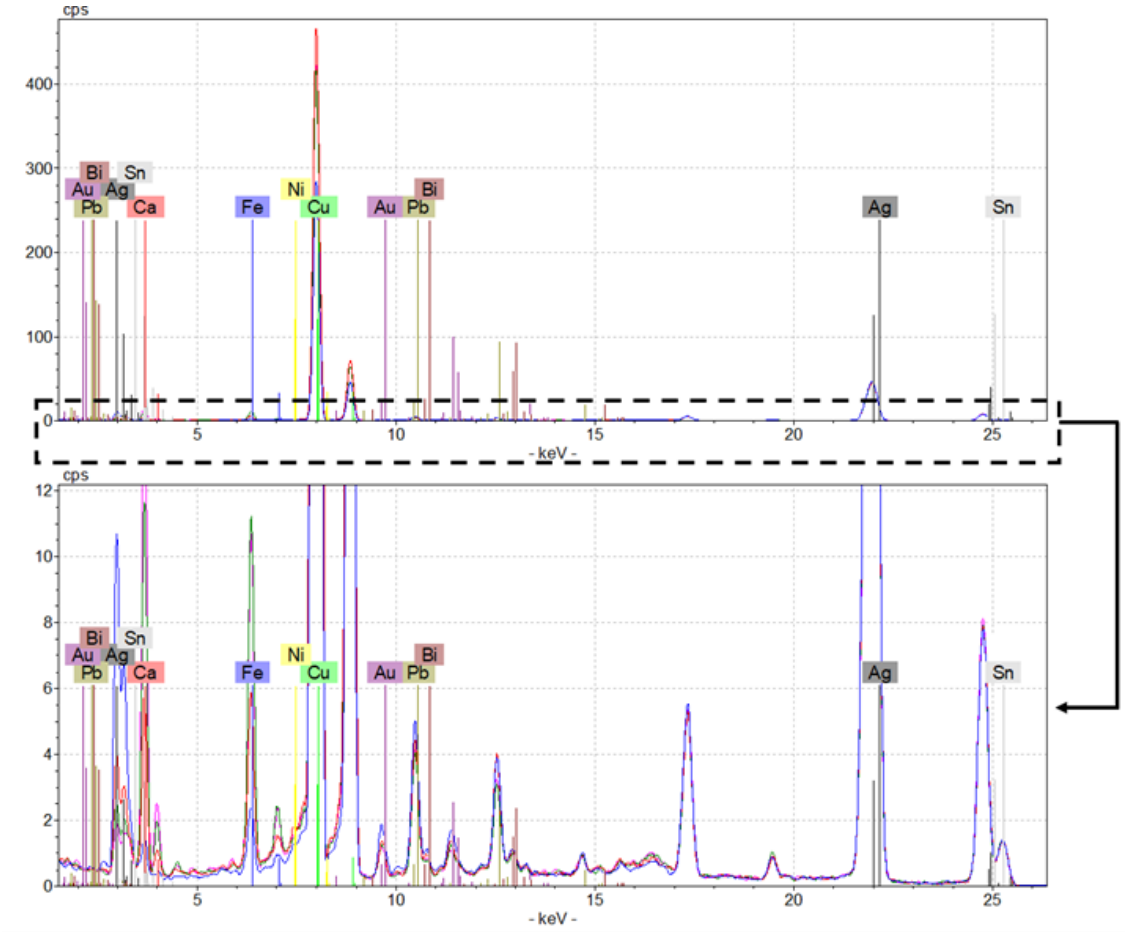

Figure 1: Four overlapped μ-EDXRF spectra of the coin no. D27. Spectrum of recto_1 in pink, recto_2 in blue, verso_1 in red, and verso_2 in green. The lower spectrum is relative to the area within the dashed frame, so that even the lower intensity peaks can be appreciated.

The higher concentration of copper and silver suggested the binary alloy nature of the coins, typically used by the Romans to mint coins during the 3rd century A.D. (Elliott, 2014), while the presence of Fe and Ca is most likely due to the interaction between the coins and the burial soil components (Manukyan et al., 2019). Subsequently, ICP−AES and ICP−MS micro−destructive analyses were carried out to quantify mainly these elements.

By calculating the area subtended by the peaks relative to the silver Kα1 line and to the copper Kα1 line, it was possible to calculate the ratio Ag/Cu in order to delineate the trend of the noble metal at the surface over the 2nd and 3rd centuries (Figure 2). An average decrease in silver can be observed, in accordance with the progression of the third−century crisis and the introduction of the antoninianus as a healing operation. In the case of the antoniniani issued by Gordian III, they showed a high surface inhomogeneity,

which resulted in spectra with little overlap in intensity and consequently a high standard deviation.

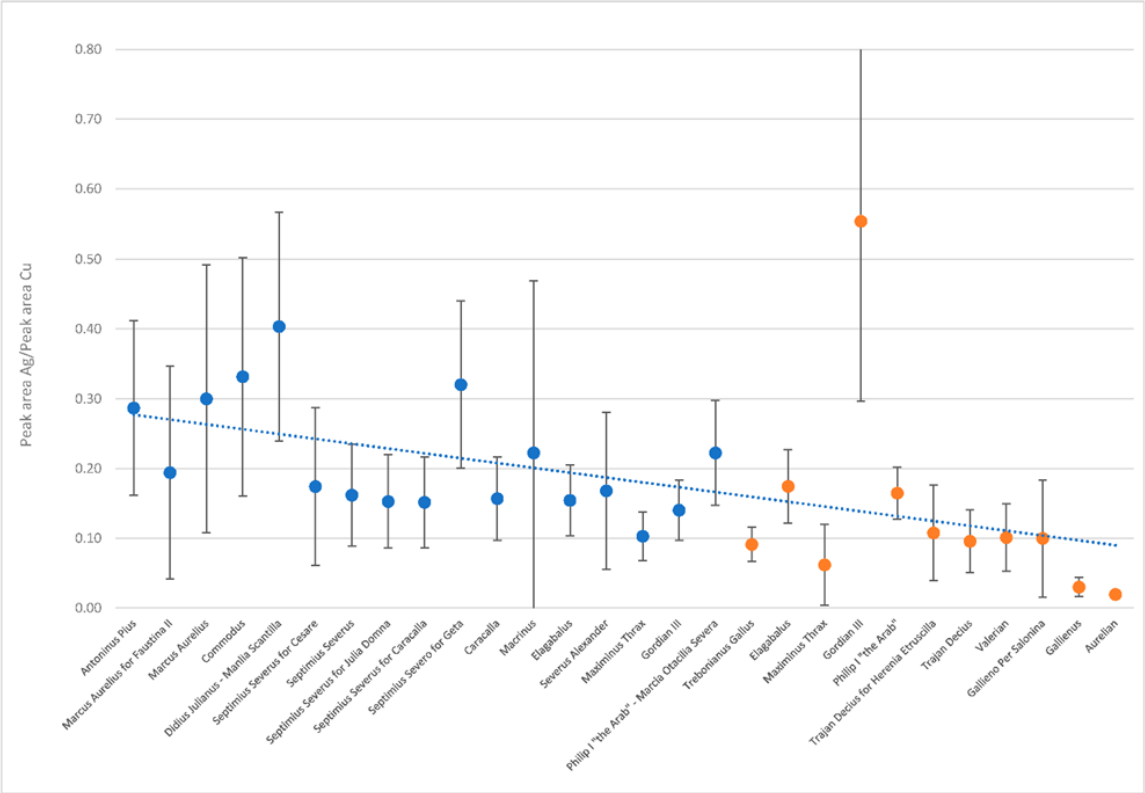

Figure 2: Average Ag/Cu ratio of the 160 coins analysed with respective error bars, denarii in blue and antoniniani in orange. The x-axis shows the emperors who issued the coins under study. The ratio reported in y-axis regards μ-EDXRF signals.

2.1.2 SEM−EDX Results

The SEM−EDX investigation was carried out on four well−preserved coins − two denarii (no. D31, D126) and two antoniniani (no. A48, A148) − in order to study the different distribution of elements on the coins' surface. These samples were chosen because, for some coins, previous XRF analysis highlighted differences in the obtained spectra in terms of peaks' intensity. Moreover, among these coins, the four samples subjected to SEM−EDX analysis were the best preserved and did not require pre−treatment for analysis. The EDX mapping (Figure 3) revealed an uneven metal distribution of Ag and Cu, and the presence of oxygen.

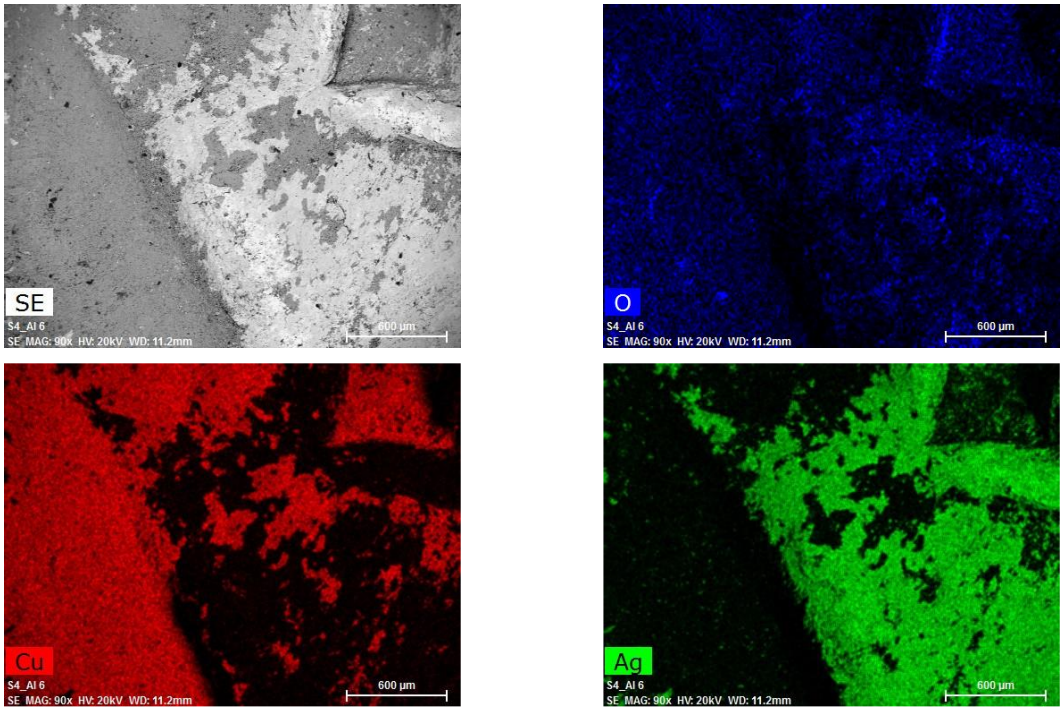

Figure 3: SE image and X-ray maps on the surface of antoninianus no. A48 obtained by SEM-EDX.

The uniform arrangement of oxygen over the entire studied area suggests that copper oxides have formed on the surface. Cuprite and tenorite are the main alteration compounds in Ag−Cu alloy artefacts. Indeed, as reported by Doménech et al. (2012), the primary patina is composed of cuprite (Cu_2O), while the patina associated to soil corrosion is mainly formed by tenorite (CuO). In some EDX spectra, the S and Cl peaks are well identified. This spectroscopic data supports the hypothesis that there may be acanthite (Ag_2S) and chlorargyrite (AgCl) as insoluble corrosion compounds in the patina.

2.2 Quantitative Analyses on the Bulk

2.2.1 ICP−AES Results

The normalised percentage concentrations − obtained by relating the mg kg^{-1} of the individual element to the sum of the ppm of all the elements detected and multiplying the ratio by 100 − of the two main elements (Ag and Cu) in the bulk are shown in Figure 4. We reported the average value of concentration calculated on two replicates from the dilution, and the corresponding standard deviations.

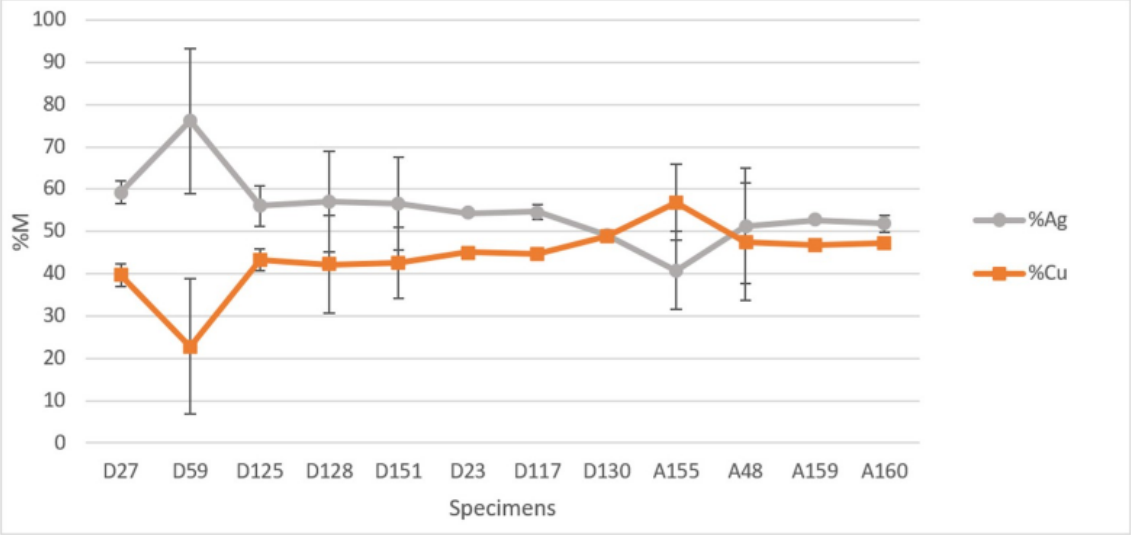

Figure 4: Relative concentration of Ag and Cu in the 12 coins (8 denarii and 4 antoniniani) analysed by ICP-AES. Data are given as mean ± RSD%.

The analysis confirmed that the coins are based on a silver−copper alloy. Since the standard deviations had no statistical significance, we performed the t−test between the two currencies (%Ag content of denarii (N = 8) and %Ag content of antoniniani (N = 4)) and the result is that the silver concentrations of the two group of currencies are significantly different by 90% ($\rho = 0.08$).

Only one of the 12 coins analysed micro−destructively had a higher Cu content than Ag percentage (antoninianus no. A155), which was minted immediately later the Caracalla reform. At the opposite, the coin with the highest Ag content, approximately 76%, was the denarius no. D59: it is the only denarius that differs significantly from the others minted in the same period in terms of Ag percentage in alloy.

It is also worth noting the different relation between %Ag and %Cu of the two currencies: in the case of the denarii, minted before 215 A.D., there is an average difference of more than 10% between the % of Ag and that of Cu, while the antoniniani show almost equal percentages of the two major elements.

2.2.2 ICP−MS Results

With regard to trace elements, Figure 5 shows the percentage elemental composition of the 12 coins analysed excluding Ag and Cu. Therefore, in this paragraph, the % of each trace element refers to the sum of trace elements concentration set equal to 100 (any % is then referred to the subgroup of trace elements, excluding Cu and Ag).

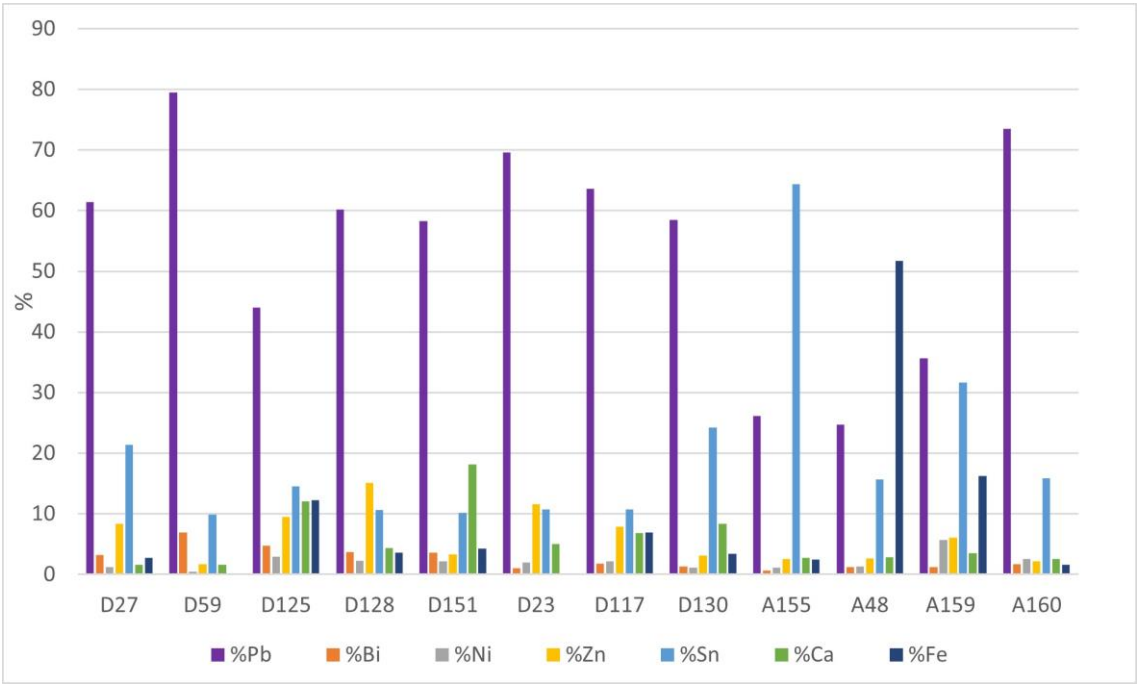

Figure 5: Average content of trace metals in the bulk of the 12 coins analysed by ICP-MS. The data are normalised excluding Ag and Cu content.

Among the trace elements, the one with the highest percentage is Pb (average content 53.1 ± 2.6 wt%), in agreement with the literature about this element in silver coins (Fabrizi et al., 2019; Ingo et al., 2006). In fact, in ancient times, this noble metal was extracted from galena (PbS), as this mineral contained appreciable amounts of silver combined as sulphur. Incomplete cupellation may leave Pb impurities in the Ag extracted (Fabrizi et al., 2019). The lead content is an indication of the effectiveness of the purification procedure. Looking at the overall data (Table 3), 5 of the 12 coins have a lead content greater than 0.5% indicating low grade silver. Bismuth is an impurity in argentiferous galena, which was often removed by the purification process: this agrees with the low concentrations found in the coins (Rodrigues et al., 2011).

The high iron content in antoninianus no. A48 (51.7 ± 0.3 wt%) is peculiar. Since this coin was well preserved and the concentration is relative to the bulk of the sample, a correlation with the burial site can be excluded. Rather, this high iron content can be attributed to an incomplete copper refining process (probably due to some processing error that was then transferred onto a certain batch of coins); in ancient times, the most

common copper ore used in metallurgy was, in fact, chalcopyrite ($CuFeS_2$, which is the most abundant copper ore in the environment) (Charalambous et al., 2014).

The average Sn content of 21.3 ± 5.8% is a clear indication that copper in the alloy was introduced in the form of brass or bronze (with their minor elements) and not directly as copper (native or extracted but anyway with a high title). In fact, it is likely that during the 3rd century old scrap metal or worn coins from previous reigns were used for the debasement of denarii and antoniniani (Caley and McBride, 1956). This is clearly detectable in the case of the antoninianus no. A155, where the highest Cu concentration (Figure 4) corresponds to the highest content of Sn (64.4 ± 0.2%, Figure 5).

Table 3: Average concentrations in percentage (wt%) and mean physical data for the 12 coins subjected to micro-destructive analysis.

Sample	Year (A.D.)	Mass (g)	Diameter (mm)	Thickness (mm)	% Ag	% Cu	% Pb	% Sn	% Bi	% Zn	% Ni	% Ca	% Fe
D27	193-211	3.4587	16.5	2.4	59.3	39.7	0.630	0.219	0.033	0.085	0.013	0.017	0.028
D59	193-211	3.3158	17.1	2.2	76.1	22.8	0.871	0.109	0.076	0.018	0.005	0.017	<LOD*
D125	193-211	3.4548	15.3	2.5	56.1	43.3	0.278	0.092	0.030	0.060	0.018	0.076	0.077
D128	193-211	3.5548	17.3	2.3	57.0	42.2	0.451	0.080	0.028	0.113	0.017	0.033	0.027
D151	193-211	3.5763	16.5	2.3	56.6	42.7	0.395	0.069	0.025	0.022	0.015	0.123	0.029
D23	198-209	4.0493	16.3	2.8	54.3	45.1	0.402	0.062	0.006	0.067	0.012	0.029	<LOD
D117	198-209	3.5017	15.9	2.2	54.6	44.7	0.392	0.066	0.011	0.049	0.013	0.042	0.043
D130	198-209	3.4990	15.6	2.3	49.1	48.9	1.193	0.495	0.028	0.063	0.023	0.171	0.069
A155	218-222	5.6444	19.9	2.4	40.8	56.9	0.598	1.470	0.014	0.059	0.026	0.063	0.055
A48	238-244	4.4082	20.8	2.2	51.3	47.6	0.269	0.171	0.014	0.029	0.014	0.031	0.564
A159	238-244	4.4958	21.5	2.0	52.7	46.7	0.219	0.194	0.008	0.037	0.035	0.022	0.100
A160	238-244	4.5434	21.6	1.9	51.8	47.3	0.669	0.145	0.016	0.020	0.023	0.023	0.015

*LOD=Limit of Detection

2.3 Correlation Matrix and Chemometric Analysis of Data

We used the average physical data and the percentage of elements (Table 3) to calculate the correlation matrix in order to identify positive or negative correlations. We noted a negative correlation between diameter and thickness (−0.60) and a positive correlation between mass and diameter (0.76). Moreover, a negative correlation was observed between Ag and Cu (−1.0), underlining that these elements are the two components of the binary alloy that constituted the coins. Sn and Cu are positively correlated (0.56), as well as Ni and Cu (0.68), supporting the hypothesis of re−melted brass or bronze for coining, instead of pure copper (Gitler and Ponting, 2007). On the other hand, Ag shows a positive correlation with Bi (0.82), as well as Pb and Bi (0.50), as foreseeable with the use of argentiferous galena as a mineral for silver extraction (Rodrigues et al., 2011).

Principal component analysis (PCA) was performed on the same dataset used for the bivariate analysis, in order to identify terms of difference between the two currencies and their different features. Examination of plots obtained by PCA allows us to understand trends and patterns within samples, correlation among variables, and relationships between samples and variables (Oliveri and Forina, 2012).

Regarding correlation among variables, by studying the loadings plot it can be concluded that there is a positive correlation among Sn, Ni, Cu, and weight. A second group of positively interrelated variables consist of Ag, Pb, and Bi. A third group, characterized by positive interrelated variables, is formed by Zn, Ca, and thickness. Finally, Ag and Cu are located in an orthogonal direction in the PC1 versus PC2 plane.

From the investigation of the biplot (see Figure 6), we can notice that PC1 is mainly associated with elemental composition: on the right−hand side of the plot (at the highest PC1 score values) is the coin with the highest copper amount (coin no. A155), while at the lowest values (on the left) is the coin no. D59, the denarius that contained about 76% of Ag. PC2 mainly explains the physical characteristics: at the top of the plot (at the highest PC2 score values) are coins with higher diameter, such as antoniniani. Whereas, specimens with larger thickness, such as coins no. D23 and no. D130, are located at the bottom of the biplot.

Moreover, thanks to the biplot, the difference between the two currencies can be clearly identified. Two separate groups are defined: one consisting of coins no. A48, A159, and A160 which have a larger diameter, a higher relative amount of Cu, and a fair percentage

of Fe (>0.5% for coin no. A48). The other group is located in the left−hand side of biplot and consists of seven denarii (coins no. D23, D27, D117, D125, D128, D130, and D151), which present a greater amount of lead and a higher average percentage of silver.

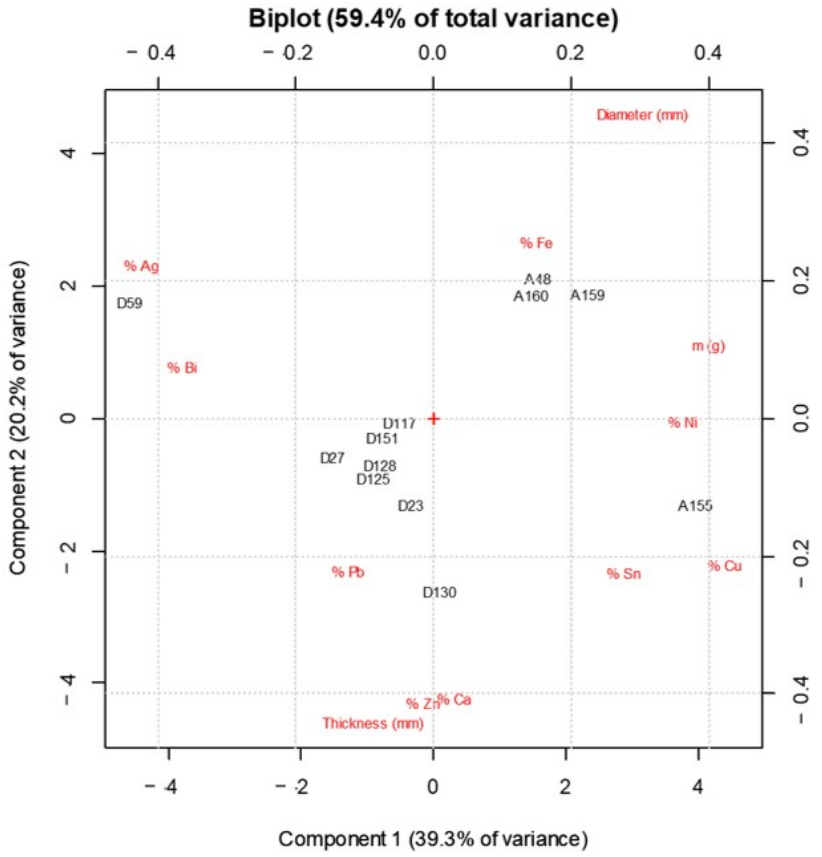

Figure 6: Biplot (score and loading scatter diagram) from PCA: scores are in black, loadings in red.

3. Material and Methods

3.1 Chemicals and Apparatuses

All chemicals used were of analytical grade. Nitric acid (67–69% v/v) was from VWR (Milan, Italy). A Millipore purification pack system (MilliQ water, Millipore, Burlington, MA, USA) was used to produce water reagent grade. For the calibration curves for ICP−AES and ICP−MS analyses, the dilution of multi−standard solutions (10 mg L^{-1}) for ICP analyses was necessary (Periodic Table MIX 1 and Periodic Table MIX 2, Sigma−Aldrich, Saint−Louis, MO, USA). The elements examined were Ag, Cu, Pb, Bi, Ca, Fe, Ni, Zn, and Sn.

A Teccpo 170 W mini drill (8000–35,000 rpm) (Teccpo, Shenzen, China) was used in the sampling procedure with HSS drill bits in W (diameter 0.5–0.9 mm). The powder resulting from drilling was weighed by means of an analytical weigh scale, Chyo JL−180 (readability: 0.1 mg; standard deviation ≤0.02 mg; stabilization time: 5 s). Thanks to Vernier callipers, it was possible to measure diameter and thickness in three places on each coin.

3.2 μ−EDXRF

An ARTAX 200 micro−XRF spectrometer (supplied by Bruker Nano GmbH, Berlin, Germany) was used to perform the elemental analysis. The instrument has an air−cooled Mo X−ray fine focus tube (max 50 kV, 1 mA, 40 W) controlled by a compact high voltage generator unit and equipped with a 650 μm collimator. It has also a Peltier cooled XFlash® silicon drift detector (10 mm^2 of active area and energy resolution <150 eV for Mn–Ka at 100 kcps) and a CCD camera (500 × 582 pixels) for sample positioning. The focal spot is 1.2 × 0.1 mm^2 with a 0.2 mm lateral resolution and a 100 μm beryllium window. For the hardware control and analytical data evaluation, the ARTAX control semi−quantitative XRF software was used (version 5.3.14.0, license of Bruker AXS Microanalysis GmbH, Berlin, Germany). Data are plotted as counts versus energy (keV). For our analyses, the instrumental parameters were set as follows: X−ray tube = 30 W, Mo target U = 50 kV, I = 700 μA, acquisition time = 45 s (live time), collimator = 650 μm (air environment). The examined elements were: Ag (line: Lα1 2.98 keV; Kα1 22.16 keV), Cu (line: Kα1 8.05 keV), Pb (line: Lα1 10.55 keV; Lβ1 12.61 keV), Zn (line: Kα1 8.64 keV), Fe (line: Kα1 6.40 keV), Ni (line: Kα1 7.48 keV), Sn (line: Kα1 25.27 keV), and Ca (line: Kα1 3.69 keV).

Two spectra were collected on the recto and two on the verso of each coin, making a total of four spectra for each specimen in order to obtain representative data of the entire coin.

3.3 SEM−EDX

Scanning Electron Microscopy with Energy Dispersive X−ray spectroscopy (SEM−EDX) measurements were performed on 4 coins in order to study the superficial inhomogeneity of the samples. A Carl Zeiss Sigma VP (Sigma−Aldrich, Saint−Louis, MO, USA) field emission scanning electron microscope (FE−SEM) equipped with a

Bruker Quantax 200 microanalysis detector was used to carry out the analyses. SEM micrographs, EDX spectra, and maps were recorded under the same conditions (20 keV, 60 µm condenser aperture) for all the samples; both secondary electrons and backscattered electrons were used as imaging signals.

3.4 ICP−AES

The major elements (Ag and Cu) were determined by analysing sample solutions with an ICP−AES spectrometer (PerkinElmer® Optima™ 8000, Waltham, MA, USA). Calibration (linear in the concentration range of 0.1–10 mg L^{-1}) was performed after the dilution of a multi−standard solution 10 mg L^{-1} for ICP analysis (Periodic table mix 1 for ICP TraceCERT®, Sigma−Aldrich). The limits of detection (LOD) in the solution sample at the operative wavelength for each element were: 0.02 mg L^{-1} for Cu at 327.393 nm and 0.02 mg L^{-1} for Ag at 328.068 nm. The coefficients of variation of repeatability (RSD %) were found to be <5%.

3.5 ICP−MS

Trace metals concentrations − Pb, Bi, Ca, Fe, Ni, Zn, and Sn − were determined by Inductively Coupled Plasma−Mass Spectrometry (ICP−MS) using a NexION 350x Spectrometer (PerkinElmer, Waltham, MA, USA) equipped with an ESI SC autosampler. In order to control and minimize cell−formed polyatomic ion interference, the analysis was performed in KED mode (Kinetic Energy Discrimination) using ultra−high purity helium (flow rate of 4.8 mL min^{-1}). The calibration of instrument (linear in the concentration range of 0.5–100 µg L^{-1}) was carried out following dilution of a multi−standard solution 10 mg L^{-1} for ICP analysis (Periodic table mix 1 for ICP TraceCERT® and Periodic table mix 2 for ICP TraceCERT®, Sigma−Aldrich). The measurements of samples were performed using the calibration curve method obtained by analysing standard solutions. The limits of detection (LOD) for each element were: Pb 0.005 µg L^{-1}; Bi 0.001 µg L^{-1}; Ca 1.5 µg L^{-1}; Fe 0.7 µg L^{-1}; Ni 0.1 µg L^{-1}; Zn 0.2 µg L^{-1}; and Sn 0.01 µg L^{-1}. The coefficients of variation of repeatability (RSD %) were <3%.

3.6 Data Processing

Bivariate analysis was performed by computation of Pearson's correlation coefficients between couples of variables, selected from the physical and chemical data. Computations were performed using MS−Excel (Microsoft Corporation, Redmond, WA, USA, Version 2019). The same data were analysed by principal component analysis (PCA), too. PCA is an unsupervised exploratory chemometric tool for the identification and visual representation of relationships: (i) among the samples (PC scores and score plots), (ii) within variables (PC loadings and loading plots), and (iii) between samples and variables (biplots) (Oliveri et al., 2020). Due to the different nature and different measurements units of data, pre−processing of the data matrices (column−autoscaling) was necessary before the multivariate analysis (Oliveri et al., 2019). Multivariate data processing was performed using the CAT (Chemometric Agile Tool, update of September 13, 2022) package, based on the R platform (R version 3.1.2, Copyright © 2014 The R Foundation for Statistical Computing, Vienna, Austria) and freely distributed by Gruppo Italiano di Chemiometria (Italy) (Leardi et al., 2019).

4. Conclusions

For the 12 coins subjected to micro−destructive analysis, a combination of μ−EDXRF, SEM−EDX, ICP−AES, and ICP−MS techniques allowed the determination of the alloy percentage (dominant elements) and the trace elements concentrations of ancient denarii and antoniniani. The multi−analytical approach enables to unveil the chemical composition of ancient coins and to speculate on raw materials' nature and minting processes, as well as to identify surface corrosion compounds (which helps to address the hypotheses on the environmental history of the finds).

The presence of Ag, Cu, Pb, Sn, Ni, Zn, Bi, Fe, and Ca and the inhomogeneity of the coins' surfaces can be deduced from the responses of the non−destructive analysis conducted on all 160 finds. Also considering the surface roughness that may affect the response of the XRF analysis, slight irregularities in the trends and imperfect superimposition of the spectra are indications of an inhomogeneous surface chemical composition. The different distribution of the two main alloy's elements was also highlighted by SEM−EDX analysis, carried out on four specimens (two denarii and two antoniniani).

Due to the great value of these historical specimens, micro−destructive analyses involved only 12 coins. In this study, a few milligrams of sample were picked up at a depth of a few millimetres. The sampling method adopted, despite some limitations mainly due to the scarcity of the available sample, provided representative samples of inhomogeneous ancient coins and allowed us to measure the elemental composition (major and minor elements) of the coins under study. We discovered that the alloy composition of the eight studied denarii is almost constant, except for denarius no. D59, which has a higher concentration of silver, and denarius no. D130, which has almost equal concentrations of Cu and Ag. The four antoniniani analysed also have a similar alloy percentage, except for antoninianus no. A155, which presents a greater concentration of Cu. However, we have clearly noticed the difference between the two currencies, with a net decrease in the % of Ag as the year of minting increases, underlining the progression of the third century economic crisis.

Among the trace elements, the high concentrations of Pb and Sn are in agreement with the use of argentiferous galena for silver extraction and old brass or bronze objects for the production of the silver−copper coins, respectively. This was confirmed also by bivariate and multivariate correlations. The latter statistical investigation identified the two groups of coins corresponding to the two currencies, providing a first basis for a numismatic database, and allowing the chemical mapping of unknown samples.

References

Beck, L., Bosonnet, S., Reveillon, S., Eliot, D., Pilon, F., 2004. Silver surface enrichment of silver–copper alloys: a limitation for the analysis of ancient silver coins by surface techniques. Nuclear Instruments and Methods in Physics Research Section B: Beam Interactions with Materials and Atoms 226, 153–162. https://doi.org/10.1016/S0168-583X(04)00831-6

Borges, R., Alves, L., Silva, R.J.C., Araújo, M.F., Candeias, A., Corregidor, V., Valério, P., Barrulas, P., 2017. Investigation of surface silver enrichment in ancient high silver alloys by PIXE, EDXRF, LA-ICP-MS and SEM-EDS. Microchemical Journal 131, 103–111. https://doi.org/10.1016/j.microc.2016.12.002

Caley, E.R., McBride, H.D., 1956. Chemical Composition of Antoniniani of Trajan Decius, Trebonianus Gallus, and Valerian. The Ohio Journal of Science 56, 285–289.

Callu, J.-P., 1984. Metallurgy in Numismatics, I, in: Revue numismatique. pp. 271–273.

Charalambous, A., Kassianidou, V., Papasavvas, G., 2014. A compositional study of Cypriot bronzes dating to the Early Iron Age using portable X-ray fluorescence spectrometry (pXRF). Journal of Archaeological Science 46, 205–216. https://doi.org/10.1016/j.jas.2014.03.006

Crosera, M., Baracchini, E., Prenesti, E., Giacomello, A., Callegher, B., Oliveri, P., Adami, G., 2019. Elemental characterization of surface and bulk of copper-based coins from the Byzantine-period by means of spectroscopic techniques. Microchemical Journal 147, 422–428. https://doi.org/10.1016/j.microc.2019.03.025

Doménech, A., Doménech-Carbó, M.T., Pasies, T., del Carmen Bouzas, M., 2012. Modeling Corrosion of Archaeological Silver-Copper Coins Using the Voltammetry of Immobilized Particles. Electroanalysis 24, 1945–1955. https://doi.org/10.1002/elan.201200252

Elliott, C.P., 2014. The Acceptance and Value of Roman Silver Coinage in the Second and Third Centuries AD. The Numismatic Chronicle 174, 129–152.

Fabrizi, L., Di Turo, F., Medeghini, L., Di Fazio, M., Catalli, F., De Vito, C., 2019. The application of non-destructive techniques for the study of corrosion patinas of ten Roman silver coins: The case of the medieval Grosso Romanino. Microchemical Journal 145, 419–427. https://doi.org/10.1016/j.microc.2018.10.056

Gitler, H., Ponting, M., 2007. Rome and the East. A Study of the Chemical Composition of Roman Silver Coinage during the Reign of Septimius Severus AD 193-211. Topoi. Orient-Occident 8, 375–397.

Hrnjić, M., Hagen-Peter, G.A., Birch, T., Barfod, G.H., Sindbæk, S.M., Lesher, C.E., 2020. Non-destructive identification of surface enrichment and trace element fractionation in ancient silver coins. Nuclear Instruments and Methods in Physics Research Section B: Beam Interactions with Materials and Atoms 478, 11–20. https://doi.org/10.1016/j.nimb.2020.05.019

Ingo, G.M., Balbi, S., de Caro, T., Fragalà, I., Angelini, E., Bultrini, G., 2006. Combined use of SEM-EDS, OM and XRD for the characterization of corrosion products grown on silver roman coins. Applied Physics A 83, 493–497. https://doi.org/10.1007/s00339-006-3533-0

King, C.E., Hedges, R.E.M., 1974. An analysis of some third-century roman coins for surface silvering and silver percentage of their alloy content. Archaeometry 16, 189–200. https://doi.org/10.1111/j.1475-4754.1974.tb00104.x

Leardi, R., Melzi, C., Polotti, G., 2019. CAT (Chemometric Agile Tool) [WWW Document]. URL http://gruppochemiometria.it/index. php/software

Linke, R., Schreiner, M., Demortier, G., Alram, M., 2003. Determination of the provenance of medieval silver coins: potential and limitations of x-ray analysis using photons, electrons or protons. X-Ray Spectrometry 32, 373–380. https://doi.org/10.1002/xrs.654

Manukyan, K., Fasano, C., Majumdar, A., Peaslee, G.F., Raddell, M., Stech, E., Wiescher, M., 2019. Surface manipulation techniques of Roman denarii. Applied Surface Science 493, 818–828. https://doi.org/10.1016/j.apsusc.2019.06.296

Oliveri, P., Forina, M., 2012. Data Analysis and Chemometrics, in: Chemical Analysis of Food: Techniques and Applications. Elsevier, pp. 25–57. https://doi.org/10.1016/B978-0-12-384862-8.00002-9

Oliveri, P., Malegori, C., Casale, M., 2020. Chemometrics: multivariate analysis of chemical data, in: Chemical Analysis of Food. Elsevier, pp. 33–76. https://doi.org/10.1016/B978-0-12-813266-1.00002-4

Oliveri, P., Malegori, C., Simonetti, R., Casale, M., 2019. The impact of signal pre-processing on the final interpretation of analytical outcomes – A tutorial. Analytica Chimica Acta 1058, 9–17. https://doi.org/10.1016/j.aca.2018.10.055

Pardini, L., El Hassan, A., Ferretti, M., Foresta, A., Legnaioli, S., Lorenzetti, G., Nebbia, E., Catalli, F., Harith, M.A., Diaz Pace, D., Anabitarte Garcia, F., Scuotto, M., Palleschi, V., 2012. X-Ray Fluorescence and Laser-Induced Breakdown Spectroscopy analysis of Roman silver denarii. Spectrochimica Acta Part B: Atomic Spectroscopy 74–75, 156–161. https://doi.org/10.1016/j.sab.2012.06.016

Rodrigues, M., Cappa, F., Schreiner, M., Ferloni, P., Radtke, M., Reinholz, U., Woytek, B., Alram, M., 2011. Further metallurgical analyses on silver coins of Trajan (AD

98–117). Journal of Analytical Atomic Spectrometry 26, 984. https://doi.org/10.1039/c0ja00252f

Tanasi, D., Greco, E., Di Tullio, V., Capitani, D., Gullì, D., Ciliberto, E., 2017. 1H-1H NMR 2D-TOCSY, ATR FT-IR and SEM-EDX for the identification of organic residues on Sicilian prehistoric pottery. Microchemical Journal 135, 140–147. https://doi.org/10.1016/j.microc.2017.08.010

SECTION 4

Enhancing Understanding of the Sasanian Dynasty: Archaeometric Investigations of Silver Drachmas (6^{th}–7^{th} Century AD) Using X−Ray Fluorescence Analysis

Abstract

X−Ray Fluorescence (XRF) analysis is widely employed in the field of cultural heritage due to its non−destructive nature. A group of 29 Sasanian drachmas belonging to a private collection at the Department of Humanities of the University of Trieste were characterised using μ−EDXRF. These coins were issued between 498 and 628 AD, during the reign of four Sasanian kings (Kavad I, Khosrow I, Hormizd IV, and Khosrow II). This study aimed to determine the elemental composition of the alloy's surface, with the objective of ascertaining the fineness of the 29 drachmas and identifying any potential forgeries or devaluation processes that may have occurred during the period covered by these coins. After cataloguing the coins and measuring their mass, diameter, and thickness, eight XRF spectra were acquired for each sample to ensure a representative result for the entire coin. The analysed drachmas were primarily composed of Ag, with traces of Cu, Au, and Pb. Using a sterling silver standard, it was possible to semi−quantitatively determine the Ag and Cu content of the 29 coins. The analysis revealed Ag contents exceeding 95% in nearly all coins, with one exception, which exhibited a high copper and mercury content, suggesting the possibility of it being a forgery.

In addition, a group of six coins minted during the reign of Khosrow II were identified: they bore the inscription "afid", indicating superior quality compared to other drachmas from the same period. Semi−quantitative analysis using μ−EDXRF revealed a silver content exceeding 99% for five of these drachmas, along with very low Pb/Au ratios, corroborating the historical hypothesis. Finally, the Au/Ag ratio, which can provide additional insights into the silver's origin, potentially identified two distinct groups of coins that may have been forged from two different minerals. However, further analyses, e.g., by LA−ICP−MS, may be required to confirm this hypothesis.

1. Introduction

Chemical analysis of ancient coins provides valuable information about the metallurgy and economy of the time when the coins were minted. The percentage composition of silver coins can be used to analyse and explain the location and identification of the mines from which the metals used in coin minting originated. It also offers insights into the economic and political conditions of the time considered (Sodaei et al., 2013). Due to the high value and rarity of ancient coins, museums and collectors of numismatic items often require chemical analyses using exclusively non−destructive techniques. This ensures that no material is removed, and the sample remains unaltered throughout the analysis process. The most commonly used non−destructive techniques for this purpose include X−Ray Fluorescence analysis (XRF), Electron Probe Micro−Analysis (EPMA), micro−X−ray analysis in a Scanning Electron Microscope (SEM−EDX), Synchrotron micro X−Ray Fluorescence analysis (SRXRF) and Particle−Induced X−ray Emission (PIXE) (Volpi et al., 2023). Among these techniques, XRF has firmly established itself in the field of cultural heritage and, more specifically, in the analysis of ancient coins due to its cost−effectiveness, non−destructive nature, speed, and its ability to analyse the sample as is, without requiring pre−treatment or cleaning (Linke and Schreiner, 2000).

In this study, 29 silver Sasanian drachmas issued by four Sasanian kings during the period between the 6th and 7th centuries AD were examined (Table 1). These specimens were part of a private collection held by the Department of Humanities at the University of Trieste.

Table 1: List of coins under study. In total there are 29 drachmas belonging to four different kings and minted in different mints of the Sasanian Empire.

Emperor	Period of issue (AD)	Number of samples	Mintmarks
Kavad I	498−531	6	AS, AY, BN, KA
Khosrow I	531−579	4	MA, AM, BYS, YZ
Hormizd IV	579−590	4	ART, LD, YZ, WH
Khosrow II	591−628	15	LYW, BYS, BBA, WYHC, DA, AHM, WYH, ML, ART, AW, SY, YZ, BN

The Sasanian dynasty, or the Sasanian Empire, was established in 224 AD, when Ardashir I defeated the last Parthian Shahanshah, Artabanus IV, on the Hormozdgan plain. The history of Sasanian dynasty concluded in 651 AD with Yazdegerd III, when the Arab conquest marked the end of Persian independence (Gariboldi, 2010). The Sasanian Empire was one of the most prosperous and influential states in the ancient world. Still, due to the limited availability of other historical evidence, its coinage remains the most critical source for the study of its political and economic history (Uhlir et al., 2016).

Like any new monarch, Ardashir I began issuing coins in his own name. Although the initial drachmas were influenced by a Parthian model and contained approximately 75% silver, Ardashir soon established a drachma type that became the standard for all Sasanian silver coin issues. The new coins, minted on a thin flan, weighed between 3 and 4.25 grams and contained 95% silver (Bacharach and Gordus, 1972). The silver content remained significantly high until the reign of Khosrow II. During the rule of Yazdegerd III (632−651 AD), the increasing weakness of the monarchy was reflected in the purity of the coinage, which declined to a silver content of 84%.

Hajivaliei et al. (2008) analysed thirty Iranian silver coins dating back to Khosrow II (592−626 AD) in order to identify any potential correlation between the composition of the coins and their time or place of minting. The researchers demonstrated that the silver content of coins minted in the western mints of the Sasanian Empire decreased in comparison to those coined in the eastern mints, possibly due to the western mints' proximity to war sites.

In addition to the primary metal, minor and trace elements are of great significance, as they may originate from different ores or processes used in silver production (Linke et al., 2004). For instance, the presence of gold in the alloy can be used as an indicator of the primary ore source since it remains unaffected by melting and cupellation (Mortazavi et al., 2018). Today, silver is usually obtained by electrolysis (patented in the second half of the 19th century) and contains traces of gold less than 0.01%, thus undetectable by XRF analysis (Gordus and Gordus, 1974). Therefore, the absence of gold in ancient specimens could suggest modern forgeries, as there was no technology in antiquity capable of completely extracting gold from ore (Constantinescu et al., 2005; Hajivaliei et al., 2008).

Although the sources of silver used in ancient coin minting may vary, it is generally believed that silver was primarily extracted from argentiferous lead ores, particularly cerussite and argentiferous galena (Harper, 1981). In these silver−rich lead ores, gold is

consistently found at a specific concentration unique to each ore (Eshel et al., 2023). Moreover, it remains unchanged throughout the various processing stages of lead mineral. The Au/Ag ratios can be valuable for distinguishing different sources of silver used for coinage. For instance, an empirical value of 0.1 wt% gold in silver objects represents the upper limit for silver derived from galena (Butcher and Ponting, 2015).

Copper is another crucial element in silver coins. Cu contents exceeding 1% suggest a deliberate addition of this element to enhance the mechanical properties and strength of the silver (Hughes and Hall, 1979). In fact, the alloy's hardness is strongly correlated with the amount of copper intentionally added to the silver (Scott, 2011). Conversely, a low copper content may indicate prosperous economic conditions (Sodaei et al., 2013).

The main aim of this study is to determine the composition of the 29 Sasanian drachmas using only multi−elemental, non−destructive micro−Energy Dispersive X−Ray Fluorescence (μ−EDXRF) technique. This analysis will enable the identification of historical forgeries. Additionally, some of the drachmas minted by Khosrow II feature the Middle Persian language inscription "afid" ("marvellous" or "excellent") on the recto, which is assumed to represent better quality compared to other coins from the same period without the inscription. This work also aims to test this hypothesis.

Table 2:Exemplary images of both obverse (recto) and reverse (verso) sides of four drachmas, each representing different kings: Kavad I, Khosrow I, Hormizd IV, and Khosrow II. The captions under the coins provide the king's name, the period of issue, and the respective mint where each coin was struck.

 	 
Drachm no. 5, Kavad I (498−531 AD) Karzi (Fars)	Drachm no. 9, Khosrow I (531−579 AD) Bishapur (Fars)
 	 
Drachm no. 12, Hormizd IV (579−590 AD) Rayy (Jibal)	Drachm no. 27, Khosrow II (591−628 AD) Yazd (Fars)

2. Results and discussion

X−ray micro−fluorescence primarily probes the surface of the material. X−photons are typically absorbed within the first 10−100 μm of the surface, depending on the material's density (Gianoncelli and Kourousias, 2007). However, previous studies (Gordus and Gordus, 1974; Hrnjić et al., 2020) have demonstrated that Sasanian coins exhibit minimal differences in silver content between their surface and the bulk. Consequently, this technique was employed for a semi−quantitative analysis to ascertain the fineness and identify minor elements. The spectra collected from both recto and verso of each coin showed considerable overlap, with estimated differences in fluorescence peak intensities ranging from 5−10%. As a result, the primary peak areas, including those for silver, copper, gold, and lead, were averaged to obtain a single value for each coin. Due to the availability of a sterling silver standard (composed of 92.5% Ag and 7.5% Cu), a semi−quantitative analysis for these two elements was conducted (Figure 1). The percentages shown in Figure 1 are obtained by assuming that the sum of the two elements concentrations is 100%.

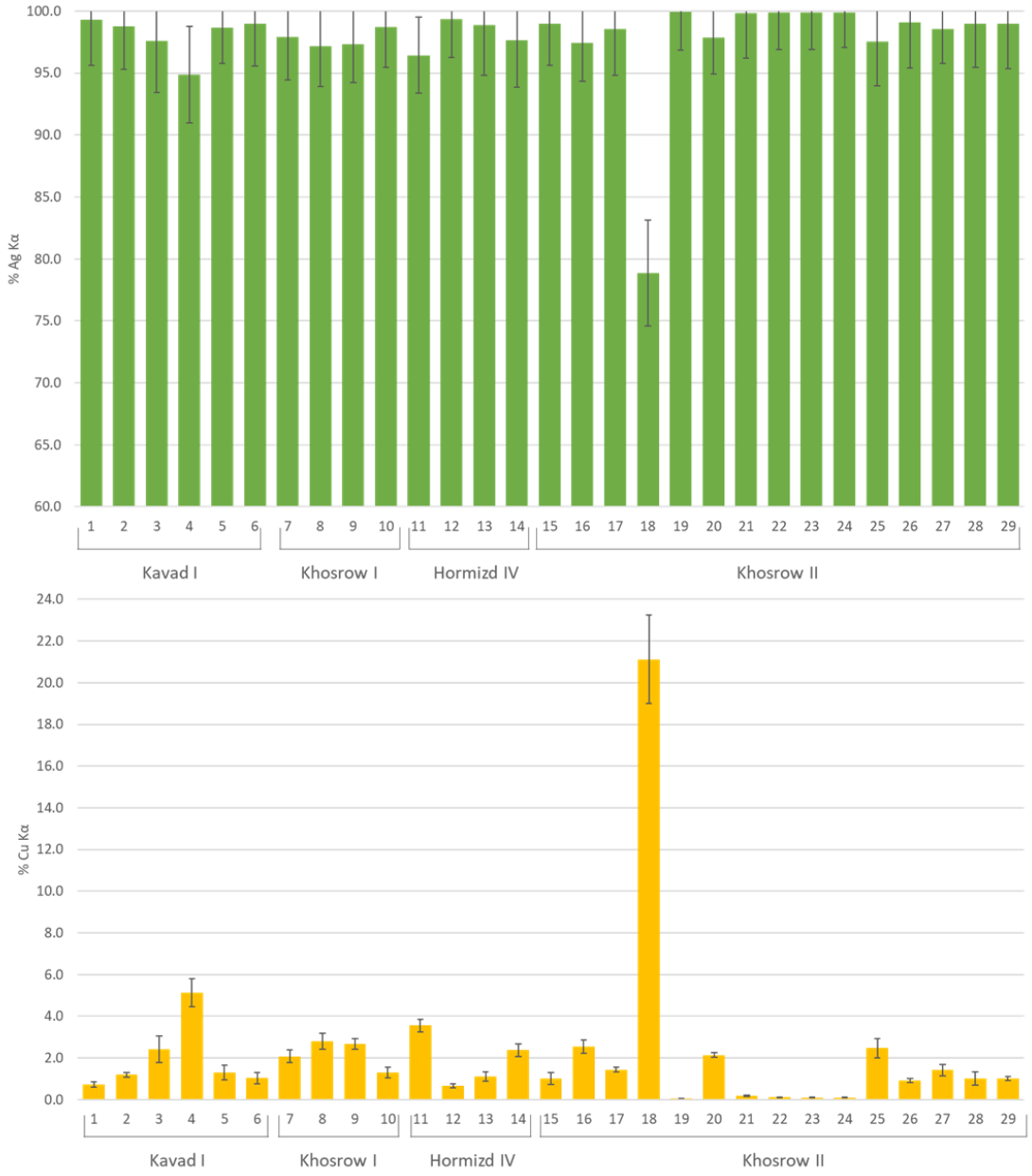

Figure 1: Average silver content in green and average copper content in yellow, estimated from the Kα fluorescence lines of the two elements. Standard deviations are expressed as error bars.

As depicted in Figure 1, the silver content was notably high on average, exceeding 90% in most cases, except for coin No. 18. This drachma not only exhibited the lowest silver content (78.9 ± 4.3%), but also the highest copper content (21.1 ± 2.1%). The inverse correlation between silver and copper was a consistent observation across all coins. Coin No. 18 exhibited this behaviour most prominently. Notably, the percentage of copper in this drachma is higher than typical silver impurity levels (3−5%) (Mortazavi et al., 2018). In addition, the analysis of the XRF spectra for this coin revealed the presence of zinc

(with a Kα peak at 8.64 keV) and mercury (with a Lα peak at 9.99 keV and a Lβ peak at 11.82 keV). While the presence of zinc can be linked to the high copper content (Meyers and Sayre, 1971), the source of mercury remains a subject of debate. Although mercury has been previously detected in studies on Sasanian drachmas (Gaudiuso et al., 2019; Heidemann et al., 2014; Meyers and Sayre, 1971; Uhlir et al., 2016), the origin of this element has yet to be determined. One hypothesis suggests that its presence on the coin surfaces may result from the application of mercury−based ointments for medical purposes, potentially contaminating coins that were frequently in contact with the skin when stored under clothing. Another hypothesis proposes that mercury may have been used in the coin casting process to enhance their lustre. Unfortunately, the question of mercury's origin remains unresolved. Given these observations and the fact that coin No.18 had the lowest mass, there is reason to suspect it may be a forgery.

Drachma No. 13 exhibited an atypical XRF spectrum with the absence of the typical gold−associated fluorescence peaks. Figure 2 provides a comparison of the XRF spectra between coins No. 13 and No. 3. It can be seen that the decrease in the intensity of the Au peaks corresponds to an increase in the intensity of the characteristic lead (Pb) peaks. The absence of gold in this coin is of particular interest, as the Sasanians had lacked the technology to extract gold from ore. This anomaly suggests that it may have been minted more recently, in the 19th century, benefiting from advances in metallurgical technology that reduced gold impurities in silver (Bacharach and Gordus, 1972). Further analyses of this coin are necessary to definitively establish whether it is a modern forgery.

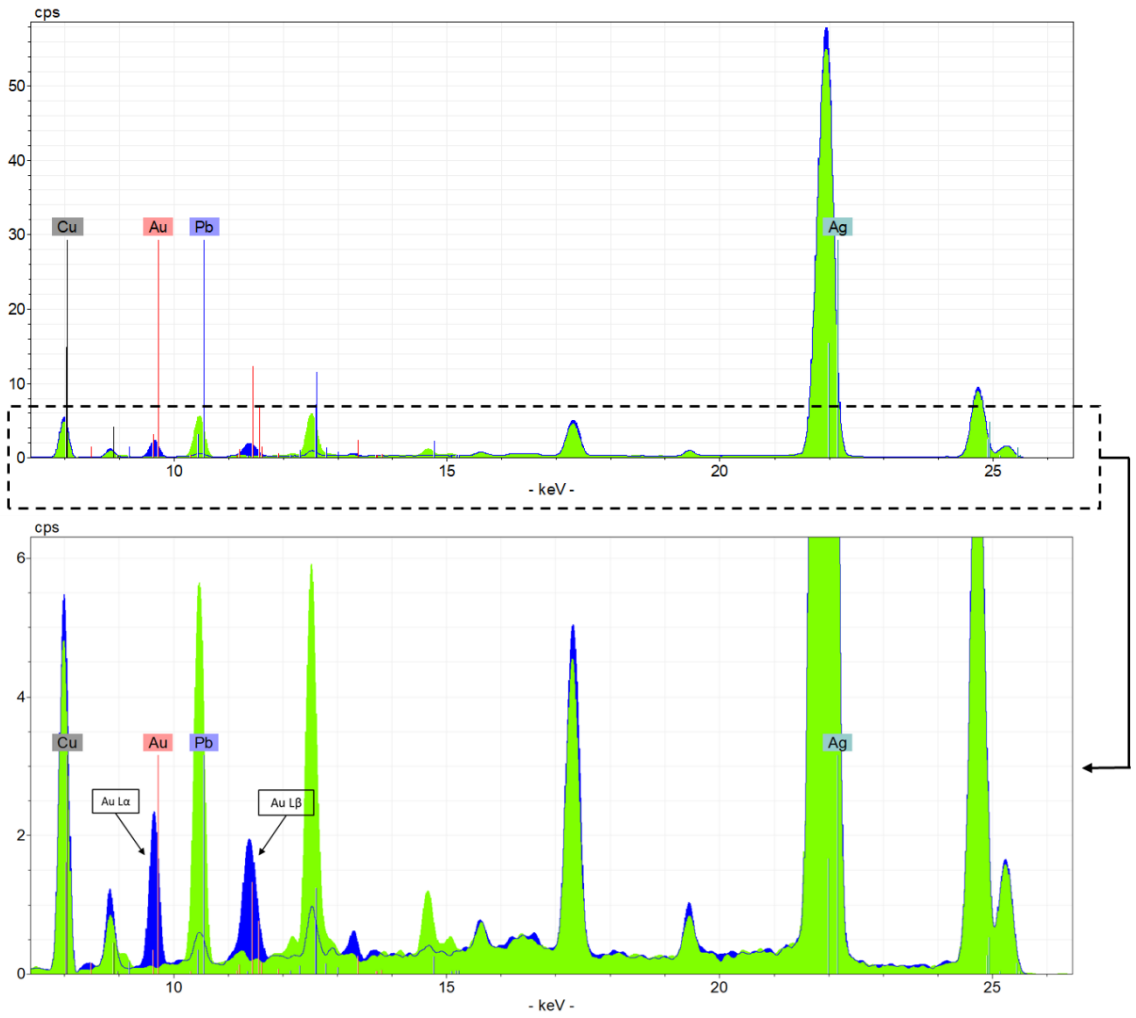

Figure 2: Average overlapped μ−EDXRF spectra of coin No. 13 (in green) and No. 3 (in blue). The lower spectrum is in relation to the region enclosed by the dashed box, where the absence of gold peaks at 9.71 keV and 11.44 keV is apparent.

The Au/Ag ratio is important for identifying the origin of the silver used in minting Sasanian coins. The relative values obtained for the 29 coins under study are shown in Table 3.

Table 3: Au Lα/Ag Kα and Pb Lα/Ag Kα ratios obtained from the areas of the XRF peaks of these elements. Au/Ag ratios higher than the average value (0.020) are highlighted in bold. Coin No. 13 lacked the typical gold peaks, while Coin No. 22 did not exhibit lead's characteristic peaks. In Coin No. 18, mercury fluorescence peaks interfered with the gold peaks, rendering the calculation of the Au/Ag ratio unfeasible.

Coin number	Emperor	Mint marks	Au/Ag	Pb/Ag
1	Kavad I	AS	0.018	0.003
2	Kavad I	AY	**0.028**	0.029

3	Kavad I	BN	**0.023**	0.007
4	Kavad I	AY	**0.024**	0.011
5	Kavad I	KA	**0.026**	0.008
6	Kavad I	AY	**0.027**	0.013
7	Khosrow I	MA	0.015	0.003
8	Khosrow I	AM	**0.023**	0.009
9	Khosrow I	BYS	0.020	0.018
10	Khosrow I	YZ	0.004	0.034
11	Hormizd IV	ART	**0.022**	0.003
12	Hormizd IV	LD	**0.021**	0.037
13	Hormizd IV	YZ	−	0.060
14	Hormizd IV	WH	0.018	0.066
15	Khosrow II	LYW	**0.025**	0.010
16	Khosrow II	BYS	0.018	0.057
17	Khosrow II	BBA	0.020	0.039
18	Khosrow II	WYHC	−	0.036
19	Khosrow II	DA	**0.022**	0.004
20	Khosrow II	AHM	**0.021**	0.018
21	Khosrow II	WYH	**0.024**	0.003
22	Khosrow II	ML	**0.024**	−
23	Khosrow II	BYS	0.006	0.016
24	Khosrow II	ART	**0.022**	0.005
25	Khosrow II	AW	**0.023**	0.034
26	Khosrow II	SY	**0.026**	0.008
27	Khosrow II	YZ	0.012	0.008
28	Khosrow II	BN	0.019	0.007
29	Khosrow II	WYH	0.019	0.002

The average value of the Au/Ag ratio (0.020) divides the 29 silver drachmas into two groups: 11 coins with a lower Au/Ag ratio and 16 drachmas with a ratio higher than 0.020. The two primary minerals from which silver was extracted in antiquity, non−galena and galena−ore, can be distinguished based on their gold content, with values respectively above and below 0.1 wt% (Wood et al., 2017). Considering the results obtained from the gold−silver ratios, it could be assumed that the two groups of coins were produced using two different minerals for silver extraction.

Regarding lead, its characteristic peaks (Lα at 10.55 keV, and Lβ at 12.61 keV) were consistently observed in all the coins except for number 22. The low Pb/Ag ratios indicate the relative purity of the drachmas, thereby highlighting the Sasanians' extensive

knowledge of metallurgy and silver purification processes during the 5th–6th centuries(Mortazavi et al., 2018; Sodaei et al., 2013).

Among the 29 coins, six featured the Pahlavi word “afid” (“good”, “excellent”) on the recto edge (Figure 3).

Figure 3: Drachma No. 19, minted during the reign of Khosrow II, serves as a prime illustration from the group of coins featuring the distinctive “afid” inscription. The word is highlighted by the red box.

This distinct category of drachmas was introduced by Khosrow II between 600 and 602 AD and possessed a slightly higher average purity than ordinary drachmas. The reason for this introduction is still uncertain. It remains unclear whether it was implemented to mark the end of a decade of civil war or to serve as a hallmark to assure recipients of the quality of the coins with which they were paid (Howard-Johnston, 2014). Analyses conducted on these coins revealed a superior quality compared to the other drachmas minted in the same period. In fact, with the exception of coin No. 20, the coins engraved with the word “afid” had silver contents of over 99.8% and the lowest contents of copper and lead (Fig. 4), elements usually present as impurities resulting from the cupellation processes. It can be concluded that these coins are indeed of better quality than the others minted by Khosrow II.

As can be seen in Figure 4, coin number 20 exhibits Cu/Ag and Pb/Ag ratios more similar to those found in coins numbered 25−29. Further analysis on this specific coin using more sensitive techniques than XRF could be useful to better understand the reason for this divergence, although coin No. 20 bears the inscription “afid” on the recto.

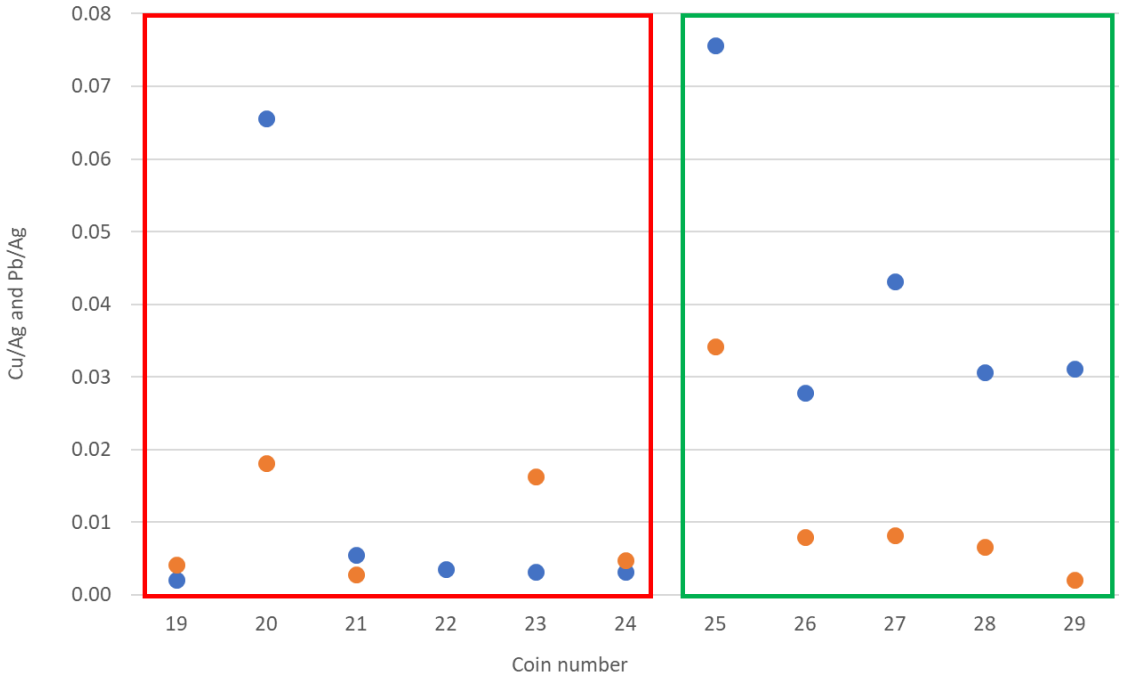

Figure 4: The Cu/Ag and Pb/Ag ratios (in blue and orange, respectively) of drachmas of Khosrow II minted during the same period. The red square highlights coins with the "afid" inscription, while the green square pertains to those without it.

In addition to silver, copper, gold, and lead, some coins exhibited fluorescence peaks of calcium (Kα at 3.69 keV) and iron (Kα at 6.40 keV). These can be attributed to the sedimentary layer on the surface of the Sasanian drachmas analysed in this work.

3. Material and methods

This work exclusively relies on the use of micro−Energy Dispersive X−Ray Fluorescence (μ−EDXRF) as analytical technique. It is undoubtedly the most common technique for analysing ancient coins, given its non−destructive nature, which eliminates the need for pre−treatment or sampling. However, it has some limitations, such as limited sensitivity, ranging from 0.1 ppm to a few percent for elements with low atomic numbers, and it can only detect elements within the atomic number range of Na to U (Z=11−92) (Linke et al., 2004; Liritzis and Zacharias, 2011). Nonetheless, this technique was well−suited for our research purposes.

All 29 Sassanid drachmas that were analysed were exceptionally well−preserved and showed no visible signs of corrosion. As coins often have uneven and irregular surfaces,

eight measurements were taken for each coin, four on the recto and four on the verso, and then average values were calculated. XRF spectra were acquired in the smoothest and cleanest regions possible to optimise the instrumental response.

The elements examined included: Ag (line: Lα1 2.98 keV; Kα1 22.16 keV), Cu (line: Kα1 8.05 keV; Kβ1 8.90 keV), Pb (line: Lα1 10.55 keV; Lβ1 12.61 keV), Au (line: Lα1 9.71 keV; Lβ1 11.44 keV), Zn (line: Kα1 8.64 keV), Hg (line: Lα1 9.99 keV; Lβ1 11.82 keV), Fe (line: Kα1 6.40 keV; Kβ1 7.06 keV), Ni (line: Kα1 7.48 keV), and Ca (line: Kα1 3.69 keV).

The standard used in this work for the semi−quantitative analysis was a silver−copper alloy sheet (Ag 92.5/Cu 7.5) (25 × 25 × 0.5 mm) supplied by Goodfellow, UK.

3.1 Experimental setup

The micro−XRF spectrometer used in this study was manufactured by Bruker Nano GmbH (Berlin, Germany), and is known as the ARTAX 200 model. Figure 5 depicts the experimental setup employed in the ARTAX 200. This instrument comprises an air−cooled X−ray tube with molybdenum anode, capable of reaching a maximum voltage, current, and power of 50 kV, 1000 µA, and 40 W, respectively. It features a Peltier−cooled XFlash® SDD (Silicon Drift Detector) with 10 mm^2 active area and energy resolution <150 eV for Mn−Kα at 100 kcps. To select the measurement point, a colour CCD camera (500 × 582 pixels) is employed. A laser dot and reticule on the video display are used to ensure the reproducibility of the measurement point and distance. The focal spot measures 1.2 × 0.1 mm^2 with a lateral resolution of 0.2 mm, and a beryllium window of 100 µm. Additionally, the system includes an interchangeable slide with three filter positions; however, no filter was employed in this study. The experimental conditions for this research were set as follows: a high X−ray tube voltage of 50 kV, anode current of 700 µA, molybdenum target, spectral acquisition time of 45 seconds (live time), a collimator diameter of 650 µm in air, and an acquisition window within the range 1−25 keV.

The control software for the ARTAX spectrometer is the ARTAX control semi−quantitative XRF software (version 5.3.14.0, licensed from Bruker AXS Microanalysis GmbH, Berlin, Germany). This software was used for both hardware control and the evaluation of the analytical data. The data are represented in terms of counts per second (cps) versus energy (keV).

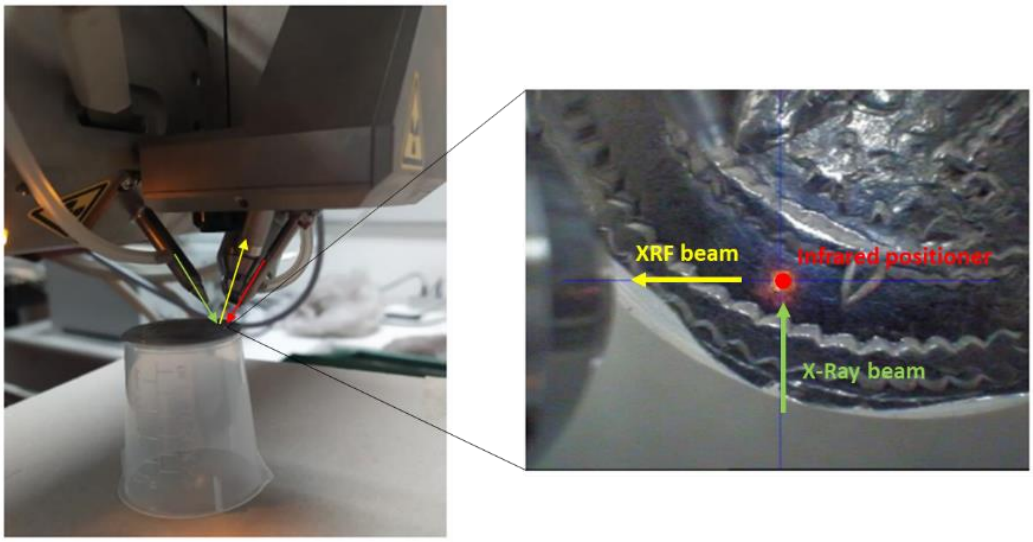

Figure 5: The experimental setup and image obtained by ARTAX 200.

4. Conclusions

In this study, 29 Sasanian drachmas were analysed. X−ray fluorescence spectroscopy revealed that the primary alloying element was silver, with impurities such as copper, lead and gold. Due to the availability of a sterling silver standard, a semi−quantitative analysis was conducted to determine the content of these two elements. This analysis unveiled a remarkably high average silver content of over 95% in nearly all the coins, indicating the prosperous period during which they were minted. Coin No. 18 is particularly intriguing due to its low silver and high copper content, along with the presence of mercury on its surface, might suggest that it is a silver−plated specimen.

The Au/Ag ratio, often useful in determining the origin of silver, was also calculated. This led to the identification of two groups, possibly indicating that the coins were produced from different minerals, galena and a non−galenic ore, most likely cerussite. Notably, the only coin that did not exhibit the fluorescence characteristic peaks of gold was coin number 13. This is fascinating because the ancient Sasanians lacked the technology to separate gold from silver, raising the possibility that this coin might be a modern reproduction of a Sasanian drachma.

Finally, a group of five coins with a higher silver content (>99.8%) was observed. These coins bear the inscription “afid” on the recto, which means “good” or “excellent” in Middle Persian. The analyses conducted in this study affirmed the superior quality of

these coins compared to similar coins minted in the same period but lacking the inscription.

To definitively assign the coins to the two groups identified by the Au/Ag ratio and to quantify the other elements detected by μ−EDXRF analysis, a quantitative analysis with a more sensitive non−destructive technique than XRF, such as Laser Ablation−Inductively Coupled Plasma−Mass Spectrometry (LA−ICP−MS), may be required. This highly sensitive technique, with low detection limits (down to ng g^{-1}), has gained popularity in recent years for investigating the provenance, material identification, and preservation of archaeological finds.

References

Bacharach, J.L., Gordus, A.A., 1972. The Purity of Sasanian Silver Coins: An Introduction. Journal of the American Oriental Society 92, 280–283. https://doi.org/10.2307/600656

Butcher, K., Ponting, M., 2015. The metallurgy of Roman silver coinage: from the reforms of Nero to the reform of Trajan. Cambridge University Press.

Constantinescu, B., Bugoi, R., Oberländer-Târnoveanu, E., Pârvan, K., 2005. Some Considerations on X-Ray Fluorescence Use in Museum Measurements – The Case of Medieval Silver Coins. Romanian Reports in Physics 57, 1021–1031.

Eshel, T., Gilboa, A., Tirosh, O., Erel, Y. Yahalom-Mack, N., 2023. The earliest silver currency hoards in the Southern Levant: Metal trade in the transition from the Middle to the Late Bronze Age. Journal of Archaeological Science, 149,105705. https://doi.org/10.1016/j.jas.2022.105705

Gariboldi, A., 2010. Sasanian Coins and History. The Civic Numismatic Collection of Milan. Mazda Publishers.

Gaudiuso, R., Uhlir, K., Griesser, M., 2019. Micro-invasive depth profile analysis by laser-induced breakdown spectroscopy (LIBS): the case of mercury layers on Sasanian coins. Journal of Analytical Atomic Spectrometry 34, 2261–2272. https://doi.org/10.1039/C9JA00165D

Gianoncelli, A., Kourousias, G., 2007. Limitations of portable XRF implementations in evaluating depth information: an archaeometric perspective. Applied Physics A 89, 857–863. https://doi.org/10.1007/s00339-007-4221-4

Gordus, A.A., Gordus, J.P., 1974. Neutron activation analysis of gold impurity levels in silver coins and art objects, in: Beck, C.W. (Ed.), Archaeological Chemistry, Advances in Chemistry. American Chemical Society, Washington, D. C., pp. 124–147. https://doi.org/10.1021/ba-1974-0138

Hajivaliei, M., Mohammadifar, Y., Ghiyasi, K., Jaleh, B., Lamehi-Rachti, M., Oliaiy, P., 2008. Application of PIXE to study ancient Iranian silver coins. Nuclear Instruments and Methods in Physics Research Section B: Beam Interactions with Materials and Atoms 266, 1578–1582. https://doi.org/10.1016/j.nimb.2007.12.101

Harper, P.O., 1981. Silver Vessels of the Sasanian Period: Royal imagery. Metropolitan Museum of Art, New York, N.Y.

Heidemann, S., Riederer, J., Weber, D., 2014. A Hoard from the Time of Yazdgard III in Kirmān. Iran 52, 79–124. https://doi.org/10.1080/05786967.2014.11834739

Howard-Johnston, J., 2014. The Sasanian state: the evidence of coinage and military construction. Journal of Ancient History 2. https://doi.org/10.1515/jah-2014-0032

Hrnjić, M., Hagen-Peter, G.A., Birch, T., Barfod, G.H., Sindbæk, S.M., Lesher, C.E., 2020. Non-destructive identification of surface enrichment and trace element fractionation in ancient silver coins. Nuclear Instruments and Methods in Physics Research Section B: Beam Interactions with Materials and Atoms 478, 11–20. https://doi.org/10.1016/j.nimb.2020.05.019

Hughes, M.J., Hall, J.A., 1979. X-ray fluorescence analysis of late Roman and Sassanian silver plate. Journal of Archaeological Science 6, 321–344. https://doi.org/10.1016/0305-4403(79)90017-7

Linke, R., Schreiner, M., 2000. Energy Dispersive X-Ray Fluorescence Analysis and X-Ray Microanalysis of Medieval Silver Coins. Microchimica Acta 133, 165–170. https://doi.org/10.1007/s006040070087

Linke, R., Schreiner, M., Demortier, G., 2004. The application of photon, electron and proton induced X-ray analysis for the identification and characterisation of medieval silver coins. Nuclear Instruments and Methods in Physics Research Section B: Beam Interactions with Materials and Atoms 226, 172–178. https://doi.org/10.1016/j.nimb.2004.03.084

Liritzis, I., Zacharias, N., 2011. Portable XRF of Archaeological Artifacts: Current Research, Potentials and Limitations, in: Shackley, M.S. (Ed.), X-Ray Fluorescence Spectrometry (XRF) in Geoarchaeology. Springer New York, New York, NY, pp. 109–142. https://doi.org/10.1007/978-1-4419-6886-9_6

Meyers, P., Sayre, E.V., 1971. The Determination of Trace Elements in Ancient Silver Objects by Thermal Neutron Activation Analysis: A Preliminary Report. International Institute for Conservation of Historic and Artistic Works 11, 29–33. https://doi.org/10.1179/019713671806030125

Mortazavi, M., Naghavi, S., Khanjari, R., Agha-Aligol, D., 2018. Metallurgical study on some Sasanian silver coins in Sistan Museum. Archaeological and Anthropological Sciences 10, 1831–1840. https://doi.org/10.1007/s12520-017-0511-8

Scott, D.A., 2011. Ancient Metals: Microstructure and Metallurgy. Lulu.com.

Sodaei, B., Hajivaliei, M., Nadooshan, F.K., 2013. Possible sources for extraction of silver by comparison of Parthian and Sasanian coins in Mede Satraps. Mediterranean Arhaeology and Archaeometry 13, 161–170.

Sodaei, Bita, Khak, P.M., Khazaie, M., 2013. A Study of Sasanian Silver Coins Employing the XRF Technique. Interdisciplinaria Archaeologica Natural Sciences in Archaeology IV, 211-215.

Uhlir, K., Padilla-Alvarez, R., Migliori, A., Karydas, A.G., Božičević Mihalić, I., Jakšić, M., Zamboni, I., Lehmann, R., Stelter, M., Griesser, M., Schindel, N., Alram, M., 2016. The mystery of mercury-layers on ancient coins — A multianalytical study on the Sasanian coins under the Reign of Khusro II. Microchemical Journal 125, 159–169. https://doi.org/10.1016/j.microc.2015.10.024

Volpi, V., Chiarantini, L., Cicali, C., Salvadori, B., 2023. Shedding light on the microstructure and chemical composition of rare early medieval coins from Italy (Berengario I) by combining pXRF and SEM–EDX analysis. Archaeological and Anthropological Sciences 15, 35. https://doi.org/10.1007/s12520-023-01726-3

Wood, J.R., Charlton, M.F., Murillo-Barroso, M., Martinón-Torres, M., 2017. Iridium to provenance ancient silver. Journal of Archaeological Science 81, 1–12. https://doi.org/10.1016/j.jas.2017.03.002

Final conclusions

Chemical analyses provide valuable insights into a wide range of multidisciplinary inquiries, encompassing historical, artistic, and archaeological aspects. These analyses provide more information about the techniques of execution, dating and provenance of archaeological artefacts. They also serve conservation and restoration purposes, helping to ascertain the condition of artefacts and identify the optimal environmental conditions to mitigate their deterioration. In addition, chemical analyses aid in monitoring the characteristics of an artefact during and after the restoration process.

This thesis presents four distinct works, each exploring the potential of analytical chemistry applied to archaeological research. Archaeological materials are notably intricate, comprising various chemical components distributed unevenly. Therefore, a comprehensive approach, combining non−destructive and micro−destructive analytical techniques, is often essential to address the queries posed by historians and conservators.

In the first section, non−destructive analysis of six copper folles dating back to the Roman−Imperial era enabled their categorisation into two distinct groups based on their discovery location. These groups corresponded to excavated coins (coins found underground) and open−air coins (coins unearthed from upper ground layers). This distinction was facilitated by the evident terrigenous incrustations and oxidation patinas observed on two of the six coins. The presence of titanium and manganese, which are typical terrigenous elements also detected in the soil sample collected from the excavation area, further substantiated the differentiation between the coins. Notably, a significant variation in copper content was also observed, suggesting different origins. Therefore, this study, conducted exclusively through non−invasive analyses such as μ−EDXRF and FTIR−ATR, demonstrated the ability to classify a subset of coins into the two groups based on their chemical and morphological characteristics. These results support numismatists who may have been uncertain about classifying all coins from the same site solely based on archaeological evidence.

In the second section, two studies on the characterisation of the composition of Late Antique gold solidi were presented. In the first study, only conventional laboratory techniques such as μ−EDXRF, ICP−AES, and ICP−MS were employed to analyse 49 gold coins. The non−destructive technique was used for the analysis of all coin samples

and, due to the availability of a 99.9% gold standard, a semi−quantitative analysis was also conducted to determine their fineness. In addition, the Pt/Pd ratio was determined to gain more insight into the origin of the metal used to mint the coins. Two distinct groups were highlighted, which could be associated with two different sources of gold. Micro−destructive analysis was carried out on only six specimens, revealing an overestimation of gold by the non−destructive surface analysis of up to 5%. This confirmed the hypothesis presented in a previous study on a single specimen that, although gold is a stable metal, surface enrichment of this metal can occur due to the long burial of ancient coins in unfavourable environments for their preservation. Regarding trace elements, the presence of tin and the low concentrations of copper and lead suggest that the gold used to produce the six coins analysed originated from alluvial sources. Positive correlations between Cr, Mn, Fe, Ni, and between Ca, Al, Sr led to the conclusion that the burial place of the coins was the soil. Following this preliminary study, four gold solidi were analysed using the most sensitive techniques with synchrotron light. These coins were three solidi and one tremisse from the mints of Ravenna and Constantinople. SR−XRF analysis identified the elements used in the minting of each piece, distinguishing the surface concretions from the elements that constitute the original coin. A semi−quantitative fitting of the XRF spectra against the metal alloy assessed the fineness of the gold and the presence of minor elements in the alloy. The results showed a variation in alloy purity of around 2% between the four specimens analysed, consistent with available literature. The same quantitative analysis was used to elucidate the nature of surface contamination by employing SR−XANES analysis on the K−edge of the iron. The results of this analysis suggest that both deposits are consistent with the Mediterranean area and that the more superficial concretions likely originate from warmer and more temperate regions, perhaps closer to the coastal areas, than the patina accumulated at greater depths.

The third section involved the multi−technical analysis of 160 denarii and antoniniani minted during the 3rd century AD. Non−destructive analysis (μ−EDXRF) revealed the presence of Ag, Cu, Pb, Sn, Ni, Zn, Bi, Fe, and Ca, along with the inhomogeneity of the coin surfaces. SEM−EDX analysis, performed on four samples, also highlighted the differing distribution of the two alloying elements (silver and copper). Micro−destructive analysis was conducted on twelve specimens, comprising eight denarii and four antoniniani. ICP−AES was used to study the alloy composition, which was found to be

relatively consistent in the eight denarii under examination. The four antoniniani analysed similarly exhibited a consistent alloy composition. A noticeable difference between the two types of coins was observed, with a significant decrease in the percentage of Ag as the year of mintage increased, underlining the progression of the economic crisis during the 3rd century. Concerning trace elements, quantified via ICP−MS, the high concentrations of Pb and Sn are in agreement with the use of argentiferous galena for silver extraction and the utilisation of old brass or bronze objects in the production of silver−copper coins, respectively. Multivariate analysis identified the two groups of coins corresponding to the two currencies. This provided an initial basis for a numismatic database and allowed for the chemical mapping of unknown samples.

Finally, the fourth section involved the exclusively non−destructive analysis (μ−EDXRF) on 29 Sasanian drachms. X−ray fluorescence revealed that the primary alloying element was silver, with copper, lead, and gold as impurities. A semi−quantitative analysis was also carried out to determine the silver and copper content, revealing an average silver content of over 95% in almost all the coins. Among the various specimens, one coin with a copper core and silver plating stood out. The Au/Ag ratio was used to identify two groups of drachmas that may have been produced from different ores. The absence of gold in one specimen suggested that it was a modern forgery, likely produced after refining the silver using modern metallurgical techniques capable of separating gold from silver. Lastly, the analysis revealed a group of five coins with a high silver content (>99.8%) and low Cu/Ag and Pb/Ag ratios. These coins bore the inscription “afid” (meaning “good” or “excellent”), confirming the historical assumption that coins with this inscription were of superior quality.

In conclusion, all the aforementioned studies underscore the importance of chemical analyses and multi−analytical approach in the study of archaeological artefacts and, particularly ancient coins. This approach offers the opportunity to determine their chemical composition, to obtain information on the nature of the raw materials used and the coinage processes, as well as to identify surface corrosion compounds, which are useful for understanding the environmental history of artefacts.

Acknowledgments

I would like to express my gratitude to ERPAC − Ente Regionale PAtrimonio Culturale della Regione Autonoma Friuli−Venezia Giulia for the provision of instruments located in the diagnostic laboratory of Villa Manin di Passariano (Codroipo, UD).

A special note of thanks goes to the team at the TrEE Lab − Trace ELements in the Environment Laboratory, whose open doors, shared workspace, and access to essential instruments were indispensable in the completion of this thesis.

I would like to thank Elettra Sincrotrone Trieste and the staff of the X−Ray Fluorescence beamline for their expertise, assistance, and support.

My gratitude also extends to the Department of Humanistic Studies at the University of Trieste, and in particular, I am deeply indebted to Prof. Bruno Callegher. Thank you for introducing me to the captivating world of archaeometry during my bachelor's thesis. I would also like to thank his collaborators, Dr. Andrea Gariboldi and Dr. Giulio Carraro. Needless to say, without all of you this thesis would not have been possible.

I have great respect for my supervisor, Prof. Gianpiero Adami. Your unwavering support since 2018, along with your precious advice and uplifting words, have been invaluable. I cannot thank you enough for the trust you placed in me and for allowing me the freedom to make my own choices.

To my "desk neighbour", Prof. Matteo Crosera, I extend my heartfelt thanks for being a constant presence over these three years. Our shared coffee breaks, your teachings, suggestions, and, most importantly, the consistent support you offered are deeply appreciated.

I would like to express my gratitude to Dr. Elena Pavoni, who graciously shared her expertise and the delicate "Miss" with me. Your attentive ear and wise counsel were invaluable.

Thank also to Prof. Enrico Prenesti for his assistance in drafting and revising the papers presented in this work.

I want to convey my appreciation to my C11 colleagues, with whom I have shared lunches, played endless games of UNO, and enjoyed aperitifs after hard days at work.

Thank you because you have gradually become more than colleagues; you are friends. In particular, I would like to thank Anastasia and Miriam for sharing not only part of this academic journey with me but also fragments of life.

To my lifelong friends and those who joined me along the way: each of you, in your unique way, has contributed to my growth. If I have reached this goal, it is because of the experiences we have shared. I would like to give a special mention to Alice and Cristina for their unwavering belief in me, even when I faltered. I hope to have made you proud again this time.

Lastly, my deepest thanks go to my family, who have consistently supported me and stood by me through the most challenging moments of this journey. A profound and heartfelt gratitude is reserved for my mum, to whom I cannot express enough how much I love her.

Twenty years from now you will be more disappointed by the things that you didn't do than by the ones you did do. So, throw off the bowlines. Sail away from the safe harbour. Catch the trade winds in your sails.

Explore. Dream. Discover.

Mark Twain

Appendix – Scientific Outreach and Didactic Activity

Publication of IF Journal

Marussi, G., Crosera, M., Prenesti, E., Callegher, B., Baracchini, E., Turco, G., Adami, G., 2023. From Collection or Archaeological Finds? A Non−Destructive Analytical Approach to Distinguish between Two Sets of Bronze Coins of the Roman Empire. Molecules, 28 (5), 2382. https://doi.org/10.3390/molecules28052382

Daka, M., Montini, T., Pengo, P., Marussi, G., Crosera, M., Adami, G., Delgado, J.J., Giambastiani, G., Fertey, P., Fonda, E., Pasquato, L., Fornasiero, P., 2023. Reduced Tiara−like Palladium Complex for Suzuki Cross−Coupling Reactions, Chemistry − A European Journal, e202301740. https://doi.org/10.1002/chem.20230174

Magnano, G.C., Marussi, G., Crosera, M., Hasa, D., Adami, G., Lionetti, N., Larese Filon, F., 2023. Probing the effectiveness of barrier creams against human skin penetration of nickel powder, International Journal of Cosmetic Science, 328, 121654, https://doi.org/10.1111/ics.12893

Magnano, G. C., Carton, F., Boccafoschi, F., Marussi, G., Cocetta, E., Crosera, M., Adami, G., Voinovich, D., Larese Filon, F., 2023. Evaluating the role of protective creams on the cutaneous penetration of Ni nanoparticles. Environmental Pollution, 328, 121654. https://doi.org/10.1016/j.envpol.2023.121654

Marussi, G., Crosera, M., Prenesti, E., Cristofori, D., Callegher, B., Adami, G., 2022. A Multi−Analytical Approach on Silver-Copper Coins of the Roman Empire to Elucidate the Economy of the 3rd Century A.D. Molecules, 27, https://doi.org/10.3390/molecules27206903

Carlomagno, I., Zeller, P., Amati, M., Aquilanti, G., Prenesti, E., Marussi, G., Crosera, M. Adami, G., 2022. Combining synchrotron radiation techniques for the analysis of gold coins from the Roman Empire, Scientific Reports, 12, https://doi.org/10.1038/s41598-022-19682-8

Magnano, G.C., Marussi, G., Larese Filon, F., Crosera, M., Bovenzi, M., Adami, G., 2022. Transdermal permeation of inorganic cerium salts in intact human skin. Toxicology in Vitro, 82, https://doi.org/10.1016/j.tiv.2022.105381

Magnano, G.C., Marussi, G., Adami, G., Crosera, M, Larese Filon, F., 2022. Assessment of dermal absorption of beryllium and copper contained in temple tips of eyeglasses. Toxicology Letters, 361, 64-71. https://doi.org/10.1016/j.toxlet.2022.04.001

Magnano, G.C., Marussi, G., Pavoni, E., Adami, G., Larese Filon, F., Crosera, M., 2022. Percutaneous metals absorption following exposure to road dust powder. Environmental Pollution, 292, 118353. https://doi.org/10.1016/j.envpol.2021.118353

Marussi, G., Vione, D., 2021. Secondary Formation of Aromatic Nitroderivatives of Environmental Concern: Photonitration Processes Triggered by the Photolysis of Nitrate and Nitrite Ions in Aqueous Solution. Molecules, 26, 2550. https://doi.org/10.3390/molecules26092550

Congress attendance

Oral presentations

Marussi G., Crosera M., Licen S., Fornasaro S., Carraro G., Callegher B., Adami G., 2023. A multi-analytical approach for the determination of the fineness of 12^{th}-13^{th} Century Emilia-Romagna Denarii. XXX Congresso Nazionale della Divisione di Chimica Analitica della Società Chimica Italiana, Book of Abstracts p. 160, Vasto (Italy), 17-21 September 2023. Presenting author: Giovanna Marussi

Greco E., Tanasi D., Hassam S. N., Pisciotta F., Marussi G., Adami G., Licen S., Barbieri P., 2022. Analyzing residues from underwater context: the case of Late Roman amphorae from the Baglio-Anselmi Museum of Marsala (Trapani, Italy). CHEMCH – 6th International Congress Chemistry for Cultural Heritage 2022, Ravenna (Italy), 4-8 July 2022. Presenting author: Dr. Enrico Greco

Carlomagno I., Amati M., Zeller P., Aquilanti G., Marussi G., Crosera M., Callegher B., Prenesti E., Adami G., 2022. X-Ray investigations on ancient gold coins: Synchrotron Radiation contribution to history and numismatics. International Conference on Accelerators for Research and Sustainable Development: From Good Practices Towards Socioeconomic Impact, Book of Abstracts p. 76-77, Vienna (Austria), 23-27 May 2022. Presenting author: Dr. Ilaria Carlomagno

Marussi G., Crosera M., Prenesti E., Callegher B., Adami G., 2021. The Third-Century monetary crisis: chemical analysis of Denarii and Antoniniani. XXVII Congresso Nazionale della Divisione di Chimica Analitica della Società Chimica Italiana, Book of Abstracts p. 299, 14-23 September 2021. Presenting author: Giovanna Marussi

Poster presentations

Marussi G., Pavoni E., Larese Filon F., Adami G., Licen S., Crosera M., 2023. Skin absorption of potential toxic metals following exposure to urban dust. XXX Congresso Nazionale della Divisione di Chimica Analitica della Società Chimica Italiana, Book of Abstracts p. 301, Vasto (Italy), 17-21 September 2023. Presenting author: Giovanna Marussi

Pavoni E., Petranich E., Floreani F., Crosera M., Marussi G., Greggio N., Campanella B., Covelli S., 2023. May biochar be a suitable amendment to mitigate mercury availability from contaminated sediments? Preliminary evidences from leaching and incubation experiments. ICOBTE & ICHMET 2023, Wuppertal (Germany), 6-10 September 2023. Presenting author: Dr. Elena Pavoni

Marussi G., Crosera M., Greco E., Callegher B., Dadà M., Prenesti E., Adami G., 2022 Multi-analytical procedure for the investigation of three byzantine seals. XXIX Congresso della Divisione di Chimica Analitica, Milazzo (Italy), Book of Abstracts p. 284, 11-15 September 2022. Presenting author: Prof. Gianpiero Adami

Barago N., Pavoni E., Crosera M., Marussi G., Lenaz D., Larese Filon F., Covelli S., Adami G., 2022. Is pXRF a suitable analytical technique for mining prospection and geochemical characterisation of contaminated sites? XXIX Congresso della Divisione di Chimica Analitica, Milazzo (Italy), Book of Abstracts p. 285, 11-15 September 2022. Presenting author: Prof. Gianpiero Adami

Greco E., Marussi G., Crosera M., Manzini D., Barbieri P., Licen S., 2022. Sensing and hyperspectral imaging Self Organized Maps: detecting altered areas in paintings. XXIX Congresso della Divisione di Chimica Analitica, Milazzo (Italy), Book of Abstracts p.326, 11-15 September 2022. Presenting author: Dr. Enrico Greco

Marussi G., Crosera M., Callegher B., Prenesti E., Cristofori D., Adami G., 2022. A multi-analytical approach on silver-based coins to reconstructing the 3rd century economy. CHEMCH – 6th International Congress Chemistry for Cultural Heritage 2022, Ravenna (Italy), 4-8 July 2022. Presenting author: Giovanna Marussi

Carlomagno I., Amati M., Zeller P., Adami G., Marussi G., Crosera M., Prenesti E., Callegher B., 2022. How X-rays can tell a story long fifteen centuries. European Conference on X-ray Spectrometry 2022, Bruges (Belgium), 26 June - 1 July 2022. Presenting author: Dr. Ilaria Carlomagno

Zanoni I., Crosera M., Pavoni E., Marussi G., Mauro M., Costa A. L., Larese Filon F., Adami G., 2021. Ex- vivo evaluation of silver nanoparticles permeation through baby porcine oral mucosa using the SP-ICP-MS technique. XVII Italian - Hungarian Symposium on Spectrochemistry: Current approaches in health and environmental protection, Turin (Italy), 14-18 June 2021. Presenting author: Giovanna Marussi

Marussi G., Carlomagno I., Aquilanti G., Amati M., Zeller P., Crosera M., Prenesti E., Callegher B., Adami G., 2021. Synchrotron X-ray Fluorescence on ancient gold coins: how trace elements can give insight into the Roman Empire. SPIE Optical Metrology - Optics for Arts, Architecture, and Archaeology (O3A) VIII, Munich (Germany), 21-25 June 2021. Presenting author: Giovanna Marussi

Didactic activity

Tutoring activity for the BSc course in Chimica Analitica II for a total of 50 hours of work. University of Trieste, Department of Chemical and Pharmaceutical Sciences. A.A. 2022-2023; A.A. 2021-2022; A.A. 2020-2021

Assistance activity for the BSc course in Chimica Analitica I. University of Trieste, Department of Chemical and Pharmaceutical Sciences. A.A. 2021-2022.

Co-supervisor of BSc thesis

Marta Baldassar 2022-2023. Assorbimento cutaneo di metalli potenzialmente tossici presenti nella polvere urbana. BSc degree in Chimica Analitica, BSc Course in Chimica. Supervisor: Prof. Matteo Crosera. Co-supervisor: Giovanna Marussi

Chiara Romanello 2022-2023. Assorbimento cutaneo di metalli in seguito a esposizione a polveri di acciaio inossidabile. BSc degree in Chimica Analitica, BSc Course in Chimica. Supervisor: Prof. Matteo Crosera. Co-supervisor: Giovanna Marussi

Giada Verk 2021-2022. Indagini archeometriche di dracme sasanidi d'argento (VI-VII sec. d.C.). BSc degree in Chimica Analitica, BSc Course in Chimica. Supervisor: Prof. Gianpiero Adami. Co-supervisors: Giovanna Marussi, Dr. Andrea Gariboldi

Stella Zucchetto 2021-2022. Determinazione multi-analitica del titolo di denari emiliano-romagnoli del XII-XIII secolo e confronto tra le tecniche ICP-AES e ED-μXRF. BSc degree in Chimica Analitica, BSc Course in Chimica. Supervisor: Prof. Gianpiero Adami. Co-supervisors: Giovanna Marussi, Dr. Giulio Carraro

Davide Della Rovere 2020-2021. Metodologie analitiche applicate allo studio di esemplari monetali argentei (Denari e Antoniniani) del III secolo d.C. BSc degree in Chimica Analitica, BSc Course in Chimica. Supervisor: Prof. Gianpiero Adami. Co-supervisors: Giovanna Marussi, Dott. Federico Floreani

Maira De Cecco 2020-2021. Elementi in tracce e terre rare: presenza e distribuzione in una sequenza sedimentaria del Golfo di Trieste. BSc degree in Chimica Analitica, BSc Course in Chimica. Supervisor: Prof. Matteo Crosera. Co-supervisors: Dr. Elena Pavoni, Giovanna Marussi

Michele Francesco Zamburlini 2020-2021. Analisi chimiche di concrezioni superficiali su esemplari monetali romani (III secolo d.C.). BSc degree in Chimica Analitica, BSc Course in Chimica. Supervisor: Prof. Gianpiero Adami. Co-supervisors: Prof. Bruno Callegher, Giovanna Marussi

Co-supervisor of MSc thesis

Matilde Ibba 2020-2021. Analisi chimiche di denari e antoniniani da uno o più ripostigli dall'area balcanica. MSc degree in Chimica Analitica, MSc course in Chimica. Supervisor: Prof. Gianpiero Adami. Co-supervisors: Prof. Bruno Callegher, Giovanna Marussi.